THESIS FOR THE DEGREE OF DOCTOR OF PHILOSOPHY

Fluidized bed plants for heat and power production in future energy systems

GUILLERMO MARTINEZ CASTILLA

Department of Space, Earth and Environment

CHALMERS UNIVERSITY OF TECHNOLOGY

Fluidized bed plants for heat and power production in future energy systems

GUILLERMO MARTINEZ CASTILLA
ISBN 978-91-7905-923-1

Doktorsavhandlingar vid Chalmers tekniska högskola
Ny serie nr 5389
ISSN 0346-718X

Department of Space, Earth and Environment
Chalmers University of Technology
SE-412 96 Gothenburg
Sweden
Telephone + 46 (0)31-772 1000

Printed by Chalmers Reproservice
Gothenburg, Sweden 2023

Fluidized bed plants for heat and power production in future energy systems

GUILLERMO MARTINEZ CASTILLA
Division of Energy Technology
Department of Space, Earth and Environment
Chalmers University of Technology

Abstract

Fluidized bed (FB) plants are used for heat and power production in several energy systems around the world, with particular importance in systems using large shares of renewable solid fuel, e.g., biomass. These FB plants are traditionally operated for base-load electricity production or for heat production, and thus characterized by relatively small and slow load changes. In parallel, as the transition towards energy systems with net-zero emissions increases the share of variable renewable energy (VRE) sources, the need for implementing variation management strategies at various timescales arises – giving heat and power plants the possibility to adapt their operations to accommodate the inherent variability of VRE sources. Following this, FB technology is envisioned for a wide range of novel applications expected to play significant roles in the decarbonization of energy systems, such as thermochemical energy storage and carbon capture and storage. In this context, research efforts are needed to investigate the technical and economic features of FB plants in energy systems with high levels of VRE.

The aim of this thesis is to elucidate the capabilities of FB plants for heat and power production in net-zero emissions energy systems. For this purpose, two main pathways are explored: **i)** transient operation as **fuel-fed plants**, and **ii)** the potential conversion into decarbonized plants, i.e., into **VRE-fed** layouts providing dispatchable outputs.

For **fuel-fed FB plants**, a dynamic model of biomass-fired FB plants has been developed, considering the two types of FB boilers (BFB and CFB) and including validation against steady-state and transient operational data collected from two commercial plants. As a novelty of this work the model describes both the gas (in-furnace) and water-steam sides such that the interactions between the two can be assessed. The results of the simulations show that i) the characteristic times for the gas side are shorter in BFB furnaces than in CFBs, albeit these times are for both furnace types not longer than those for the water-steam side; ii) the computed timescales for the dynamics of FB plants fall well within those required for offering complementing services to the grid; and iii) the use of control and operational strategies for the water-steam side can confer capabilities superior to fuel-feeding control in terms of avoiding undesirable unburnt emissions and providing temporary overload operation. The retrofit of fuel-fed FB plants into poly-generation facilities cogenerating a combustible biogenic gas is also assessed, revealing that partial combustion of this gas can be used to provide faster inherent dynamics than the original configuration.

For **VRE-fed FB layouts**, techno-economic process modeling has been carried out for large-scale deployment of solar- and electricity-charging processes based on three different chemical systems: i) carbonation/calcination (calcium); ii) thermally reduced redox (cobalt oxides); and iii) chemically reduced redox (iron oxides). One attractive aspect of these layouts is the possibility to build part of them by retrofitting current fuel-fed FB plants. While the technical assessment for solar applications indicates that cobalt-based layouts offer the highest levels of efficiency and dispatchability, calcium-based processes present better economics owing to the use of inexpensive calcium material. The results also show that electricity-charged layouts such as iron looping can play an important role in the system providing variation management strategies to the grid while avoiding costly H_2 storage. Further, the economic performances of VRE-fed FB layouts are benefitted by the generation of additional services and products (e.g., carbon capture and on-demand production of H_2), and by scenarios with high volatility of the electricity prices.

***Keywords*:** operational flexibility, thermal power plant, process control, combined heat and power, biomass combustion

List of publications

The thesis is based on the following appended papers, which are referred to in the text by their assigned Roman numerals:

I. G.M. Castilla, R.M. Montañés, D. Pallarès and F. Johnsson.
"Dynamic modeling of the reactive side in large-scale fluidized bed boilers".
Industrial and Engineering Chemistry Research, **2021,** 60, 3936-3956.

II. G.M. Castilla, R.M. Montañés, D. Pallarès and F. Johnsson.
"Comparison of the transient behaviors of bubbling and circulating fluidized bed combustors".
Heat Transfer Engineering, **2023,** 44, 4, 303-316

III. G.M. Castilla, R.M. Montañés, D. Pallarès and F. Johnsson
"Dynamics and control of large-scale fluidized bed plants for renewable heat and power generation".
Applied Thermal Engineering, **2023,** 219, 119591.

IV. G.M. Castilla, R.M. Montañés, D. Pallarès and F. Johnsson.
"Dynamics of large-scale bubbling fluidized bed combustion plants for heat and power production".
Fuel, **2023,** 341, 127748.

V. G.M. Castilla, D.C. Guío-Pérez, S. Papadokonstantakis, F. Johnsson and D. Pallarès.
"Techno-economics of solids-based thermochemical energy storage systems for high-temperature applications at large scale".
Submitted for publication, **2023**.

VI. G.M. Castilla, D.C. Guío-Pérez, S. Papadokonstantakis, D. Pallarès and F. Johnsson.
"Techno-economic assessment of calcium looping for thermochemical energy storage with CO_2 capture".
Energies, **2021,** 14, (11) 3211.

VII. D.C. Guío-Pérez, G.M. Castilla, D. Pallarès, H. Thunman and F. Johnsson.
"Thermochemical energy storage with integrated district heat production – a case study of Sweden".
Energies, **2023,** 16, (3) 1155.

Guillermo Martinez Castilla is the principal author of **all papers** and performed the modeling and analysis for all seven papers. Diana Carolina Guío-Pérez contributed to the method development, editing and discussion in **Papers V-VII** and shares first authorship of **Paper VII.** Rubén M. Montañés contributed to the method development, editing and discussion in **Papers I-IV**. David Pallarès contributed to the method development, editing and discussion in **all papers**. Filip Johnsson contributed with discussion and editing in **all papers**. Henrik Thunman contributed with discussion and editing in **Paper VII.** Stavros Papadokonstantakis contributed with discussion and editing in **Papers V** and **VI.**

Publications not included in this work

Additional publications by the author related to the work are listed below but have not been included in the thesis as they are either outside the scope of this thesis or overlap with the appended papers.

- G.M. Castilla, M. Biermann, R.M. Montañés, F. Normann and F. Johnsson.
  "Integrating carbon capture into an industrial combined-heat-and-power plant: performance with hourly and seasonal load changes".
  International Journal of Greenhouse Gas Control, **2019,** 82, 192-203

- G.M. Castilla, A. Larsson, L. Lundberg, F. Johnsson and D. Pallarès.
  "A novel experimental method for determining lateral mixing of solids in fluidized beds – Quantification of the splash-zone contribution".
  Powder Technology, **2020,** 370, 96-103.

- G.M. Castilla, D.C. Guío-Pérez, D. Pallarès and F. Johnsson.
  "Calcium looping for combined CO2 capture and thermochemical energy storage",
  in Book *Circular Economy Processes for CO_2 Capture and Utilization. Strategies and Case Studies*, **2023**, Paperback ISBN: 9780323956680

- G. M. Castilla, R.M. Montañés, D. Pallarès and F. Johnsson.
  "Dynamic modeling of the flue gas side of large-scale circulating fluidized bed boilers".
  In Proceedings: CFB-13 conference, Vancouver, Canada, **2021**

- G.M. Castilla, D.C. Guío-Pérez, S. Papadokonstantakis, D. Pallarès and F. Johnsson.
  "Techno-economic assessment of calcium looping for thermochemical energy storage with CO_2 capture".
  In Proceedings: 11th International Trondheim CCS Conference TCCS, Trondheim, Norway, **2021.**

- G.M. Castilla, R.M. Montañés, D. Pallarès and F. Johnsson.
  "Dynamics of large-scale bubbling fluidized combustion plants for heat and power production".
  In Proceedings: FBC-24 conference, Gothenburg, Sweden, **2022**

- A. Köhler, G. Gustafson, G.M. Castilla and D. Pallarès.
  "Extension of the product portfolio of fluidized bed boilers by bed-sectioning – effects on the original boiler system".
  In Proceedings: FBC-24 conference, Gothenburg, Sweden, **2022**

Acknowledgments

It might sound illusory but pursuing a PhD is a teamwork. Or at least it has been for me. Thus, I would like to start by thanking my four (four!) teammates aka supervisors. First and uttermost to David, from whom I have learnt tons of not only scientific (which are quite many) but life lessons. Special thanks for your openness, for your patience and for your trust, and for making these 5 years a comfortable, yet exciting and fun journey. Thank you, Carolina, for enlightening my studies with love for the detail, scientific curiosity, and passion for good, hard work. Also thank you for all the non-work aspects that have led me to call you "friend". Rubén, thanks for always being there. Despite the distance, you have been the only constant of these 6 years of work at Chalmers, and I will always be thankful for your implication and for the role you have played in my life. Last but not least, thank you Filip for always finding the time to discuss both work and non-work aspects, and for doing it with such a great temper. It has been an honour to learn so much from you.

My gratitude goes also to my examiner Henrik Thunman, whose busy office and challenging drawings have always been available to me. Very special thanks to Fredrik, Max and Stavros for opening me the doors of the division five and a half years ago and initiating this longer-than-expected adventure.

Thank you Bioshare for a great collaboration and useful discussions, all the luck for the exciting projects you have ahead! Thanks also to Karlstad and Övik Energi for an impressive work answering to all our requests. Special thanks to Greene for believing in Modelica and trusting my expertise. It has been (and is) a pleasure to push the limits and keep learning with you.

Thanks also to Javier and Cameron for teaching me how to teach. Your brilliant work not only was a constant training for me, it is also part of this thesis now.

Regarding my co-workers at Energy Technology, I would like to thank Marie and Katarina for their everlasting good and helping mood that we all should learn from. Thanks to my PhD colleagues (some of you now friends) for lunches, discussions, afterwork sessions, board games, volleyball and more. Sharing this adventure with you all has been crucial for me. Thank you, Alla Toktarova, for existing and for crossing paths with me. Special thanks also to my office mates Anna and Tove. Your positive, respectful, and caring energy are also part of this thesis. To the Fluidization group, thanks for our Monday meetings when we needed them the most and for the fun travels around the globe. Lastly, thanks to the Heat and Power team for being the best teaching group one could have asked for.

To all my friends around the world in Spain, Iceland, Italy, Austria, Netherlands… Thanks for being a constant source of love and fresh air. Special thanks to Javier and Paco, os quiero. I would like to thank Gothenburg for allowing me to spend these crucial years of my life among its streets, its people and its winters and summers. Big thanks to all the friends who have contributed to make this city my home. Schmidt, thank you for the unconditional friendship and for one or two nights out.

Thank you to my parents, for being the reason of this all. Thank you for teaching me how to live, for always allowing me to be me, and for your love. Thank you, Marina and Mario, I have you with me day after day. Lastly, thank you Stefanía, for being the light, the warmth, and the grounding force during all these years.

Guillermo Martinez
Gothenburg, August 2023

Table of Contents

Abstract iii

List of publications v

Acknowledgments vii

1. Introduction 1

1.1. Background 1

1.2. Thesis overview 2

1.2.1. Aim and scope 2

1.2.2. Contributions 3

1.2.3. Limitations 3

1.2.4. Outline 4

2. Technical background 7

2.1. Characteristics of future energy systems 7

2.1.1. VRE generation and variability 8

2.1.2. Flexibility of thermal power plants 9

2.1.3. Carbon capture and storage 10

2.2. Fluidized bed plants for solid fuel conversion 11

2.2.1. Dynamic modeling of FBC plants 14

2.3. Solids looping processes for TCES 16

2.3.1. Carbonate looping 17

2.3.2. Redox looping 18

3. Methods 19

3.1. Dynamic process modeling and simulation 21

3.1.1. Input data 21

3.1.2. Formulation of the models 24

3.1.3. Calibration and validation 26

3.1.4. Dynamic analyses 28

3.1.5. Summary of the cases studied 30

3.2. Techno-economic process modeling and simulation 31

3.2.1. Material selection and process formulation 32

3.2.2. Process modeling 34

3.2.3. Cost estimation 36

3.2.4. Technical assessment 37

3.2.5. Economic assessment 37

3.2.6. Summary of the cases studied 38

4. Selected results 39

4.1. Load-changing capabilities of fuel-fed FB plants 39

4.1.1. Validation of the dynamic process model 39

4.1.2. Load-changing dynamics 42

4.2. Techno-economics of VRE-fed FB plants 47

4.2.1. Solar-charged layouts 47

4.2.2. Electricity-charged layouts 51

5. Discussion 55

5.1. Transient operation of FB plants 55

5.2. Provision of variation management strategies 57
5.3. Additional products and services 61
5.3.1. Combustible biogenic gas 61
5.3.2. CO_2 capture from nearby facilities 62
5.3.3. H_2 on-demand 63
6. Conclusion ***65***
7. Recommendations for further work ***67***
Appendix A. Linear cost optimization model ***69***
Appendix B. Retrofit of a fuel-fed FB plant for CHP into a poly-generation plant ***71***
References ***73***

Nomenclature and definitions

Abbreviations and Acronyms

ADV	average duration of variations
AP	absolute percentage error
BESP	breakeven electricity selling price
BF	boiler-following
BFB	bubbling fluidized bed
BHSP	breakeven heat selling price
BSP	breakeven selling price
CaL	calcium looping
CCS	carbon capture and storage
CFB	circulating fluidized bed
CHP	combined heat and power
CoL	cobalt looping
CSP	concentrated solar power
DFB	dual fluidized bed
DH	district heating
ESP	electricity selling price
FB	fluidized bed
FBC	fluidized bed combustion
FeL	iron looping
HX	heat exchanger
IncomeCC	Carbon capture-derived income
NPV	net present value
OEA	oxygen-enriched air
O&M	operation and maintenance
SP	set-point
STC	steam to clients
TCES	thermochemical energy storage
TES	thermal energy storage
TF	turbine-following
UF	utilization factor
VMS	variation management strategies
VRE	variable renewable energy

Symbols

C	cost [M$]
C_0	reference cost [M$]
CF_i	cash flow in year *i* [M$]
Cp	heat capacity [J/K]
$\dot{E}_{net}$	net energy flow [MW]
f	scaling factor
F_i	mass flow rate of component *i* [kg/s]
F_{steam}	live steam mass flow rate [kg/s]
M_i	total mass of species *I* [kg]
$M_{solids,stored}$	total inventory mass of stored solids [kg]
P_{el}	electrical power [MW]
P_{steam}	live steam pressure [bar]
Q_{DH}	district heating load [MW]

Q_{in}	net heat input [MW]
$Q_{out,disch}$	heat flow output from the discharging section [MW]
Q_{walls}	heat transfer to the waterwalls [MW]
r	discount rate [%]
r_{disp}	dispatchability ratio
S	sizing capacity of a given equipment
S_0	reference sizing capacity
t_{ch}	operation time of the charging section [h/day],[h/year]
T_{db}	temperature in the dense bed [°C]
$T_{DH,out}$	temperature of the outlet district heating line [°C]
t_{disch}	operating time of the discharging section [h/day],[h/year]
t_s	stabilization time [s][min]
T_{top}	temperature in the furnace top [°C]
x_m	measured process variable
x_s	simulated process variable
y_0	initial state of a certain process variable before the change is introduced
y_∞	final state of a certain process variable after reaching stabilization
τ_{FD}	characteristic time of the fluid dynamics[s]
τ_{HT}	characteristic time of the heat transfer [s]
τ_{FC}	characteristic time of the fuel conversion [s]
τ	residence time, [s]
ΔH_R	enthalpy of reaction, [kJ/mol]
η_t	overall energy efficiency
$\eta_{t,el}$	overall electrical efficiency

Definitions

The following terms are recurrently used throughout the thesis:

Controlled dynamics: Transient behavior of a plant/furnace when running with closed (i.e., activated) control loops.
Dynamic analysis: Investigation of different aspects related to the transient operation of fluidized bed plants.
Fuel-fed plants: Fluidized bed plants combustion plants converting solid renewable fuels.
Gas side: Reaction and transport chambers in which the fuel, bulk solids and gas are located. In some contexts, also referred as *in-furnace*. Note that the furnace walls and flue gas path are in this work considered part of the water-steam side.
In-furnace mechanism: Each one of the physical-chemical phenomena present in a fluidized bed reactor, namely: heat transfer, fluid dynamics and chemical conversion.
Inherent dynamics: Transient behavior of a plant/furnace when running with open (i.e., deactivated) control loops.
Model calibration: Fine-tuning of model parameters to adjust the model output so that it resembles more accurately a specified operational dataset of a certain reference unit.
Model formulation: Writing and balancing of the model, i.e., of the system of equations consisting of mass and energy balances.
Model validation: Use of the calibrated model to predict steady-state and transient operational datasets others than the one used for calibration, and thereby check the model reliability.
Open-loop: Uncontrolled response of the system variables after a step-change in one of the inputs.
Reference units: Commercial-scale fuel-fed fluidized bed plants used for collecting operational data.
TCES-focused: Layouts where the storage of variable renewable energy is maximized.
VRE-fed plants: Fluidized bed plants converting and storing variable renewable energy into dispatchable heat and power (and optionally other outputs).
Water-steam side: All the equipment related to the water-steam loop conforming the Rankine cycle, i.e., the convective flue gas path (economizers and superheaters), evaporator tubes and in-furnace walls, steam drum, steam lines and valves, steam turbines, condensers, deaerators, feedwater heaters, pumps, and valves.

List of figures

Figure 1. Overview of the investigated FB processes and layouts and their relationships to the papers included in this thesis. 4
Figure 2. Overview of the topics covered in this section and their relationship with this thesis. 7
Figure 3. Schematic side views of the two types of FB furnaces for heat and power production. 12
Figure 4. Schematic of a fuel-fed FB plant for heat and power production including both the reactor (gas side) and Rankine cycle equipment (water-steam side)..... 13
Figure 5. Schematic of a DFB steam gasifier. 13
Figure 6. General scheme for thermochemical energy storage.. 17
Figure 7. Overview of the methods used in this thesis and their connections to the appended papers 20
Figure 8. Overview of the dynamic process modeling and simulation methodology. 21
Figure 9. Simplified process schematic of the reference plant including the main process variables used throughout the work 22
Figure 10. Simplified process schematic of the reference plant including the main process variables used throughout the work. 23
Figure 11. Input/output scheme of the integrated dynamic model including the master control. 25
Figure 12. Operational datasets acquired from the reference fuel-fed FB plants..... 27
Figure 13. Schematic showing how the stabilization time is computed from the transient trajectory of a specific process variable 29
Figure 14. Schematic P&ID of the boiler-following and turbine-following control strategies..... 30
Figure 15. Schematic process diagram of the turbine bypass. 30
Figure 16. Overview of the techno-economic process modeling and simulation methodology. 31
Figure 17. General scheme of the VRE-fed processes assessed in this work. 33
Figure 18. Inputs to the model for the transient validation of the CFB mode. Source: **Paper III**..... 40
Figure 19. Comparison of the model outputs (simulation) and the plant measurements of the CFB plant. 40
Figure 20. Inputs to the model for the transient validation of the BFB mode..... 41
Figure 21. Comparison of the model outputs (simulation) and the plant measurements of the BFB plant. 41
Figure 22. Stabilization times of the CFB and BFB reference furnaces after load changes of different magnitudes. 42
Figure 23. Stabilization times of the CFB reference plant (gas and water-steam sides) after load changes of different magnitudes..... 45
Figure 24. Power output of the CFB reference plant with after ramping rates of different magnitudes with turbine-following (TF) and boiler-following (BF) control structures in place..... 46
Figure 25. Pressure of the live steam prior to the steam control valve for the ramping rates and control structures tested. 46
Figure 26. Simulated responses of the electrical power output and DH production for different bypass flows when the valve is open and closed..... 47
Figure 27. Net electrical production *(per year)* of the charging and discharging sides, energy efficiency ($\eta_{t,el}$) and dispatchability ratio (r_{disp}) for each of the processes assessed. S 48
Figure 28. Disclosure of the total investments (in M$), total costs (distribution between OPEX and CAPEX) and BESP of the four solar-charged FB plants assessed.. 50
Figure 29. Dispatchability ratios and energy efficiencies (electricity-to-heat, η_t) of the electricity-charged FB plant layouts with low and high temperature electrolyzers. Source: **Paper VII** 51
Figure 30. Resulting sizes of the reduced material stored (in tonnes) and equivalent volumes in order to store electricity for the objective time periods under the nine cases investigated..... 52
Figure 31. Capacities of the charging reactor, i.e., F_{ch} (in kg/s of solid material) and electrolyzers (in MW) for the nine cases investigated. 53

Figure 32. Disclosure of the total investments (in M$), total costs (distribution between OPEX and CAPEX) and BHSP of the electricity-charged FB plants for the three different electricity mixes considered.....54
Figure 33. Stabilization times of the reference CFB plant after the addition of a FB gasifier.....62
Figure 34. Economic performance the *CaL-TCES-CCS* process layout expressed as a capture cost. 63
Figure 35. Schematic of an electricity-fed FB plant layout with on-demand production of H_2.....64

List of tables

Table 1. Variation challenges in the grid for different timescales.....8
Table 2. Design data of the reference CFB plant. 22
Table 3. Design data of the reference BFB plant. 22
Table 4. Calibration factors used in each side of the dynamic model. 27
Table 5. Process variables tracked to characterize the inherent dynamics.....28
Table 6. Summary of the dynamic analysis carried out in this thesis for the fuel-fed FB plants.....31
Table 7. Summary of the VRE-fed process layouts assessed in the present work, including their charging type, chemical system, naming, input, main outcome, power block and additional product or service generated, if any.....34
Table 8. Key process sizing parameters of the solar-charged FB process layouts.....35
Table 9. Key process sizing parameters of the electricity-charged FB process layouts.....36
Table 10. Summary of the specific VRE-fed FB processes investigated in this thesis.....38
Table 11. Overview of the steady-state performance of the gas and water-steam side models on CFB and BFB configurations. The comparison with the measured values is carried out using the absolute percentage error (%).....40
Table 12. Characteristic times of the main in-furnace mechanisms of CFB and BFB furnaces. 43
Table 13. Simplified expressions for the dependency of the stabilization times (t_s) of the gas side on the characteristic times (τ) of the three in-furnace mechanisms.....44
Table 14. Summary of the inherent stabilization times of the gas and water-steam sides of the investigated fuel-fed FB plants.....55
Table 15. Estimation of the characteristic times of the in-furnace mechanisms within the different VRE-fed FB reactors evaluated in this thesis.....56
Table 16. VMS explored in this thesis together with their pros, cons, and energy system types that would benefit the most from each. 58

1. Introduction

Variable renewable energy (VRE) such as electricity from wind and solar power is experiencing a tremendous growth as a strategy to decarbonize energy systems worldwide. Due to the inherent variability of VRE sources, dispatchable power technologies such as thermal conversion will play crucial roles in balancing the grid and driving the increasing penetration of VRE in the coming decades. In this context, fluidized bed (FB) combustion plants are of particular interest owing to their abilities to convert renewable fuels efficiently, and due to their potential integration with various novel technologies (such as CO_2 capture and energy storage). Against this background, this thesis aims to elucidate the capabilities and potentials of FB plants for heat and power production in the forthcoming energy systems with high penetration levels of VRE.

1.1. Background

Anthropogenic CO_2 emissions resulting from the combustion of fossil fuels represent 65% of the total greenhouse gas emissions and are the main cause of climate change [1]. As of Year 2022, 40% of these CO_2 emissions are linked to electricity and heat generation [2], making energy supply the single-largest contributor to climate change. Thus, towards mitigating global warming, energy systems have undergone deep transformations during the past decades, and more changes are required in the upcoming years for the transition towards sustainable and net-zero emissions energy systems [3]. The main focus of these transformations is on shifting primary energy generation from fossil fuels to renewable energy sources. As of Year 2021, 17% of the global electricity and heat generation comes from renewable sources, and this share is envisioned to surge to 48% in Year 2050 [4]. In particular, variable renewable energy (VRE) sources, such as wind and solar power technologies, are experiencing dramatic growth, as they represent well-developed, low-cost alternatives for fossil fuels, not only with respect to electricity generation but also for energy in adjacent sectors, such as transportation and heavy industries [5]. Consequently, the fluctuations in net load, i.e., the demand curve after subtracting the generation from VRE sources, are expected to become larger, more frequent, and more uncertain [6]. Thus, as the penetration of VRE sources increases, there is an urgent need for strategies that ensure the balancing of demand and supply at all times. In this context, the development of energy storage technologies is especially attractive for energy systems with a large penetration of VRE, especially when it allows storage plants to output dispatchable energy at high temperatures.

Today, thermal power plants are often the most-frequently applied power generation technology covering the net load [4]. Thermal plants are typically operated as base-load units since they are characterized by high start-up costs and high minimum load. Nevertheless, in future scenarios with higher penetration of VRE (often occurring simultaneously with the decommissioning of nuclear power plants that are capable of covering base-load), several authors [7], [8] have highlighted the need for thermal plants to help balance the grid providing electricity generation when the shares of wind and sun are low. On the other hand, a large proportion of the thermal power plant fleet is currently fueled by fossil feedstock (coal and natural gas), which is disregarded in most of the future energy pathways [9] unless deployed with carbon capture and storage (CCS). Thus, when it comes to balancing the grid in future

energy systems, the need for thermal power plants that are able to convert renewable fuels with high load flexibility is envisioned.

Fluidized bed (FB) combustion plants (extensively deployed for heat and power production in various regions, such as the Nordics, Canada and China) are the technology of choice when dealing with low-grade fuels (to which the renewable solid fractions typically pertain), such as biomass and waste. However, the furnaces in FB power plants have a large inventory of solid material, which yields delayed process responses during operation, strong coupling of control parameters, and non-linear behaviors [10]. Thus, conventional operation of FB plants is characterized by smaller and slower load changes compared to other technological alternatives for solid fuel conversion, such as pulverized coal [11]. Moreover, when deployed for combined heat and power (CHP) generation, FB plants are typically dispatched following the demand for heat. This situation leads to very low utilization rates (e.g., in the case of Sweden, the capacity factor of FB-CHP plants is around 40% [12]), which makes them susceptible to decrease as biomass prices surge and, thus, alternative technologies become more competitive. Thus, FB plants operating in CHP schemes face the challenge of complementing their conventional roles as heat-following providers with new operational strategies in order to remain cost-competitive, while responding to the challenges posed by the future energy systems. In addition, a new array of roles is envisioned for FB plants in the heat and power sector, being in the spotlight of a wide range of novel applications, including: thermochemical energy storage (TCES) [13]–[15]; carbon capture processes [16]–[18]; and the generation of combustible biogas [19], [20].

In summary, owing to their fuel flexibility properties, heat and mass transfer capabilities, efficient conversion of renewable fuels, and prospective application in novel processes, FB plants for heat and power production have the potential to promote the penetration of VRE generation, thereby contributing strongly to the decarbonization of energy systems. Nevertheless, research efforts are needed to identify the opportunities and define the roles of FB plants in the future energy systems, evaluating their capabilities in terms of both flexible load operation and new applications such as TCES and poly-generation systems.

1.2. Thesis overview

1.2.1. Aim and scope

The overarching aim of this thesis is to elucidate the capabilities of FB plants for heat and power production in the forthcoming energy systems that have high penetration levels of VRE. Towards this goal, two main alternatives are explored: **i)** a technical assessment of the capabilities in terms of dynamic operation as **fuel-fed** plants; and **ii)** a techno-economic assessment of the potential for conversion into decarbonized plants, i.e., **VRE-fed** layouts. The scope of this work includes: both the reactor and plant levels; commercial-scale (50–500 MW_{th} input); and bubbling and circulating fluidized bed plants (BFB and CFB, respectively). With regards to the inputs, woody biomass is considered in the fuel-fed case, and high-temperature heat (e.g., concentrated solar) and electricity are considered for the VRE-fed case.

The specific research questions of the present thesis are:

1. What are the mechanisms governing the dynamics of the gas side of fuel-fed FB plants and what are their characteristic times in comparison to those of the water-steam side?
2. Can control and operational strategies enable faster load-changing capabilities than those required today in fuel-fed FB plants?
3. Which FB-based process layouts can offer large-scale energy storage to the system?
4. What are the technical and economic performances of the layouts formulated in 3) and how do they depend on the characteristics of the energy systems in which they are deployed?

1.2.2. Contributions

While fulfilling the aim and the research questions listed above, this thesis provides new insights into the fields of fluidization, process systems engineering, thermal power plant flexibility and thermochemical energy storage. The main scientific contributions of this thesis can be summarized as follows:

- Increased knowledge on the description of the dynamics of fuel-fed BFB and CFB plants, including model validation at steady-state (at different load levels) and transient conditions against operational datasets acquired from commercial-scale plants.
- Improved understanding of both the gas side and the water-steam side of large-scale FB plants when dealing with a wide range of fast load changes, both controlled and uncontrolled.
- Characterization of the process dynamics within the furnace as a function of the key in-furnace mechanisms, namely heat transfer, fluid dynamics and fuel conversion. General expressions as a function of these three mechanisms have been formulated, to allow predictions regarding the stabilization times of gas-side variables both for BFB and CFB combustors.
- Formulation, assessment, and comparison of large-scale TCES process layouts for the main solids systems considered to date (metal carbonates, and both thermally and chemically reduced metal oxides) including the evaluation of several process alternatives for each system.

1.2.3. Limitations

The methodology used in this thesis does not account for the lifetimes of process components nor modeling of the energy system. Accounting for these aspects is mandatory for more refined analyses intended for investment decision-making.

In the analysis of VRE-fed layouts, this thesis excludes the design and assessment at the component level, focusing instead on the process level. Thus, component-level concerns, such as the energy supply to charging (endothermic) reactors or the design and performances of solids-solids heat exchangers, are not studied, despite their impacts on process performance. Further, the plants are assumed to be charged and discharged instantaneously (or at the rate required by the system). The validity of this assumption is discussed in Section 5.1.

1.2.4. Outline

This thesis consists of the present summary and seven appended papers (**Papers I–VII**). The summary comprises seven chapters that cover the key outcomes of the appended papers. After the introductory **Chapter 1**, **Chapter 2** presents the technical background of the work by reviewing the characteristics of future energy systems, the FB technology for thermochemical conversion of solid fuels, and the state of the art with regards to solids looping processes. **Chapter 3** gives an overview of the research methods applied, namely dynamic process modeling and techno-economic process modeling. Selected findings from the appended papers are described in **Chapter 4** and discussed in **Chapter 5**, together with their implications for net-zero energy systems. **Chapter 6** provides the summary and conclusions of the thesis, and additional reflections about further work are presented in **Chapter 7**.

Figure 1 displays a schematic visualization of the content of the thesis and the linkages between the appended papers. First, the capabilities in terms of dynamic operation of large-scale FB combustion plants are investigated through the development and utilization of a dynamic process model in **Papers I–IV**. Subsequently, the potentials for FB plants to operate and be deployed as VRE-fed plants for heat and power production (providing energy storage to the grid) are explored from the techno-economic perspective in **Papers V–VII**. A more detailed description of the topics covered by each of the appended papers is given below.

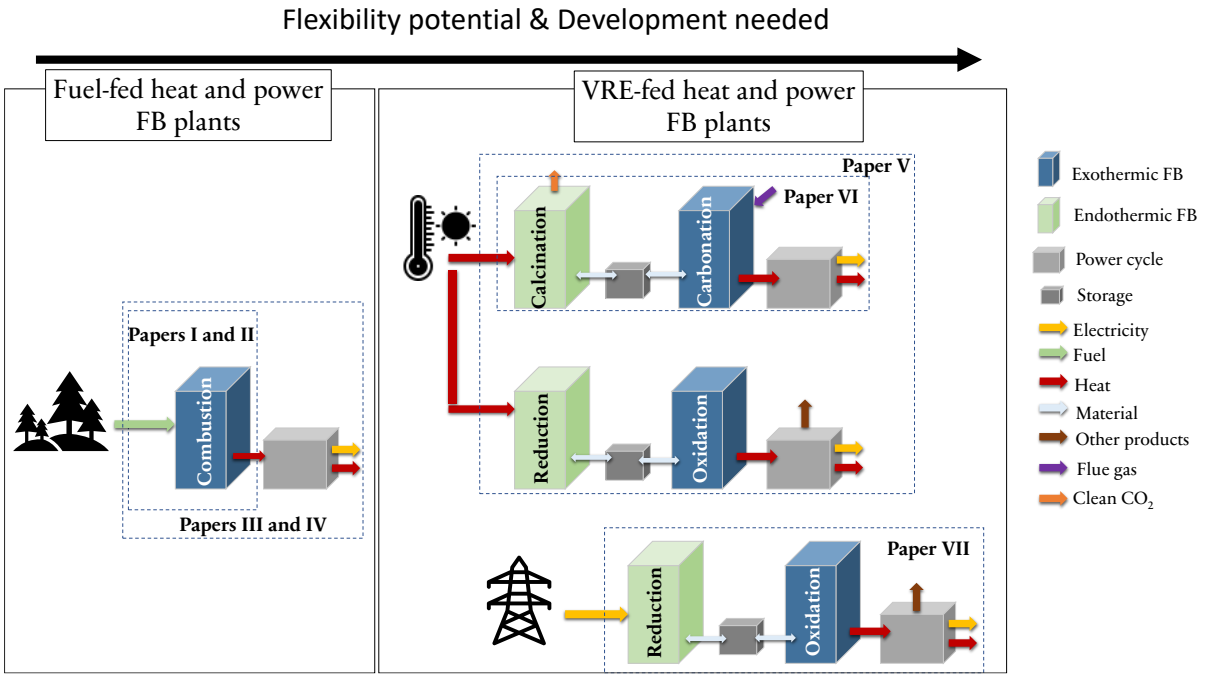

Figure 1. Overview of the investigated FB processes and layouts and their relationships to the papers included in this thesis. The processes are sorted from left to right by means of flexibility potential and development needed.

Paper I presents the formulation, calibration and validation of a dynamic model of the gas side of large-scale BFB and CFB combustors. Thereafter, the model is used to assess the part-load performances of the two reference units (a 100 MW_{th} CFB and a 140 MW_{th} BFB), as well as to study the resulting inherent timescales after changes in load and fuel composition.

Paper II utilizes the model presented in **Paper I** to compare the transient performances of BFB and CFB combustors. In addition, the paper characterizes the stabilization times of the main

variables (such as temperatures and heat extraction) as a function of the characteristic times of the dominant in-furnace mechanisms (fluid dynamics, heat transfer and fuel conversion).

Paper III and **Paper IV** expand the analysis to the plant level, i.e., including the dynamics of both the gas and water-steam sides of a CFB and BFB plant, respectively. For this purpose, the model presented in **Paper I** is integrated into a dynamic process model of the water-steam side. The resulting integrated plant model is validated against steady-state and transient operational data acquired from two reference plants. Several control and operational strategies are simulated to assess the capabilities of large-scale CFB and BFB plants to provide load changes at different ramp rates.

Paper V describes a techno-economic evaluation of the main solids-gas systems for large-scale thermochemical energy storage (TCES). Assuming a renewable input of intermittent and high-temperature heat, six different process layouts are formulated based on state-of-the-art research studies of solids looping cycles for both carbonates and metals. The technical performances of the processes are assessed through computations of mass, energy and exergy balances, and the economic feasibility of each process is evaluated according to the breakeven electricity selling price (BESP).

Paper VI explores in detail the techno-economics of calcium looping for energy storage (one of the options considered in **Paper V**), as it allows FB plants to add carbon capture to their services portfolio. The layout is designed for the storage of high-temperature, non-dispatchable heat, in scenarios where a CO_2-containing flue gas is available nearby.

Paper VII evaluates the potential of FB plants to be deployed with TCES, using electricity as the energy input. This case is highly relevant for countries that have a large penetration of VRE-based electricity and an existing fleet of FB plants. Thus, a Swedish case study is used to assess the proposed scheme. Mass and energy balances are solved at the plant level, and the technical and logistical implications at a national level are discussed, together with additional implementation alternatives.

2. Technical background

The achievement of net-zero emissions energy systems will rely, *inter alla*, on VRE generation, mechanisms to balance differences in the energy supply and demand, and carbon capture and storage. FB plants for heat and power production have the potential to contribute to these requirements, through i) load-following operation and/or ii) moving away from carbonaceous fuels and providing thermochemical energy storage.

This chapter covers the technical background required to understand the formulation of models as well as the relevance of the results and discussion of this thesis. For this, Figure 2 displays the key aspects included in this chapter and their connection with the capabilities of FB plants in future energy systems. The chapter provides overviews of: Section 2.1), the characteristics of the future energy systems with high levels of VRE; Section 2.2, the FB technology for the conversion of solid fuels and its operational patterns; and Section 2.3, the different solids looping cycles for energy applications that exploit the FB technology.

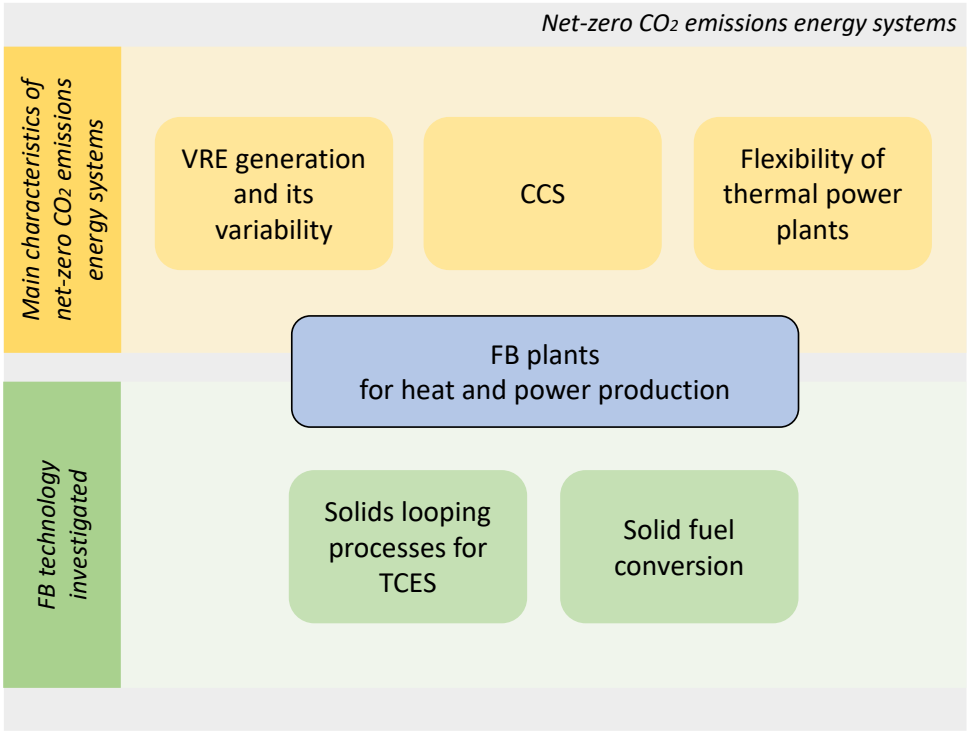

Figure 2. Overview of the topics covered in this section and their relationship with this thesis.

2.1. Characteristics of future energy systems

In order to meet climate targets, energy systems are required to transform into net-zero emissions carbon systems later in this century [1], i.e., such that there will be net addition of CO_2 to the atmosphere. While decarbonization of some services (such as heating and cooling, among others) may be relatively easy to achieve through electrification (especially in regions such as the Nordic countries due to the rapid progress of wind power), in some other sectors (e.g., aviation and other long-distance transport and industries) elimination of emissions is more challenging. Thus, the achievement of net-zero emissions energy systems will involve

combinations of different existing and under-development technologies that vary between sectors, as well as a coordinated integration across these sectors [21]. While many technological pathways exist, the typically recognized elements of net-zero energy systems include: availability of vast amounts of inexpensive, emissions-free electricity; mechanisms to balance time-variable differences (often uncertain) between electricity supply and demand; and mechanisms for carbon capture and storage (CCS). The following subsections review the elements of net-zero emissions energy systems that are of key importance in this thesis.

2.1.1. VRE generation and variability

Generation of electricity through VRE technologies, namely wind turbines and solar photovoltaic, has an associated inherent variability, as it is subject to wind speeds and solar irradiation levels. Oppositely, the energy demand follows a regular pattern over time, linked to human activity. The resulting net load curve when the shares of VRE in the system are large is highly variable, which translates into a greater need for flexibility, to be covered by the remainder of the electricity generators in the system. The needs for balancing supply and demand range across different timescales (see example of the main challenges in Table 1), as the variations presented by solar and wind electricity production units are inherently different. On the one hand, energy systems dominated by solar power exhibit mainly day-night and seasonal variations (and to a lesser extent, variations that extend over a few days in cloudy regions) [22]. On the other hand, the variations seen in wind-dominated energy systems expand from the hourly to the weekly scale, as well as between seasons. In addition to the variations on the hours-to-weeks scale that are linked to the availability of power generation, there are additional challenges to be solved at shorter timescales (from ms to min) in relation to grid stability, i.e., voltage and frequency control [8].

Table 1. Variation challenges in the grid for different timescales.

Timescale	Variations
Milliseconds	Inertia
Seconds	Frequency control
Minutes	Voltage control
Hours	Energy availability (solar)
Weeks	Energy availability (wind)
Seasons	Energy availability

Thus, the penetration of VRE creates an opportunity for strategies capable of shifting in time large amounts of energy across different timescales, which are sometimes referred to as variation management strategies (VMS). According to Göransson and Johnsson [23], VMS can be divided into three groups that differ with respect to the ways in which they balance a varying supply and demand (note that alternative ways to divide them exist, see e.g., [24]):

- **Shifting strategies**. Strategies that store energy for later use, i.e., shifting it in time.
- **Absorbing strategies.** Strategies that utilize excess electricity generation when required to convert it into another energy form or carrier.
- **Complementing strategies.** Strategies that can generate dispatchable energy to complement VRE when needed.

As these three types of VMS fulfill different needs with different cost structures, energy systems benefit from combining several VMS so as to increase the penetration of VRE [25]. The present thesis investigates the opportunities of FB plants to contribute as shifting (**Papers V-VII**), absorbing (**Paper VII**) and complementing (**Papers I-IV**) strategies through different layouts and operating regimes.

2.1.2. Flexibility of thermal power plants

Several studies have highlighted the flexible use of thermal power as a complementing VMS able to provide services in the minute-hour timescale [8], [26]. Thus, as the shares of VRE in the energy system increase, thermal power plants are required to modify their conventional operational patterns (from base-load to load-following) in order to remain competitive. Consequently, several studies exploring the flexibility properties of both conventional and innovative thermal technologies have been published in the last few years, mostly focusing on gas- and coal-fired plants (see e.g., [7], [27]). Nevertheless, the term *flexibility* becomes vague as it may refer to various aspects. To clarify this issue, a recent work by Beiron [28] defined the following categories of the flexibility at the plant level:

Operational flexibility. Defined as the ability to change the production level, i.e., load. Operational flexibility is the most intensively investigated flexibility type in thermal power plants, especially for condensing plants (i.e., producing electricity as single output). Operational flexibility includes the following key aspects [29]:

- Cycling capabilities: increasing the speed of load ramping and start-up/shutdown allows the plant to provide a wider range of power services and act as a complementing VMS in shorter timescales.
- Part-load efficiency: as thermal power plants are displaced in the merit order owing to the penetration of VRE, part-load operation becomes more frequent and it lasts for longer periods. Thus, off-design performance becomes crucial from both the economic and environmental perspectives.
- Operational boundaries: refers to the overload capacity (e.g., 105% - 110% load as compared to the design values) and the minimum load. The former allows the plant to deliver excess output at times when additional output generation is beneficial (i.e., expanding the plant capabilities as complementing VMS). The latter, offers the possibility to reduce the production level when desired while avoiding the costs associated with start-up/shutdown procedures.

Product flexibility. This relates to the ability to change the production level by manipulating the product ratios, regardless of whether this involves a change in boiler load. Thus, product flexibility is strictly linked to the production of two or more outputs, which means that it has been explored much less extensively. In CHP schemes, product flexibility typically refers to the ability to adjust the power-to-heat ratio (see [30] and [31]) although it can also include the provision of ancillary services (e.g., frequency control or congestion management) [32]. As the thermal plants incorporate new products such as biofuel production [33] or carbon capture services [34], the product flexibility gains additional complexity and importance. In contrast to the operational flexibility defined above, product flexibility is independent of time, i.e., it is a steady-state characteristic.

Load shifting flexibility. This refers to the capability to shift production in time, i.e., it is only possible when energy storage is available at the plant. In thermal power plants, load shifting is essentially reduced to the presence of a thermal energy storage (TES), which enables the decoupling of the boiler load from production of heat [35], [36].

As suggested and reviewed by several authors (e.g., [37], [38]), dynamic modeling and simulation is the preferred choice for investigating operational flexibility. This thesis explores the operational (**Papers I-VII)** and product flexibilities **(Papers III** and **IV)** of fuel-fed FB plants using a dynamic model that is parametrized and calibrated/validated using design and operational data collected from two commercial plants. In addition, the product flexibility and load-shifting capabilities of VRE-fed FB plants are explored in **Papers V-VII** by evaluating their techno-economic feasibility**.**

It is important to mention that the control system of a thermal power plant regulates and coordinates all the involved subsystems, so as to fulfil a certain operational objective while ensuring safe operation [39],[40]. The control structure and objectives of a given plant largely reflect on economic considerations. Thus, the control solutions currently deployed in industry are often based on traditional practices and are not necessarily optimized for fast load changing or maximal plant efficiency. However, as the need for flexibility increases, the effective design, tuning and deployment of advanced control strategies gain relevance as tools to increase the operational and production efficiencies of the plant, thereby avoiding expensive retrofits [41]. This thesis (**Papers III and IV**) investigates the use of control strategies as a way to enhance the operational and product flexibilities of fuel-fed FB plants.

2.1.3. Carbon capture and storage

While decarbonizing the generation of electricity and heat is today a realistically achievable goal thanks to the cost reductions of VRE, other emitting industries need to undergo profound transformations in order to comply with the net-zero emissions pledges. In fact, direct industrial emissions account for 26% of the global CO_2 emissions [4], so reducing their levels is crucial for achieving net-zero emissions systems. A way to reduce these carbon emissions is via carbon capture and storage (CCS), a group of technologies that capture and permanently store CO_2 that would otherwise have been emitted to the atmosphere. That CCS is as a necessary mechanism in most pathways directed towards limiting global warming has been highlighted for several years [42] owing to its capability to reduce emissions at-scale [43]. While there are several types of CCS technologies (typically grouped as post-combustion, pre-combustion and oxy-combustion), post-combustion CCS (i.e., separation of CO_2 from a process gas or flue gas) and in particular amine separation is especially attractive as it theoretically offers the possibility to be coupled to any point source of CO_2 while the source remains unaltered [43]. Typical disadvantages of post-combustion CCS (as compared to pre-combustion and oxy-combustion CCS) are: more space-intensive and larger associated operating costs [44].

The number of planned CCS projects has experienced a noticeable surge within the past years due to the raised public awareness concerning climate change and the increased political will, among other factors [45]. Nevertheless, the IEA has emphasized [2] that even if all the projected large-scale CCS units are realized, the amount of CO_2 captured would still be well below the 1600 Mt/yr expected by the scenarios that reach the climate goals [9]. Among the reasons for the relatively slow development of CCS, two are critical in the context of this thesis:

i) the large investment and operational costs associated with the technology, which hinder the economic feasibility of CCS projects; and ii) the lack of cross-sectorial collaborations that would reduce the financial risk for each actor.

The present thesis (**Papers V** and **VI**) explores the techno-economic potentials of the FB plants that could be utilized as CO_2 capture facilities to offer capture services to nearby emitters, while simultaneously providing VMS services to the energy system.

2.2. Fluidized bed plants for solid fuel conversion

A gas-solids FB consists of a vessel in which a bed of bulk solid particles (referred to as bed material) adopts a fluid-like behavior when a gas is injected from the bottom of the vessel. Fluidized beds are known to exhibit strong mass and heat transfer due to the relatively high mixing rates of both the solid phase and gas phase [46]. Thus, FBs are typically used in applications where the heat and mass transfer are to be maximized, such as separation, coating and gas-solid chemical reactions. Originally patented in the 1920s for the gasification of coal [47], the thermochemical conversion of solid fuels (mainly combustion but including also gasification and pyrolysis) remains as the major application of gas-solids FB reactors [48]. Among the characteristics of FB combustion (FBC) plants, the thermal capacity associated with the large mass of bulk solids is especially advantageous as it yields relatively homogeneous furnace temperatures, which are linked to higher efficiency and lower emissions. These features make FB reactors especially attractive for the thermochemical conversion of low-grade solid fuels [49] to which renewable fuels typically pertain, i.e., biomass and renewable waste fractions. In addition, FBCs enable the in-bed capture of CO_2 through the use of sorbents as the bed material, and allow the efficient handling of different fuel types and even mixtures thereof [50].

Within an FB reactor, different zones can be defined based on their fluid-dynamic characteristics. A general distinction is made between the dense bed, which is located at the bottom of the reactor and is characterized by a high concentration of solids, and the freeboard, which is located immediately above the dense bed. In the freeboard, a splash zone characterized by a sharp decrease in solids concentration with height is established due to the backmixing of the solids ejected from bubbles erupting at the dense bed surface. While this summarizes the picture for the simpler type of reactors (i.e., BFB, depicted in Figure 3a), in CFB units a combination of higher gas velocities and finer solids yields entrainment of solids above the splash zone (in the so-called transport zone) and the establishment of a significant solids flow also at locations higher up in the furnace (see Figure 3b). This disperse solids flow backmixes gradually to the furnace walls and, eventually, a minor share of the solids is recirculated externally to the furnace after being separated from the gas in a cyclone. In FB boilers, heat is extracted from the furnace via a working fluid (typically water) through membrane tube walls, as well as from the convective flue gas path, where economizers and superheaters are located (see Figure 3). In CFB units, which typically have larger thermal capacities and sizes, there are usually additional heat transfer surfaces in the furnace, cyclone and/or loop seal, in order to keep an operational temperature in the furnace temperature at around 850°C.

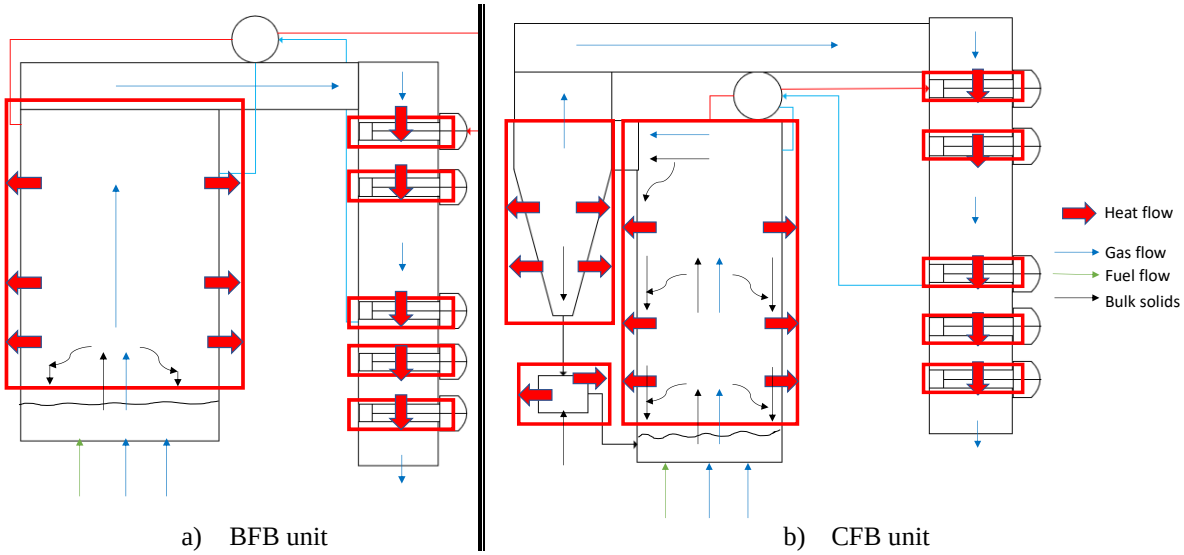

Figure 3. Schematic side views of the two types of FB furnaces for heat and power production.

At present, large-scale FBC plants are typically deployed with a water-steam circuit (Rankine cycle) to produce electricity, heat, or a combination of these (CHP) (see Figure 4). In the first case, CFB units are the preferred option as they offer a higher power output per specific cross-sectional area (in the range of 4-5 MW/m^2). Due to the larger investment cost associated with CFB configurations, FB units for electricity production are typically coal-fed units with sizes in the range of 100-500 MW_{el}. In addition, due to the low volatile content of coal the combustion of char is the principal chemical reaction. Thus, distributing the combustion throughout the furnace (as it is the case in CFB units) is beneficial for a homogeneous temperature distribution. In contrast, BFB units are characterized by lower investment costs and lower specific capacities (around 1 MW/m^2). Thus, BFB plants are the preferred alternative for converting locally collected fuels such as biomass and waste, and are typically linked to the production of heat or CHP in plants of sizes that range from 30 to 150 MW_{th}. Furthermore, biomass and waste fuels have high content of volatiles, which causes the combustion to be distributed throughout the furnace without the need for solids circulation. This thesis utilizes two commercial-scale FB plants to investigate the operational flexibility of fuel-fed FB plants (a 100 MW_{th} CFB plant is used in **Papers I-III** and a 140 MW_{th} BFB plant is used in **Papers I, II** and **IV**). Both plants are operated with biomass as fuel and are deployed as CHP plants.

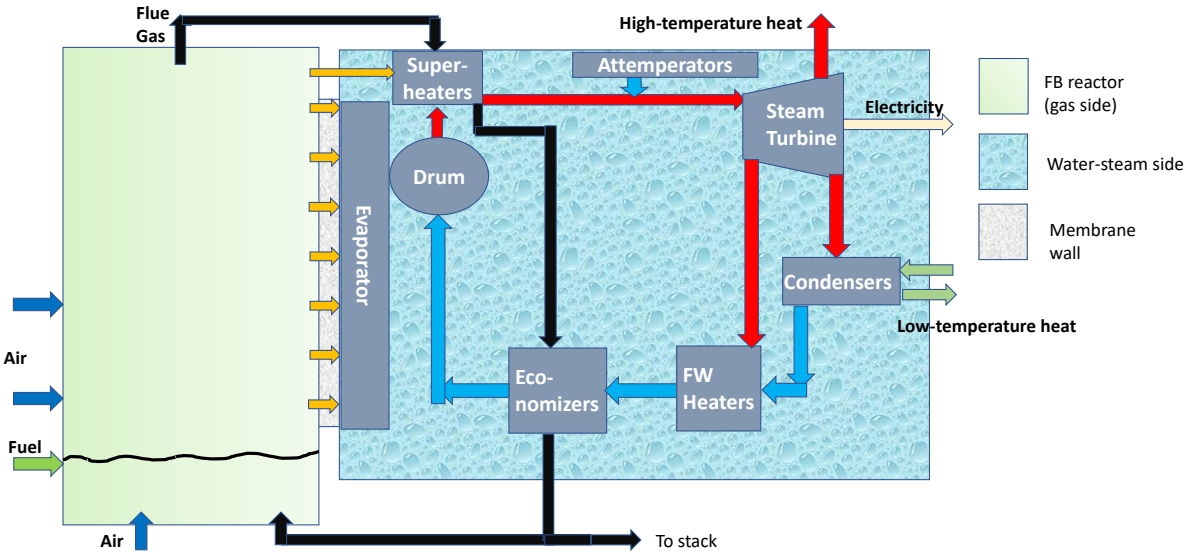

Figure 4. Schematic of a fuel-fed FB plant for heat and power production including both the reactor (gas side) and Rankine cycle equipment (water-steam side). Source: **Paper IV.**

Applications of FB conversion other than combustion (namely biomass gasification) via the double fluidized bed (DFB) setup have experienced a surge in research and development during the last two decades with the aim to develop net-zero emissions energy systems (see Section 2.1). Gasification involves the thermal decomposition of a solid fuel into gaseous products such as CO, H2 and CO_2, and an autothermal layout is preferred for industrial operation. In DFB gasifiers (schematic depicted in Figure 5), the heat required by the endothermic gasification reactor is generated in the combustor and transferred in the form of hot sand [51]. This type of unit offers a large degree of flexibility as in theory it can be operated in two ways [52]: i) maximizing heat and power production (in the combustion chamber) with combustible gas as a side revenue, or ii) as a biogas production facility with the combustor producing the exact amount of heat than required by the gasifier.

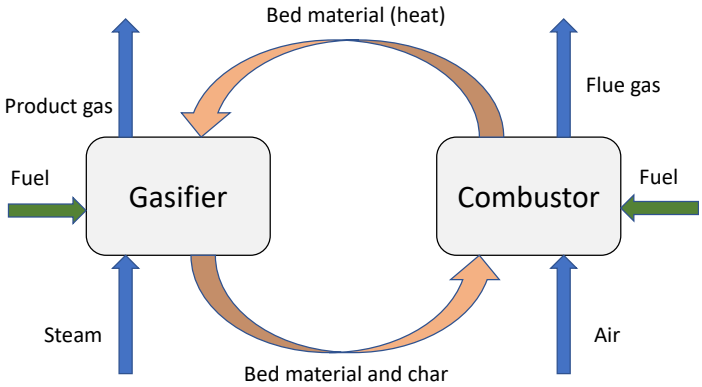

Figure 5. Schematic of a DFB steam gasifier.

2.2.1. Dynamic modeling of FBC plants

In the two most commonly used FBC setups presented above (i.e., larger CFB units for electricity production and smaller BFB plants for heat or CHP generation), the operation is governed by slow and small load changes. This is because the plants are: i) dispatched based on the electricity generation typically covering base-load production, ii) governed by the generation of district heating following weather patterns and iii) governed by the generation of industrial heat following the industrial operational patterns. Thus, modeling-based investigations of FB furnaces and plants have traditionally focused on steady-state operation (see [53] for a review on steady-state FBC modeling) as a way to improve knowledge regarding the design and the efficient and clean operation of FB plants. As a result, the limits related to the transient capabilities of FB plants (linked to the operational flexibility described in Section 2.1.1) remain largely unexplored. Indeed, the importance of mastering the dynamic operation of FBC plants has been highlighted by several authors [54], [55].

Dynamic process modeling is gaining attention as a tool that can provide insights into the transient behaviors of power plants, as it allows operators and plant owners to evaluate various operational and control strategies that can lead to increased profits in the present and future energy markets [56], [37]. However, different type of models exists with different reliability and applicability levels. While unit-specific models for conventional operation of existing furnaces and plants can be developed based on correlations derived from site measurements, general model formulations with a more solid theoretical ground are needed to study unit designs, sizes and operations outside the scope covered by site measurements. In particular for FB combustors, low-order models represent an optimal trade-off between accuracy, generic applicability, and low computational cost to be integrated into dynamic process models [20]. Particularly attractive are the so called semiempirical models, i.e., models that make use of empirical expressions (normally related to the fluid dynamics of solids and gas phases) together with first principle equations [57].

Over the last decade, extensive research studies have been published regarding the dynamic modeling of power cycles, such as Rankine cycles for coal-fired power plants [35],[58], combined-cycle plants [59], [60], waste-fired units [61], [62], nuclear plants [63], and concentrated solar power [64]. Nevertheless, one of the aspects that most of these investigations share is the assumption that the gas side of the boiler (in-furnace side) has a much faster response to operational variations than the water-steam side, and so its dynamics can be neglected. Although the validity of this assumption has been proven for gas-fired combustion [65], [66], it has not been explored for FBC plants.

When it comes to modeling the dynamics of the in-furnace of FB boilers, most of the available literature has focused on CFB units. Several 0D models [67]–[69] have been presented and used in the literature, although they are not capable of describing the special distribution of the solids throughout the furnace, which is a crucial aspect of CFB operation. One of the first 1D dynamic models published was that of Park and Basu [70]: a mathematical representation of a 0.3 MW furnace that was capable of predicting the transients of char and O_2 concentrations. A 1D model was presented by Majanne and Köykkä [71], in which an evaporator model was linked to the in-furnace side, allowing simulations of the steam pressure and mass flow after a change in fuel moisture, with stabilization times of the water/steam side in the order of 10 minutes. Recently, Deng et al. [72] have modeled the 1D dynamic behavior of the solids flow of a 350 MW unit, observing abrupt transients when increasing the gas velocity. More detailed

models include the internal recirculation of solids through the wall layer. The 1D models that include this feature are typically called 1.5D models. Among these, the model presented by Chen et al. [73] of a 410 t/h coal-fired unit stands out as having being validated with operational data from an industrial site. After presenting and validating the model, the work focused on the qualitative analysis of the trajectories of the main in-furnace variables after a load change. More recently, Kim et al [74] have presented a 1.5D model of the in-furnace side of CFB units that was validated with design data from a coal-fired 795 MW plant. The model was then applied to investigate the effect of the solids flow on the transient responses of the CFB loop, revealing overshoots in the temperature responses for certain load changes. A 1.5D dynamic model presented by Ritvanen et al. [75] and based on a previous publication [76] has been widely used for simulation and control studies [77]–[79]. Haus et al. [80] have presented a dynamic model of the in-furnace side of interconnected FB reactors with the focus on chemical looping combustion. That model was successfully validated against tests conducted in an experimental facility. Lastly, it is important to mention that some other groups have developed dynamic models of the in-furnace side as a way to design and test control strategies (see for instance [81]), where the high level of interaction between variables was highlighted.

Regarding the in-furnace side of BFB units, Kataja et al. [82] have presented a 1D model connected to a model of the steam drum and evaporator, and used this to simulate the boiler responses after a step-change in fuel flow. A detailed model has been described by Selcuk [83], who have presented a validation of the model with steady-state and transient data obtained from a 0.3 MW unit. This model was subsequently used to investigate the dynamics of the unit, identifying inverse responses in the char inventory of the dense bed after a load increase. More recently, Yasar et al. [84] have presented a transient model of BFB combustion units coupled to a 3-D radiation model, which was validated against a lignite-fired 0.3 MW unit A model of a biomass-fired BFB combustor has been developed and used by Galgano et al. [85], who uncovered substantial differences in the dynamics of the dense bed and in the freeboard caused by the differences in heat capacity between the different regions.

Other studies have investigated the transient behaviors of FBC plants by focusing on the dynamics of the water-steam side, especially in coal-fired CFB units. Hultgren et al. [86] utilized the CFB model presented previously [76] to perform a control design analysis of a coal-fired CFB plant, identifying significant interactions between the control loops, i.e. the manipulation of one input affects several outputs. Their work was further expanded upon [87] to create an integrated control process design (ICPD) to optimize the transient performance of the steam side, resulting in very good load-tracking performance during boiler-following operation. Nevertheless, the authors stated the need for a detailed mechanistic model to improve the robustness of the study. Gao et al. [10] have presented and validated a 0D model of a CFB furnace that accounts for the water-steam side tubes. Following linearization, this model was used by Zhang et al. [11] for model predictive control (MPC). The 1.5D model of the in-furnace side presented in [74] was integrated into a model of the water-steam side by [88] and utilized to quantify the responses of the steam temperature after changes in the fuel and feedwater flows. Recently, Stefanitsis et al. [78] have used the CFB model originally published in [76] to evaluate the transient performance of a boiler after implementing a thermal storage in the form of hot bulk solids, and they concluded that the stabilization time for load changes is reduced when adding the storage. In recent times, some authors have investigated the transient behaviors of waste-fueled CFB plants. Zimmerman et al. [89] have exploited a 0D model of the in-furnace side presented earlier [67] to compare different control strategies,

identifying feed-forward (FF) MPC as the optimal strategy in terms of disturbance rejection. Beiron et al. [62] have presented and validated a detailed dynamic model of the water-steam side of a waste-fired CFB unit, and have further applied the model to investigate the inherent dynamics of the process. Regarding BFB plants, it is worth mentioning the recent work of Zlatkovij et al. [68], in which a 0D dynamic model of a BFB furnace integrated into a simplified model of the water side was used to test and compare MPC strategies, concluding that FF-MPC was the preferred option.

The literature review presented in this chapter in combination with more dedicated literature reviews included in **Papers I-IV** shows that the following important items are lacking:

1. simultaneous description of the dynamics of both the gas side and the water-steam side, when assessing the transient behavior of FBC units;
2. study of the transient performances of biomass-based units for the production of CHP;
3. validation of models against steady-state and transient operational data obtained from large-scale commercial FBC plants, and
4. systematic assessment of control strategies for FBC-CHP plants.

The present thesis describes the formulation, validation and utilization (**Papers I-IV**) of a comprehensive dynamic process model of FBC plants that aims to fill the knowledge gaps identified above.

2.3. Solids looping processes for TCES

Given their high heat and mass transfer capabilities described in Section 2.2, FB reactors are often the preferred option for other novel solid-gas processes with energy applications [90]. In particular, the so-called looping processes offer a wide range of possibilities for the fields of clean combustion, energy storage and carbon capture. In this section the concept of solids looping for TCES using FB reactors is presented.

The general concept underlying the solids-gas looping process for TCES is the cyclic endothermic-exothermic reaction of a solid material in two different reactors according to the general scheme depicted in Figure 6. Note that the endothermic reaction is driven by renewable thermal energy that can be provided by several mechanisms (directly irradiated reactors [91] or oxy-combusted green H_2 [92], among others). The reaction product can be stored at ambient temperature and for long periods of time, which facilitates transportation of the material in which the energy is stored, if desired. The stored energy is subsequently discharged by promoting the reverse exothermic reaction. The kinetics and thermodynamics of the discharging reaction determine the temperature and reaction conditions required for each of the two steps (the heat absorption and the heat released), thereby dictating whether the energy released can be transformed into electricity making use of regular power cycles [15].

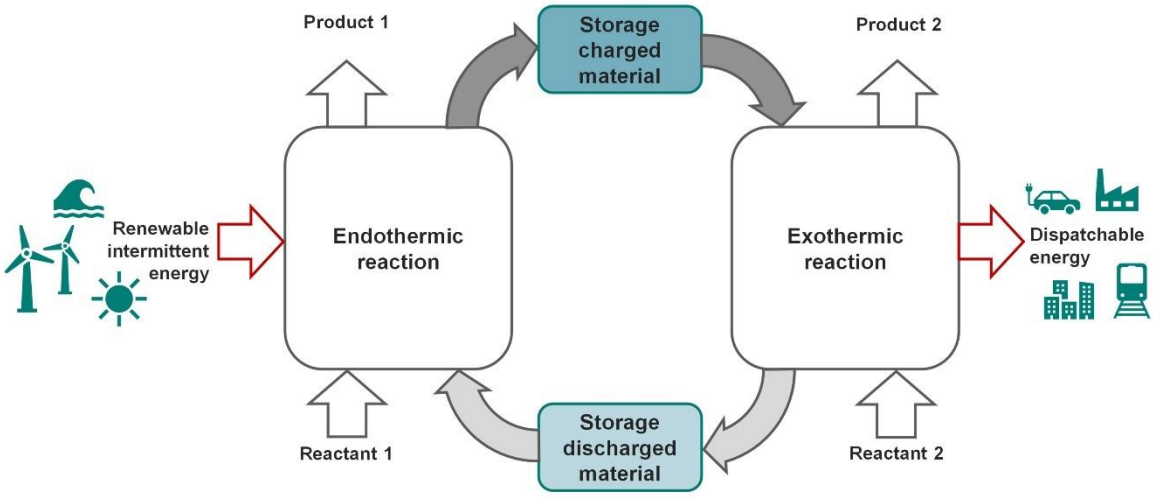

Figure 6. General scheme for thermochemical energy storage. The endothermic reaction is charged using renewable intermittent energy. The stored energy is released by promoting the reverse (exothermic) reaction and the product is stored back for charging.

For a chemical system to be suitable for the TCES scheme, it must be reversible and entail a considerable enthalpy of reaction, among others. While many different systems could be considered [15], the ones with the strongest industrial potential are those in which the reactions occur at high temperatures and with widely available precursor materials. In this regard, the two chemical systems that are typically highlighted in literature as prime candidates for large-scale TCES and that are investigated in this thesis are the carbonation/calcination of a metal carbonate (briefly reviewed in Section 2.3.1) and the reduction/oxidation of a metal oxide (Section 2.3.2). Due to the characteristics described in Section 2.2, FB reactors are shown to be a suitable technology for large-scale implementation in terms of both reactions and heat exchange [93].

2.3.1. Carbonate looping

Carbonates have been in the spotlight of high-temperature TCES research for years due to their high volumetric energy densities (1200-3300 MJ/m^3), efficient conversion at low pressures and high temperatures, lack of toxicity and non-corrosiveness [94]. Some of the most-promising carbonates include those of Ca, Sr, Ba, Pb and Mg. Nevertheless, $CaCO_3$ is by far the most investigated system when it comes to TCES due to the good availability and low price of natural Ca-based minerals such as limestone and dolomite [93]. In addition, $CaCO_3$ calcination and carbonation reactions present very high reversibility and fast kinetics [95]. The reversible calcination/carbonation reaction of the CaO/$CaCO_3$ system is shown in Equation 1.

$$CaCO_3(s) \leftrightarrow CaO(s) + CO_2(g) \quad \Delta H_R > 0 \tag{1}$$

Note that since the carbonation step requires a stream of CO_2, the calcium looping process has long been researched as a post-combustion carbon capture technology [96]. By introducing a flue gas into the combustion reactor, the CaO reacts with the CO_2 present in the flue gas (with typically 10%-15% CO_2 content). The absorbed CO_2 is subsequently released in the calcination reactor.

In recent years, research on $CaCO_3$ for TCES has focused on increasing the dispatchability of high-temperature solar power plants, such as concentrated solar power (CSP) plants. For such

process setup, the performance and optimal conditions have been identified and tested in numerous studies (see [95] and references therein). The calcium looping process for TCES is still at pilot and demonstration scales, and upscaling possibilities depend on problems related to the deactivation and agglomeration of the material after multiple cycles [97]. Possible suggested solutions involve hydration during or after calcination, as well as by the addition of stabilizing particles that lead to synthetic sorbents (see e.g., [98]).

2.3.2. Redox looping

Several metal oxides have been investigated for TCES applications during the last decades [99] owing to their high energy storage densities (700-3000 MJ/m^3), generally high operating temperatures (although they range from 200°C to 1,700°C), and low environmental impacts. In addition, the literature regarding these systems is abundant, as they have already been extensively investigated as oxygen carriers for multiple high-temperature applications such as chemical looping combustion (CLC) [100], H_2 production via water splitting [101] and syngas production through CO_2 splitting [102]. The general reaction form of thermally and chemically reduced metal oxides is described by Equation 2 and 3 respectively (note that the scheme depicted in Equation 3 can be endothermic or exothermic depending on the system and agent chosen):

$$M_xO_y(s) \leftrightarrow M_xO_{y-1}(s) + {}^1/_2\, O_2(g) \qquad \Delta H_R > 0 \tag{2}$$

$$M_xO_y(s) + A \leftrightarrow M_xO_{y-1}(s) + {}^1/_2\, AO_2(g) \qquad \Delta H_R \lesseqgtr 0 \tag{3}$$

Metal oxides can undergo thermal and chemical reduction at different temperature levels. Metal oxides that can be thermally reduced at temperatures <1100°C have traditionally been the preferred option for TCES systems. Yet, chemically reduced metal oxides have recently been gaining attention as the development of electrolyzers has advanced, allowing the use of electricity to generate a chemical reduction agent (typically H_2) that can lower the temperature required for the reduction step [93], [103].

Among the most-attractive thermally reduced oxides, systems based on Co, Mn, Ba and Cu have been highlighted as potential candidates by several researchers [104], [105] owing to their very high energy densities (up to ~980 kJ/kg) and good kinetics and reversibility. Regarding the chemically reduced alternatives, most of the focus has been on Fe-based materials due to their good availability and the large body of research that exists on chemical looping combustion systems [93]. Mixed metal oxide systems such as (Co,Ni)Fe_2O_4 [106] are often considered as a way to enhance the properties of pure metal systems, given that the addition of a secondary oxide increases the concentration of anion vacancies and enhances the mass transfer, thereby improving the long-term redox performances of the materials [94]. The disadvantages of metal oxide systems for TCES applications differ according to the system considered, with high material costs and sintering often being problematic.

Although many investigations have been carried out on the theoretical use of TCES, the literature is deficient when it comes to connecting the chemical behavior with large-scale process feasibility. This thesis (**Papers V-VII**) proposes large-scale layouts based on the FB technology and assesses the techno-economic performances of the most-promising high-temperature solid-gas systems for TCES.

3. Methods

Two main methods are used to investigate the capabilities of FB plants for heat and power production in future energy systems: dynamic reactor and process modeling; and techno-economic process modeling. Dynamic process modeling is used to simulate the load-changing capabilities of commercial-scale FB plants. For this purpose, design and operational data for two reference plants (a CFB and a BFB biomass-fired boilers) are acquired and used as inputs to the dynamic models at reactor and plant levels. The models are then calibrated and validated, and later used to gain insights into the plant dynamics.

Techno-economic process modeling in turn is used to carry out a preliminary assessment of low-technology readiness level (TRL) process configurations, i.e., VRE-fed layouts with energy storage. Chemical and reaction data from the literature are used to formulate process layouts, for which the energy and mass balances (steady-state process modeling) are solved. The results are used to estimate the plant costs, thereby enabling technical and economic assessments of each layout. The specific cases investigated include solar-charged and electricity-charged FB plants.

This chapter provides an overview of the different methods developed and applied in this work to address the aim and objectives introduced in Chapter 1. This thesis is based on the process modeling and simulation of different configurations of FB plants for heat and power production. Figure 7 presents an overview of the two main modeling techniques (dynamic process modeling and techno-economic process modeling) used in this thesis, as well as their connections to the topics of the appended papers.

Dynamic process models can describe both the steady-state behaviors at several load levels (i.e., design and off-design behaviors) as well as the transient behaviors when the operating conditions are changed. For accurate and reliable predictions of the process dynamics, dynamic modeling requires extensive design data from the process equipment as well as operational datasets for model calibration and validation. In addition, plant-specific aspects such as the regulatory and supervisory control layers are needed when modeling operation of an industrial site. Thus, the use of reference plants is mandatory for comprehensive formulation and utilization of the dynamic models. In this thesis, a reactor-level model of FB combustors resembling both the BFB and CFB layouts has been developed making use of semiempirical formulations briefly presented in Section 3.1.2 (and described in detail in **Papers I and II)**. Subsequently, the reactor model was expanded to the plant level by connecting it to a process model of the water-steam side that was built upon model components from the Thermal Power library from Modelon [107]. Note that this was done for two reference plants: a CFB plant (**Paper III**) and a BFB plant (**Paper IV**).

Preliminary techno-economic process modeling provides an early assessment of the process performance when the analyzed process has a lower TRL, and therefore, data for large-scale facilities are not available. Techno-economic process modeling is based on steady-state process simulations and computation of the equipment sizing for a given operational point. These results are the inputs to the cost estimation, which allows comparisons of the different processes from a technical and economic feasibility perspective. In this work (**Papers V-VII**), techno-economic process modeling is applied to assess the technical and economic performances of various VRE-fed FB plants for heat and power production.

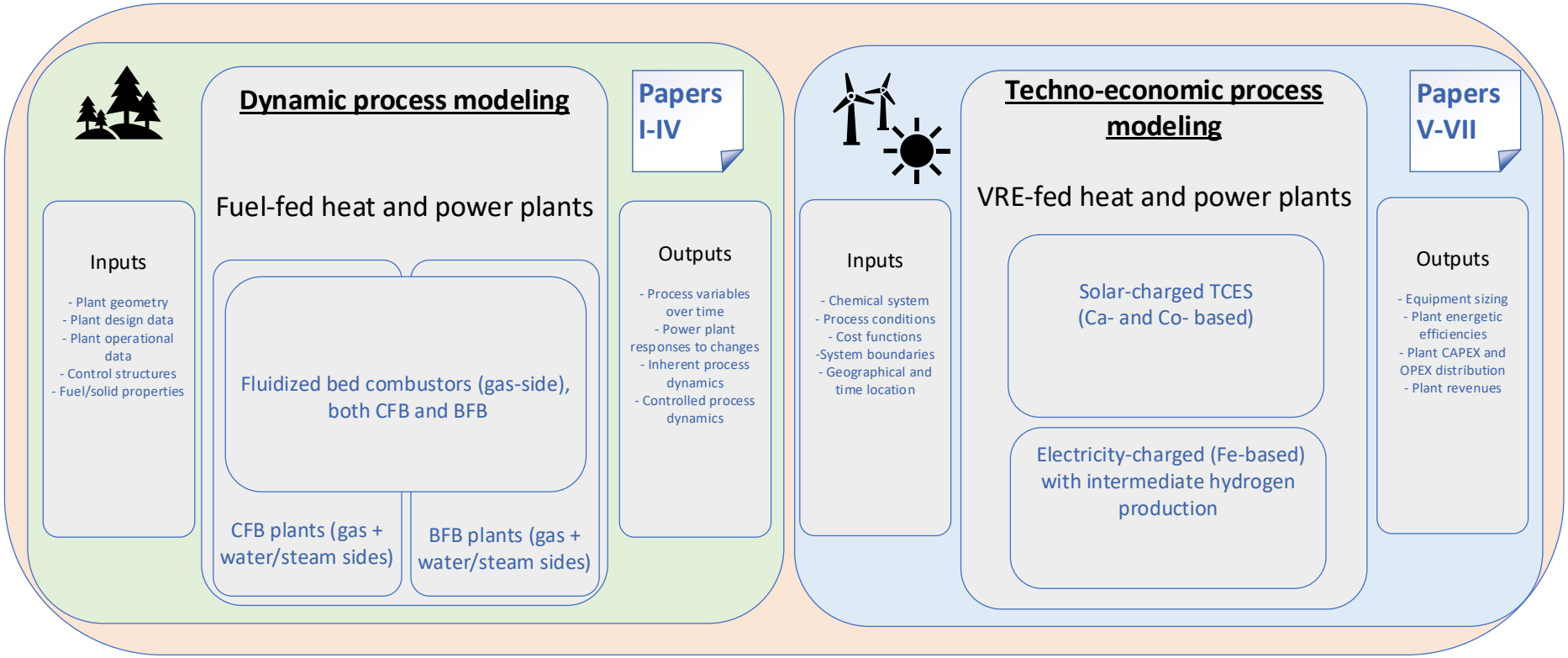

Figure 7. Overview of the methods used in this thesis and their connections to the appended papers.

3.1. Dynamic process modeling and simulation

Figure 8 displays a schematic of the methods included within dynamic process modeling and simulation and their links to the following subsections. First, two commercial-sized FB plants are used to collect design and operational data, which then serve as inputs (Section 3.1.1) for the modeling and simulation tasks. Second, the formulation of the dynamic process models both at the reactor (gas side) and plant (water-steam side) levels is presented (Section 3.1.2). Simulation methods (yellow boxes in Figure 8) include: i) calibration and validation (Section 3.1.3); and ii) the use of the calibrated models to compute the dynamic analyses (Section 3.1.4). Lastly, Section 3.1.5 briefly summarizes the specific cases studied.

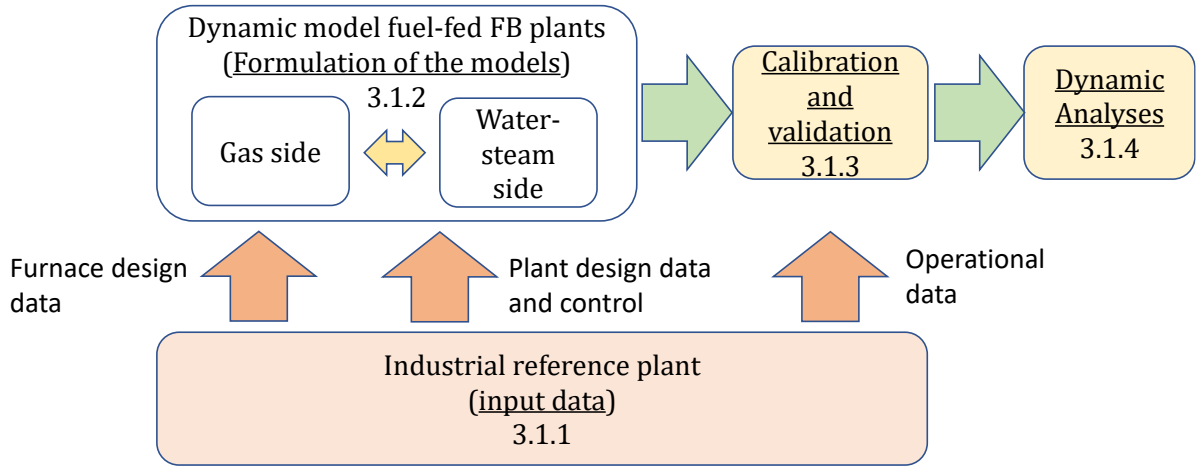

Figure 8. Overview of the dynamic process modeling and simulation methodology.

3.1.1. Input data

CFB reference plant

Detailed descriptions of the CFB furnace and plant are provided in **Paper I** and **III**, respectively. The plant is a 100 MW_{th} biomass-fired CFB boiler located in Karlstad (Sweden) that normally operated with wood chips with a moisture content in the range of 50%–55% (for the detailed fuel composition, see **Paper I**). A simplified process diagram with the main process components is shown in Figure 9 together with the main process variables used in this work (for details, see Section 3.1.4). The plant consists of: i) the CFB furnace; ii) a convective flue gas path; iii) an in-furnace superheater; iv) a steam drum; v) a steam turbine with two intermediate extractions; vi) a steam condenser in which DH water is produced; and vii) one closed and one open feedwater heater. Table 2 lists the main design data for the reference plant operated at full load.

The plant is operated with a conventional boiler-following strategy (for details, see Section 3.1.4 and **Paper III**). Note that due to the absence of a condenser operating with cooling water, the output of the plant follows a constant power-to-heat ratio.

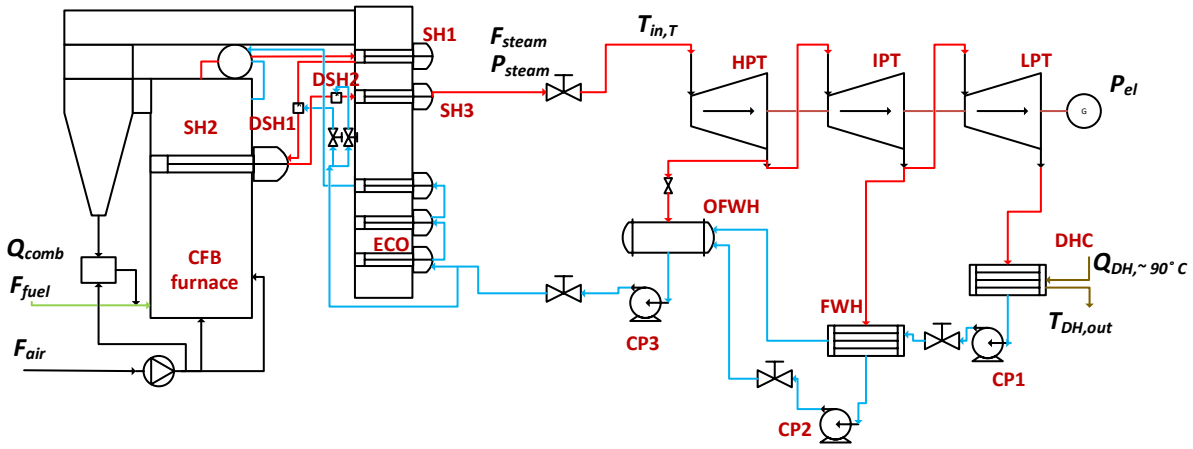

Figure 9. Simplified process schematic of the reference plant including the main process variables used throughout the work. Red is used for steam lines and water for water lines. SH: Superheater. DSH: desuperheater. ECO: economizer HPT: high pressure turbine. IPT: intermediate pressure turbine. LPT: low pressure turbine. DHC: District heating condenser. FWH: feedwater heater. CP: centrifugal pump. DHC: district heating condenser. Source: **Paper III**

Table 2. Design data of the reference CFB plant. Source: **Paper III**.

Combustor thermal load	100	MW_{th}
Live steam mass flow	28.9	kg/s
Live steam temperature	505	°C
Drum temperature	74.3	bar
Electrical power	20.2	MW
District heating load (DHC)	56.8	MW
Power-to-heat ratio	0.36	-

BFB reference plant

The industrial BFB-CHP plant used here is located in Örnsköldsvik, Sweden. This 140 MW_{th} biomass-fired (wood chips and forest residues) plant delivers medium-pressure steam to industrial facilities, i.e., steam to customers (STC), power to the grid and DH to the nearby municipality. Table 3 summarizes the main plant characteristics and design values, and detailed descriptions of the furnace and plant can be found in **Papers I** and **IV** respectively.

Table 3. Design data of the reference BFB plant. Source: **Paper IV**.

Combustor thermal load	130	MW_{th}
Live steam mass flow	53.4	kg/s
Live steam temperature	540	°C
Drum pressure	151.5	bar
Electrical power	37	MW
District heating production	60	MW

Figure 10 shows a process schematic of the reference plant, along with the main process variables used in this work (for details, see Section 3.1.4). For bed temperature control, the BFB furnace uses flue gas recirculation from the bottom of the furnace. Several superheater (SH) tube bundles are vertically immersed in the wingwall of the freeboard (upper furnace). The remaining superheaters and economizers (ECO) are located across the flue gas flow in the convection path. The steam turbine train consists of six stages, which are distributed across the

high-pressure train (HPT) and the low-pressure train (LPT). Steam from the third HPT outlet is extracted and delivered as STC, while the two low-pressure condensers are used for DH production (DHCs).

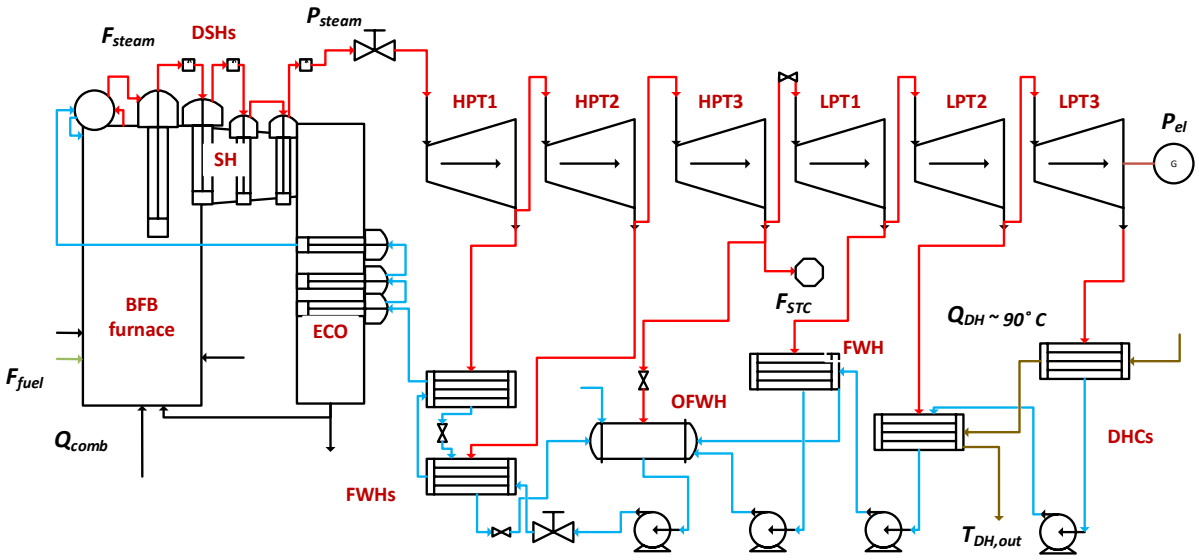

Figure 10. Simplified process schematic of the reference plant including the main process variables used throughout the work. Red is used for steam lines and water for water lines. SH, superheater; DSH, desuperheater; ECO, economizer; HPT, high-pressure turbine; LPT, low-pressure turbine; DHC, district heating condenser; OFWH, open feedwater heater; FWH, feedwater heater. Source: **Paper IV.**

Data acquisition

Both operational plant data and design information of the main process components were collected from the above presented reference plants. The following steps summarize the data acquisition process followed for collecting and processing the datasets used in this work:

- **Step 1 – Component, instrument and data selection**: Studying the piping and instrumentation diagrams (P&IDs) that display the flows, vessels, controllers, and instruments conforming the plants is a mandatory first step. This is followed by the selection of the process components that will be modeled and what will be excluded. Subsequently, the instruments of interest, i.e., the measurements and set-points containing variables of interest for the model development are selected and requested. Variables of interest include temperatures, pressures, flows, levels and concentrations. In parallel, geometric design data for the modeled equipment which include dimensions, pitch and number of tubes, existence of fins, or metal thicknesses, were selected.
- **Step 2 - Time period selection**: For the steady-state calibration and validation of the model, different operational periods during which the plants were running under diverse load levels were requested. Steady-state datasets involved periods of 1-2 hours of operation. Regarding transient operation, periods during which the load was increased or decreased were requested. The transient datasets used in this work represent periods of 3 hours of operation. The resolution of both the steady-state and transient datasets was the minimum that the plant instruments could provide, i.e., 60 seconds.

- **Step 3 - Post-processing data**: The steady-state data used in this work were calculated as the averages of 30-minute measurements (for details, see **Paper I**). For the transient validation (see Section 3.1.3), the measured transient datasets were linearly interpolated from the sampling time scale of 1 minute into a time scale of 1 second.

3.1.2. Formulation of the models

This section summarizes the formulation of the overall dynamic model, which results from integrating two dynamic models developed within this thesis: one describing the gas side of FB plants (described in detail in **Paper I**), and one describing the water-steam side (presented in detail **Papers III** and **IV**). The model also includes regulatory components such as controllers, ramps, steps and other mathematical blocks.

The external inputs required for the integrated model are:

- Geometry of the boiler and peripheric equipment, including the locations of the fuel and air feeding injections.
- Bulk solids properties: namely the density and size of the in-furnace bulk solids.
- Riser pressure drop.
- Fuel and gas compositions and properties, including the feeding temperatures.
- DH inlet conditions: flow, temperature and pressure of the return DH entering the plant.
- Operational conditions dictating the operation of the reference plant, i.e., set-points for the load level, live steam temperature and/or pressure, etc.

Figure 11 shows a schematic of the input/output flow diagram of the two integrated models, including the master control that governs the plant operation and the internal model variables through which the two sides are connected. The following aspects of the model integration are particularly noteworthy:

- The flue gas stream leaving the gas side enters the water-steam side model *via* the convection path.
- The furnace waterwalls transfer heat from the gas side for evaporating the biphasic water-steam flow, which in combination with the thermal inertia of the wall material determines the dynamics of the wall temperature. This heat transfer through the walls and the wall temperatures are represented in Figure 11 by a single arrow for simplification. However, these are handled in the model as control volumes, for each of which a dynamic energy balance is solved.
- The superheaters that are immersed in the furnace at height *h* extract heat from the corresponding control volumes of the gas side while simultaneously superheating steam in the water-steam side.

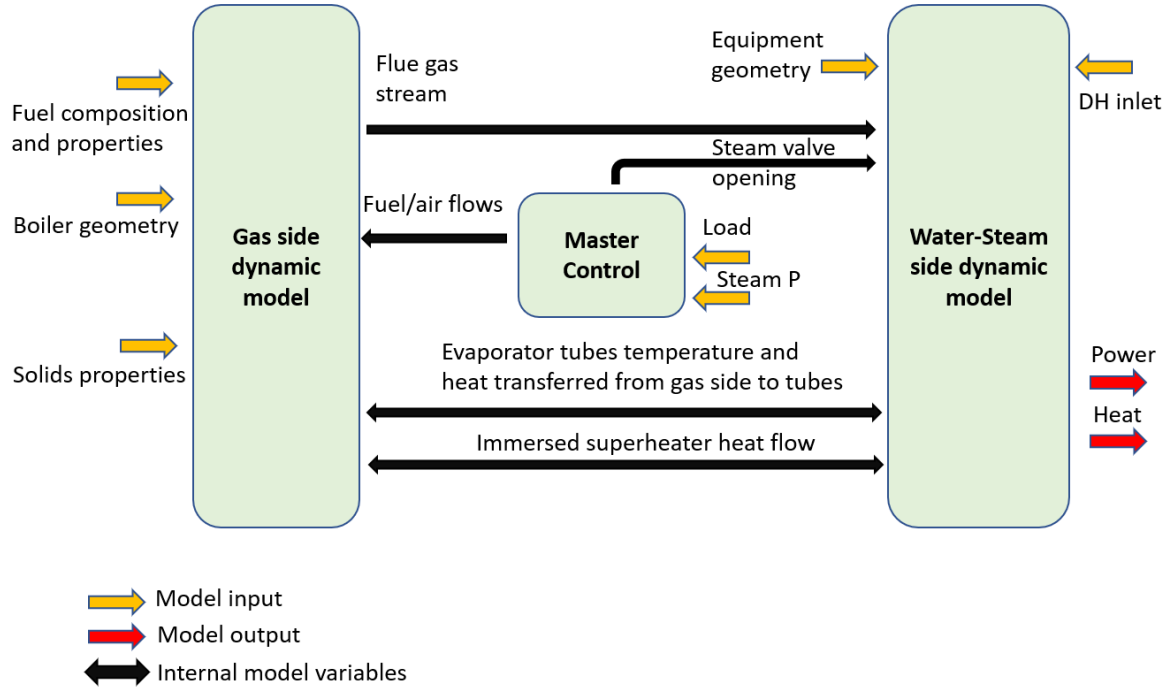

Figure 11. Input/output scheme of the integrated dynamic model including the master control. Source: **Paper III**.

Gas side

The gas side (see glossary for the definition and boundaries, respectively), whose detailed model formulation is presented in **Paper I**, is described by a number of perfectly mixed control volumes (CSTR) that exchange mass and energy. The domain is divided into the different fluid-dynamic regions generally identified from experimental studies conducted in large-scale FBCs [108]–[110]: the dense bed and the freeboard, and for CFB boilers, additionally the exit zone, cyclone and loop seal. The regions that are known to exhibit a plug-flow behavior, and thereby deviate from the assumption of perfect mixing (such as the gas in the dense bed or the gas and solids in the freeboard), are described in terms of consecutive CSTRs. The model accounts for three phases consisting of the: gas (comprising an ideal gas mixture of nine phase components); fuel (modeled as three phase components – fresh, dry devolatilized, and char – to account for the changes in size and density that occur during conversion); and bulk solids (represented by a mean size and density). The model solves the intercoupled dynamic energy and mass balances for each of the control volumes, calculating the temperatures and heat flows, as well as the concentrations and mass flows of each of the phase components. These energy and mass balances are governed by the three main mechanisms defined below:

- Fluid dynamics: 1.5D description of the gas and solids flows within the furnace [110], [111], [112].
- Fuel conversion: drying, devolatilization and homogeneous and heterogeneous combustion of the fuel [113], [114], [115].
- Heat transfer: transport of thermal energy within the furnace and from/to the waterwalls [116], [117].

Water-steam side

The different components have been modeled using the lumped parameter approach, which is known to be a valid assumption when describing power plants at the process level [118]. Regarding those components for which such a 0D representation is not appropriate, e.g., a tube, a 1D discretization is applied. For all the components, geometric data, initialization values and nominal values for correlations were fed into the model according to the design data derived from the reference plants (Section 3.1). A detailed formulation of the water-steam side model is presented in **Paper III** and **Paper IV**.

In the convection path, the heat transfers on the gas and water-steam sides of the superheaters and economizers are modeled according to Nusselt number correlations from [119], while the evaporator tubes model uses a correlation based on the Dittus-Boelter equation. The wall separating the two sides is modeled as a 1D domain, while assuming heat accumulation with a thermal resistance function of the wall thickness, area and conductivity.

The steam drum is modeled according to [120], solving the dynamic energy and mass balances for the liquid and vapor volumes. Heat transfer through the drum walls and heat accumulation in the walls are neglected. The natural circulation of the two-phase flow through the evaporator tubes is modeled with an ideal height difference that yields a certain pressure head. The steam turbine is described by a quasi-static model, an assumption that is found valid when comparing its characteristic time with those of other plant components such as condensers [121]. The power generation is calculated based on the inlet and outlet steam enthalpies with a constant dry isentropic efficiency [122]. The off-design performance is modeled according to Stodola´s law of cones. Lastly, the steam condensers are modeled as horizontal cylindrical vessels with a hotwell at the bottom where the condensate is accumulated. The model assumes thermodynamic equilibrium between the two phases. A wall model separates the condensing steam from the cooling fluid, with a heat transfer correlation for condensing steam over horizontal tubes and one based on the logarithmic average of the inlet and outlet temperatures for the cooling media, as derived from [119]. The deaerator is modeled in a similar manner, albeit without cooling tubes and neglecting the heat transfer through the walls.

The supervisory controllers are modeled as proportional-integral (PI) controllers that are tuned according to the PID tuning rules described by Skogestad [123]. Note that for tuning the supervisory control structures, the regulatory control layer needs to be already tuned and retained in a closed loop. For cascade control loops, the slave controller (i.e., the internal, faster controller) is tuned first.

3.1.3. Calibration and validation

The dynamic models result in a differential-algebraic system of equations (DAE), which is solved by means of the numerical solver Radau IIA [124]. To capture the fast-transient events that are ypical of combustion processes, the selected time resolution for the simulation was 1 second. This was increased to 100 seconds for the steady-state analyses. Initialization of the model was done by assigning design values to the main state variables.

Figure 12 summarizes the datasets used for calibration (green boxes) and validation (grey boxes), respectively. As indicated, for the reference CFB plant the model is calibrated to match

the steady-state operational dataset at 100% load. For the BFB reference plant, the model is calibrated with steady-state data at 100% and 40% loads.

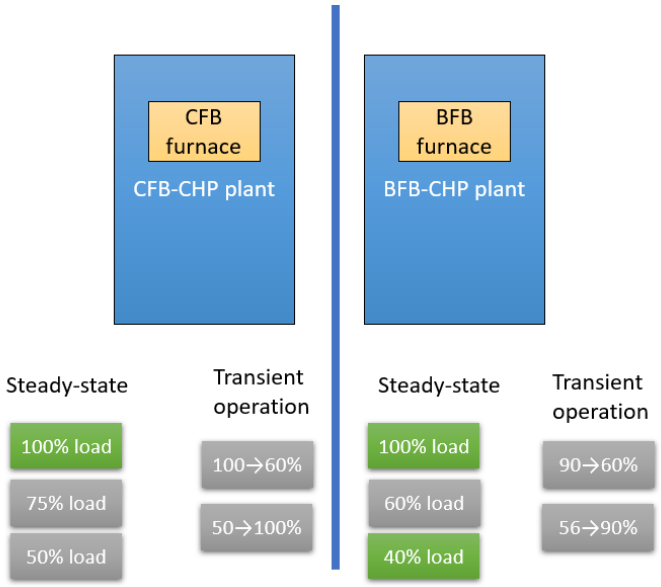

Figure 12. Operational datasets acquired from the reference fuel-fed FB plants and used for the calibration (green) and validation (grey) of both steady-state and transient model performance.

The sets of calibration parameters of the combustor gas-side model differ depending on the operation mode (BFB or CFB) as depicted in Table 4 (and described in detail in **Paper I**). For CFB conditions, which are characterized by a large amount of entrained solids in the riser, the model is calibrated by tuning the mean particle diameter of the bulk solids, which differs from the mean size of the fed particles due to particle attrition and size segregation phenomena. For BFB conditions, where the heat transfer to the walls is assumed to be driven exclusively by radiation, the entrainment of miniscule amounts of solids fines is known to have a significant impact on the emissivity of the freeboard cells. As this is a complex mechanism to model, it is here handled as a calibration factor through tuning the effective absorptivity of the freeboard cells. Lastly, the gas mixing rate governing the homogeneous reactions is used as a calibration factor in both BFB and CFB operations. Regarding the water-steam side, the present work follows the common practice in dynamic process modeling of calibrating the model by tuning a pre-exponential factor in the correlations for the heat transfer coefficients. The specific values of the tuned calibration factors are presented in **Papers I-IV**.

Table 4. Calibration factors used in each side of the dynamic model.

			Calibration factors
Gas side	CFB mode	-	Gas mixing
		-	Bulk solids size
	BFB mode	-	Gas mixing
		-	Absorptivity of the gas-solids suspension
Water-steam side		-	Heat transfer correlations

The steady-state validation of the models is carried out by means of the absolute percentage error (*AP*) between the measured (x_m) and simulated (x_s) process variables of interest (see Section 3.1.4) as depicted in Equation 4. Validation of the transient performance of the models is carried out by comparing the output of the model with measurements taken over a several hours of transient operation during load changes (the specific load changes reproduced in each model are shown in Section 4.1). Note that for an accurate validation the supervisory control strategies of the reference plants need to be activated when simulating the dataset for transient validation.

$$AP = 100\frac{|x_m - x_s|}{x_m} \tag{4}$$

3.1.4. Dynamic analyses

Inherent dynamics

The inherent dynamics of a system are usually evaluated through open-loop tests. These tests involve the introduction of individual step-changes in the key process inputs when the system is uncontrolled. After that, the time trajectories of the output variables of interest are computed. Thus, an open-loop analysis allows an assessment of how the system reacts to a specific change without the influence of the control loops. Executing these types of tests in industrial plants is often not an option due to safety and operational restrictions, and due to the presence of non-optimal control loops that would influence the results. Therefore, dynamic models are a potent alternative for the study of the process inherent dynamics.

Process variables that are typically important for operation are used to characterize the transient performances of the gas and water-steam sides, included in Table 5. The responses of these variables are assessed in terms of the total stabilization time (t_s, see Equation 5), which is defined as the time that it takes for a certain process variable *y* to remain within an error band of ±10% of the total change in steady-state values. Figure 13 includes a simplified representation of how t_s is computed.

Table 5. Process variables tracked to characterize the inherent dynamics.

Gas side
Temperature of the dense bed, T_{db} [˚C]
Temperature at the top of the furnace, T_{top} [˚C]
Total heat transferred to the waterwalls, Q_{walls} [MW]
Water-steam side
Power produced, P_{el}, [MW]
DH load, Q_{DH}, [MW]
DH water outlet temperature, $T_{DH,out}$ [˚C]
Live steam mass flow, F_{steam} [kg/s]
Live steam pressure, P_{steam} [bar]

$$t_s = \tau\rfloor_{y_0 \rightarrow y_\infty \mp 0.1(y_0 - y_\infty)} \tag{5}$$

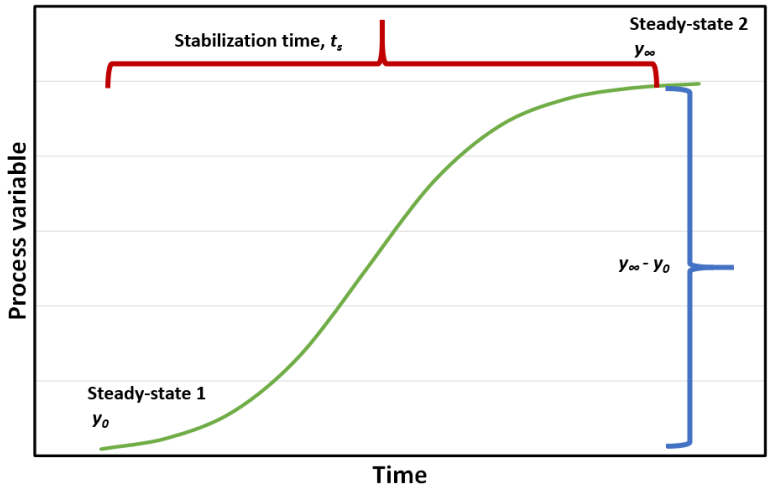

Figure 13. Schematic showing how the stabilization time is computed from the transient trajectory of a specific process variable.

Paper II describes a comprehensive comparison of the transient performances of the gas sides of BFB and CFB furnaces of the same size. For this, the stabilization times of the different variables listed in Table 5 are studied using open-loop tests as a function of the characteristic times of the main gas-side mechanisms (i.e., fluid dynamics, heat transfer and fuel conversion; see Section 3.1.2 and Section 4.1.2).

Controlled dynamics

The supervisory control layer of a process plant is responsible for regulating the variables of importance from the production point of view, i.e., driving the plant economics in a longer timeframe [41]. In thermal power plants, the supervisory control structure works on a minute-hour timescale, handling variations in the fuel composition and load. In particular in steam-generating plants, such as those investigated in this work, the supervisory control system modulates the steam flow, temperature, and pressure, so as to target production values. Complementary to this, the regulatory control layer ensures stabilization pf the process so that it does not drift away from acceptable operating conditions during disturbances. This entails the control of vessel pressures, levels, and in some cases, temperatures.

Supervisory control strategies for boilers differ according to whether the power plant output (i.e., generated power and heat) is controlled by the combustion load (i.e., air and fuel flows into the furnace) or the live steam control valve. The operational implications of each of the standard boiler control strategies used to provide rapid load changes in FB plants are briefly described below. An schematic diagram is shown in Figure 14 and the detailed review is presented in **Paper III**.

- **Turbine-following (TF)**: In this operation mode (blue lines in Figure 14) the turbine follows the response of the combustor. Thus, the master controller uses the combustion fuel load to control the power plant output, and the steam valve is used to maintain the steam pressure at the desired set-point.
- **Boiler-following (BF)**: The basis for BF control (red lines in Figure 14) is the opposite of that for TF control: the master load controller now manipulates the live steam control valve, and the combustor fuel load is used to control the steam pressure.

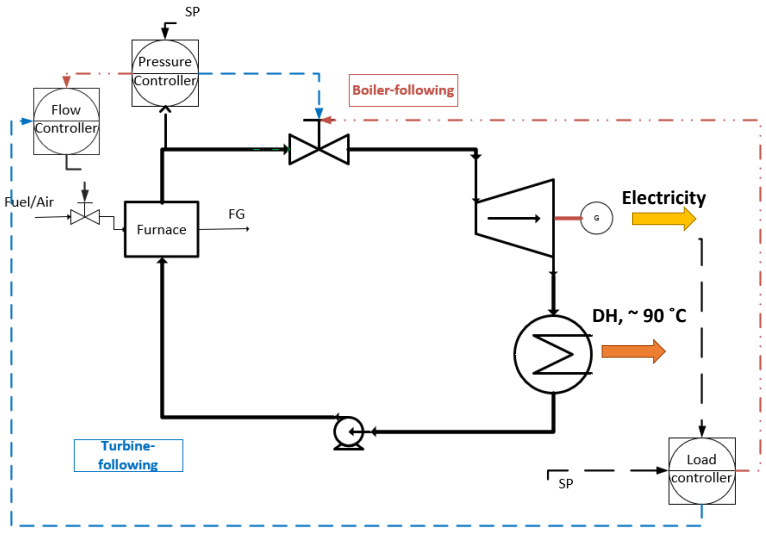

Figure 14. Schematic P&ID of the boiler-following and turbine-following control strategies. Source: **Paper III**.

Paper III evaluates the load-changing performances of the CFB reference plant when operated under different control strategies and for several ramping rates (see Section 3.1.5). The rise time of the generated power, i.e., the time that it takes for the output power to go through the 10%–90% response window [125], is used in **Paper III** to assess the performance of each control strategy.

In addition to the control strategies described above, a steam bypass is tested and placed on the high-pressure line, i.e., before the steam turbine (see Figure 15 and **Paper III**). The bypassed steam is condensed in the DH condenser to produce DH water. Note that a valve is added to regulate the steam pressure down to the pressure of the DH condenser.

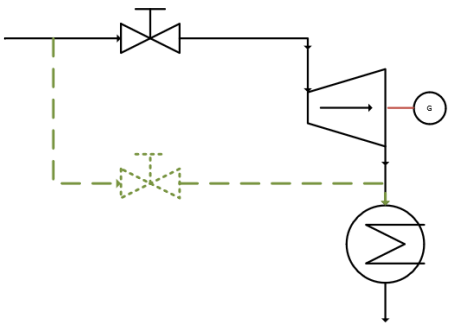

Figure 15. Schematic process diagram of the turbine bypass. Source: **Paper III**.

3.1.5. Summary of the cases studied

An overview of the simulated cases for the fuel-fed FB plants studied in this thesis is shown in Table 6 (note that cases related to calibration and validation of the model are not included). The load level pre-change refers to the steady-state in which the unit operates before the specific change is introduced. The changes applied are expressed in Table 6 as percentages of the pre-change load. Note also that while the inherent dynamics (i.e., open-loop tests) are investigated for both the CFB and BFB reference plants, the analyses of control and operational strategies are only simulated within the CFB plant.

Table 6. Summary of the dynamic analysis carried out in this thesis for the fuel-fed FB plants.

Analysis	FB plant type	Level	Load level pre-change	Changes applied	Change rate
Open-loop tests	BFB/CFB	Reactor	High	-10%, -25%,-50%	Step
		Plant*	High, low	±25%	Step
Controlled ramping rate	CFB	Plant	High	-50%	very fast (-5%/s), fast (-0.5%/s), slow (-0.05%/s) and very slow (-0.005%/s)
Turbine bypass	CFB	Plant	Medium, low	Bypass opened (3, 7, 5 kg/s), Bypass closed	Step

* The inherent dynamics of retrofitted fuel-fed plants for the production of heat, power and combustible gas were also evaluated. See Section 5.3.1 and Appendix B.

3.2. Techno-economic process modeling and simulation

Figure 16 displays a schematic diagram of the methods included within the techno-economic process modeling and simulation used in this thesis, and their links to the following subsections. Three subsequent steps are carried out prior to the technical and economic assessments (Sections 3.2.4 and 3.2.5 respectively): i) large-scale process layouts are formulated based on chemical system data retrieved from literature (Section 3.2.1); ii) the steady-state energy and mass balances of each of the layouts are computed and the main process equipment are sized (Section 3.2.2); and iii) the cost of each process layout is estimated and analyzed in relation to variables of interest (Section 3.2.3). The input data relevant to each task are described within the pertinent subsection. Lastly, Section 3.2.6 briefly summarizes the specific cases studied.

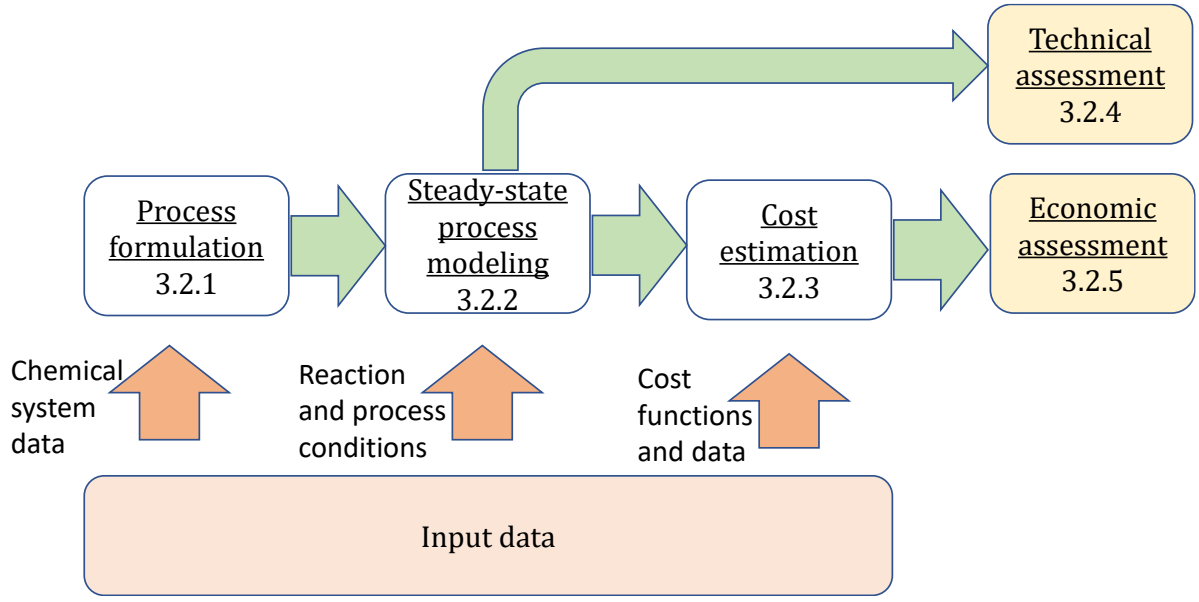

Figure 16. Overview of the techno-economic process modeling and simulation methodology.

3.2.1. Material selection and process formulation

The process layout, process conditions and associated costs vary depending on the chemical system chosen. Thus, representative candidate materials are selected from the literature for each of the chemical systems that are capable of providing high-temperature TCES, and thereby allowing the transformation of fuel-fed FB plants into VRE-fed layouts. The general criteria for the selection of the chemical systems are summarized below. More in detail motivations for the three specific selected cases are presented in **Paper V**:

- The system should have been described (in terms of key parameters such as energy density) in previous studies as promising with respect to large-scale deployment.
- A sufficient body of literature concerning the testing of the reactor and process conditions should be available.
- Only single-metal compounds are considered (disregarding mixtures and synthetic materials).
- Both the charging and discharging reactions should have rapid kinetics and conversion rates to minimize reactor size.
- The temperature levels of the reactions should be within the range of 650-1000 ˚C in order to i) match the temperatures reached at CSP solar receivers; and ii) maximize the production of electricity in the discharging side.
- The solids should hold physical stability over large number of cycles to minimize the make-up requirements.

Based on the above, the selected chemical systems for each of the solid looping types described in Section 2.3 are:

- $CaCO_3/CaO$ for metal carbonates.
- CoO/Co_3O_4 for thermally charged metal redox.
- FeO/Fe_2O_3 for chemically charged metal redox.

This thesis formulates a total of five large-scale process layouts based on the chemical systems identified above. Figure 17 depicts the general scheme of the VRE-fed layouts formulated in this work, detailed descriptions of which are given in **Papers V-VII**. Note that the units represented with dashed-line boxes are only present in some of the process layouts.

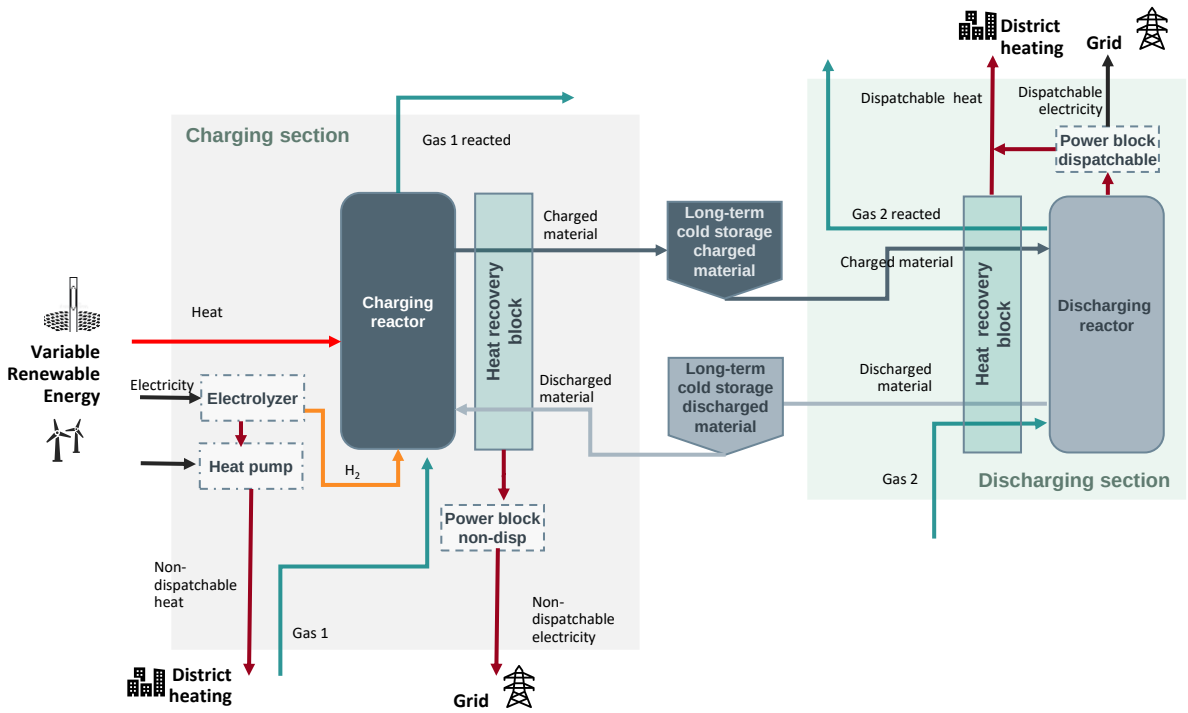

Figure 17. General scheme of the VRE-fed processes assessed in this work. The charging section is fed with renewable, intermittent energy (which can be in the form of high-temperature solar heat or electricity) and the discharging section produces dispatchable energy (DH or electricity). A fraction of the output is produced as non-dispatchable energy when the charging section is in operation. Storage of charged and discharged solids under ambient conditions is considered. Dashed-line boxes are only present in some process layouts, see Table 7.

Storage of the solid material under ambient conditions is considered in all the layouts. This allows for heat recovery between the hot and cold streams through the utilization of solid-solid and solid-gas heat exchangers, as well as conventional gas-gas heat exchangers. Solids storage under ambient conditions enables possibilities to operate the charging and discharging sections independently, and to introduce freighting of charged and discharged material without altering the energy efficiencies computed herein. To feed the charging section, availability over an intermittent source of energy is assumed, which depending on the process layout can either be i) heat at temperatures in the range of 650 to 1000 ˚C (e.g., a solar receiver in a CSP plant); or ii) electricity. In the latter case, an electrolyzer producing H_2 from water is included in the process formulation (and in the case of low-temperature electrolyzers, together with a heat pump for recovering waste heat).

While the main output of all the processes is dispatchable energy (in the form of electricity or heat), some of the processes offer the possibility to generate additional products or services. Table 7 lists the process layouts studied in this thesis, with their corresponding names, chemical system, additional product or service, and the type of energy input to the charging section.

Table 7. Summary of the VRE-fed process layouts assessed in the present work, including their charging type, chemical system, naming, input, main outcome, power block and additional product or service generated, if any.

Charging	Chemical system	Name	Non-dispatchable Input	Main dispatchable output	Additional product/service	Power block dispatchable	Detailed description
Thermally	$CaCO_3/CaO$	*CaL-TCES**	Heat	Electricity	-	Brayton	**Paper V and VI**
		CaL-TCES-CCS	Heat	Electricity	CO_2 capture	Rankine	
	Co_3O_4/CoO	*CoL-TCES-OEA**	Heat	Electricity	O_2-enriched air (OEA)	Brayton	**Paper V**
		CoL-TCES-O_2	Heat	Electricity	O_2	Brayton	
Chemically	$Fe_3O_4/Fe_2O_3/FeO$	*FeL-TCES-DH***	Electricity	District heating	-***	-	**Paper VII**

* Herein considered as *TCES-focused* layouts, i.e., maximizing the storage of energy.
** Two different schemes for low-temperature and high-temperature electrolyzers are assessed.
*** A layout to produce on-demand H_2 is suggested in **Paper VII** and discussed in Section 5.2 although its techno-economic performance has not been computed.

3.2.2. Process modeling

The present subsection summarizes the methodology that was followed to compute the energy and mass balances of each process layout, for which the following main assumptions were made:

- 0-D components, i.e., uniform pressure and temperature.
- No heat or pressure losses in the reactors and pipelines.
- Static process operation (i.e., despite some units turning on and off, the dynamics of the processes are not accounted for, and each section is modeled as steady-state).

The charging side is sized to be operated during a limited amount of time according to the availability of renewable energy, in contrast to the discharging section, which is sized so as to be operated following the energy demand. This is possible due to the presence of the storage tanks, which decouple the charging and discharging sides. Thus, the charging reactor is modeled to produce sufficient charged solids for the discharging section to operate continuously at the maximum capacity of dispatchable energy. This means that the molar flow rates into each reactor F_{ch} and F_{disch} can be linked according to Equation 6, where t_{ch} and t_{disch} represent the hours per day or year that the charging and discharging sections, respectively, are operating (see subsections below):

$$F_{disch} \cdot t_{ch} = F_{ch} \cdot t_{disch} \quad (6)$$

For the selection of t_{ch} and t_{disch}, as well as of the reactors capacities (i.e., F_{ch} and F_{disch}), different boundaries linked to the reactor and process conditions are applied depending on the type of VRE input (i.e., solar heat and electricity). Thus, they are presented independently in the subsections below. **Papers V** and **VI** cover in detail the method used for the solar-charged processes while those used for the electricity-charged processes are presented in **Paper VII**.

Solar-charged layouts

The solar-charged processes are evaluated and sized in this work as FB plants coupled to a high-temperature solar plant, i.e., a CSP plant, with the purpose of providing a storage possibility and enhance its dispatchability. For all the solar-charged processes, the assumed energy input consists of a heat flow, Q_{in}=100 MW_{th}, that is intermittently available for periods of t_{ch}=12 h/day (see Table 8), at the temperature level required by the chemical system selected

(i.e., required by the charging reaction to take place at the selected pressure). The impact of the net capacity on the economic feasibility of the processes is evaluated by considering in the analysis Q_{in}-values of 50 MW_{th} and 250 MW_{th} too. Regarding the discharging section, it is assumed to operate continuously at full capacity for 24 h/day (t_{disch}). Further details of the sizing and process modeling of the solar-charged processes are given in **Paper V**.

Table 8. Key process sizing parameters of the solar-charged FB process layouts.

Parameter	Value
Net renewable heat input to the process, $\dot{Q}_{in}$ (MW_{th})	100 (50,250)*
Charging time, t_{ch} (h/day)	12
Discharging time, t_{disch} (h/day)	24

* Three different values of Q_{in} are considered, in order to assess the impact of the net capacity of the plant.

Electricity-charged layouts

The electricity-charged layout (*FeL-TCES-DH*) proposed in this work utilizes H_2 as the reducing agent [126]. Thus, non-dispatchable electricity (from VRE) is used to run an alkaline electrolyzer at times when electricity is available at competitive prices, and the dispatchable energy is produced in the form of DH. The assessment of this layout carried out in **Paper VII** considers the use of existing fuel-fed FB plants, i.e., retrofitting the existing exothermic reactor (i.e., furnace) as a discharging reactor and coupling it to a newly constructed charging section. Therefore, the capacity of the discharging section is here fixed at 100 MW (see Table 9), which corresponds to a common size of a fuel-fed FB plant with DH demand [12]. The plant is modeled to follow the same operational profile after the retrofit, which is here assumed to be full-load operation during the winter months, i.e., 6525 h/year (t_{disch}), and switched off during the summer [127]. The sizing of the charging section and the storage units depend on the availability of electricity. Here, different electricity price profiles simulated by the electricity system investment model "hours-to-decades" (H2D) [128] are used. The profiles used are for the south of Sweden and represent different ratios of wind power and nuclear generation capacity within the system. Three different thresholds in electricity price are selected for triggering the charging section (i.e., the price of electricity considered to be competitive to run the charging process), corresponding to different t_{ch} values (for details, see Table 9 and **Paper VII**). Each threshold is, therefore, applied to each price profile resulting in nine different scenarios.

- **Price threshold 1, *Only_VRE*** – the charging section makes use of only wind-dominant periods.
- **Price threshold 2, *UF_50*** – the charging section utilizes electricity for 50% of the year, i.e., it has an utilization factor (UF) of 0.5.
- **Price threshold 3, *No_peak*** – the charging step avoids only peak price events, characterized by sharp increases in the price duration curves.

The storage is sized to cover for the average duration of the variations (*ADV*) of each price profile as expressed by Equation 7 and explained in detail in **Paper VII**. In contrast to the thermally charged processes, and due to the lack of experimental studies, the reactors are modeled assuming chemical equilibrium and based on the Gibbs free energy minimization model [129].

$$M_{solids,stored} = F_{disch} \cdot ADV \quad (7)$$

Table 9. Key process sizing parameters of the electricity-charged FB process layouts.

Parameter		Value
Net dispatchable heat output, $\dot{Q}_{out,disch}$ (MW_{DH})		100
Charging time, t_{ch} (h/year)		
	Only_VRE	1487-5295*
	UF_50	4380
	No_peak	8502-8605*
Discharging time, t_{disch} (h/year)		6525

* Different values are obtained for each electricity price profile (only the extremes are shown).

3.2.3. Cost estimation

The estimation of the plant cost is done following a bottom-up approach that includes i) the calculation of the process equipment costs, CAPEX (for every unit in each of the process layout defined in Section 3.2.1); ii) the addition of the installation and indirect costs, calculated according to [130]; and iii) the fixed and variable plant operating costs, OPEX. In this work the loading of inventory solid material is accounted for as part of the initial investment and is therefore annualized over the plant lifetime. Note that the estimation of the CAPEX utilizes the equipment sizing obtained from the process modeling (Section 3.2.1) and subsequently scaled up/down from the known cost of a reference component of size S_0 and a scaling parameter f, through the expression defined in Equation 8:

$$C = C_0 \left(\frac{S}{S_0}\right)^f \tag{8}$$

While most of the cost functions used in this thesis are taken from the literature, four different equipment cost functions were developed based on available economic data: i) externally heated endothermic FB reactors, ii) adiabatic FB reactors, iii) exothermic FB reactors with steam generation and iv) solids-solids heat exchangers. For the detailed equations, see **Papers V** and **VI**. Up-to-date costs and selling prices are obtained from literature.

For the solar-charged processes the inputs for the cost estimation are directly obtained from the process modeling stage (equipment sizes, utilities and input/output flows), with a cost for renewable high-temperature heat estimated from [131]. For the electricity-charged layouts, both the sizing (see Section 3.2.2) and the operational costs depend on interplaying factors (described in **Paper VII**) related to the electricity price profile. Thus, for the economic evaluation of electricity-charged layouts a cost-minimizing model developed by Cortés et al. [132] (see Appendix A) is used to assess the cost-optimal layout under the three different electricity profiles defined in Section 3.2.2.

3.2.4. Technical assessment

The outcome of the mass and energy balances described in Section 3.2.2 is used to compute several performance metrics, so as to assess the technical performance of each process layout. First, for the solar-charged process layouts producing electricity only, the overall energy efficiency $\eta_{t,el}$ is computed according to Equation 9, which includes the time-weighted average of the energy inputs and outputs:

$$\eta_{t,el} = \frac{\dot{W}_{net,ch} t_{ch} + \dot{W}_{net,disch} t_{disch}}{\dot{Q}_{in} t_{ch}} \quad (9)$$

where $\dot{W}_{net}$ represents the net electrical output (i.e., after subtracting the parasitic losses) and $\dot{Q}_{in}$ represents the heat input. Second, for the electricity-charged process layout producing heat only, the overall energy efficiency η_t is computed according to Equation 10:

$$\eta_t = \frac{\dot{Q}_{out,ch} t_{ch} + \dot{Q}_{out,disch} t_{disch}}{\dot{W}_{in} t_{ch}} \quad (10)$$

Third, the dispatchability ratio r_{disp} is used to evaluate how the energy input is distributed between dispatchable energy and non-dispatchable energy and is defined according to Equation 11, wherein $\dot{E}_{net,dis}$and $\dot{E}_{net,char}$ represent the energy flows (heat or electricity depending on the process layout) produced in the discharging and charging sections, respectively. This factor also represents the fraction of absorbed energy that can be delivered with a displacement in time (and potentially in space), i.e., a metric of how much non-dispatchable energy input is actually stored (for details, see **Paper VII**).

$$r_{disp} = \frac{\dot{E}_{net,disch} t_{disch}}{\dot{E}_{net,ch} t_{ch} + \dot{E}_{net,disch} t_{disch}} \quad (11)$$

3.2.5. Economic assessment

This work utilizes the breakeven selling price (BSP) as the main indicator of the economic performance of each processes that is assessed. The BSP of each process is computed by setting the net present value (NPV) to zero, i.e., the BSP represents the output price at which the annualized revenues and costs of the plants are breakeven after a given lifetime of the plant (set at 20 years). When the main outcome is electricity (solar-charged processes) the BSP is in the form of the breakeven electricity selling price (BESP), while the breakeven heat selling price (BHSP) is used in those cases with DH output (electricity-charged process).

Thus, the economic assessment of the processes relies on the calculation of the NPV, which is computed from the discounted annual cash flows CF_i according to Equation 12. The annual cash flows include also the side revenues from selling additional byproducts, if any (see Section 3.2.1). The selling prices of products and services such as OEA, O_2, and CCS are taken from the literature. More details on the BSP computation can be found in **Papers V** and **VI**.

$$NPV = \sum_{i=1}^{n} \frac{CF_i}{(1+r)^i} \quad (12)$$

3.2.6. Summary of the cases studied

An overview of the cases studied in this thesis concerning VRE-fed FB plants is shown in Table 10. As the thermally charged solid systems are evaluated assuming availability of high-temperature solar heat influx, a solar-intensive region (e.g., Spain) is taken as reference, for which the production of heat is not considered a valuable output. Moreover, such countries with a high share of solar CSP are typically lacking FB plants for heat and power production. Thus, a greenfield approach is followed (i.e., the plant is built from a totally undeveloped state). In contrast, the chemically charged processes are studied here as electricity-charged layouts. For this, a northern European country (i.e., Sweden) is taken as reference, for which access to competitively priced renewable electricity is guaranteed, and a demand for DH is in place. As such countries are characterized by a large installed capacity of fuel-fed FB plants, the investigation considers the retrofit of an existing plant.

Table 10. Summary of the specific VRE-fed FB processes investigated in this thesis.

VRE input	Charging	Location	Plant construction	Dispatchable output	Fixed boundary condition	Sizing criteria
Solar CSP	Thermally (Ca, Co)	Solar-intensive	Greenfield	Electricity	Solar input (12 h/day)	24 h/day discharging
Electricity	Chemically (Fe)	Northern Europe	Retrofit	District heating	DH output (6525 h/year)	Function of electricity price variations*

* The optimization model [132] summarized in Appendix A is used for the cost estimation.

4. Selected results

The selected results of this thesis are presented in two sections. First, the load-changing capabilities of fuel-fed FB plants are presented and analyzed. Secondly, the technical and economic performances of the VRE-fed layouts are assessed.

4.1. Load-changing capabilities of fuel-fed FB plants

4.1.1. Validation of the dynamic process model

The dynamic process model of fuel-fed FB plants is calibrated and validated prior to its utilization as a simulation tool. For this, the calibration parameters are first tuned to match the calibration datasets. Subsequently, the performance of the calibrated model is compared with additional operational datasets. The validation presented in this section contains multi-load steady-state datasets as well as transient events, and it includes process variables for both the gas side and water-steam side of BFB and CFB plants. The results of the validation show that the model resembles both steady-state and transient operations of large-scale plants with sufficient accuracy (< 5% error between key variables) for the intended purpose.

A summary of the steady-state validation for both the CFB and BFB model configurations is shown in Table 11, which includes the average absolute percentage error (*AP*) of the gas and water-steam sides respectively. The results in Table 11 indicate that the model can reproduce multi-load, steady-state operation with a reasonable level of agreement, as all average deviations are < 5% with an average *AP* of 2% and 3.6% for the calibration and validation cases, respectively. It can be noted that for most cases, the *AP* is somewhat higher at lower loads than at full load. This might be attributable to i) the fact that full load was used for calibration, ii) some of the semiempirical expressions used to formulate the model were obtained for a full-load situation and iii) some of the model assumptions become less realistic at lower loads, e.g., perfect vertical mixing of the fuel in the dense bed. An additional potential source of discrepancies between the model and the measured values is the input data of some process variables (such as incoming DH flow) which were back-calculated It should be noted that inherent instrument error in large-scale plants typically lies within 1% - 5%. Thus, it can be inferred that the dynamic process model can predict steady-state operation of fuel-fed CFB and BFB plants with a reasonable level of agreement within the operational windows of interest in this work. Detailed results of the prediction of each of the key process variables (as well as other variables not included in Table 11) can be found in **Paper I** (for the gas-side) and **Papers III and IV** (for the water-steam side).

Table 11. Overview of the steady-state performance of the gas and water-steam side models on CFB and BFB configurations. The comparison with the measured values is carried out using the absolute percentage error (%).

Model configuration	**Model side (key variables accounted)**	***AP* (%)**	
		Load level 1 – full load (calibration)	Load level 2 – partial load (validation)
CFB	Gas side (Q_{wall}, T_{db}, T_{top}, X_{CO2})	2.2	5.5
	Water-steam side (P_{el}, Q_{DH}, F_{steam})	3.4	1.3
BFB	Gas side (Q_{wall}, T_{db}, T_{top}, X_{CO2})	1.8	3.3
	Water-steam side (P_{el}, Q_{DH}, F_{steam})	0.6	4.4

Regarding the transient validation, Figure 18 shows the transient input values used for validating the CFB plant model, where Figure 18a depicts the inputs into the gas-side and Figure 18b those related to the water-steam side, i.e., those connected to the inflowing DH line. The simulated and measured transient values of the main process variables used for validation are shown in Figure 19, where gas-side variables are plotted in Figure 19a and water-steam side variables in Figure 19b. It can be noted that the measured temperature at the upper region of the furnace drops whenever the secondary air injection is sharply increased. This effect is not captured by the model as it is believed to be attributed to a local cooling phenomenon around the measuring instrument rather than effective cooling of the entire volume represented by a model cell.

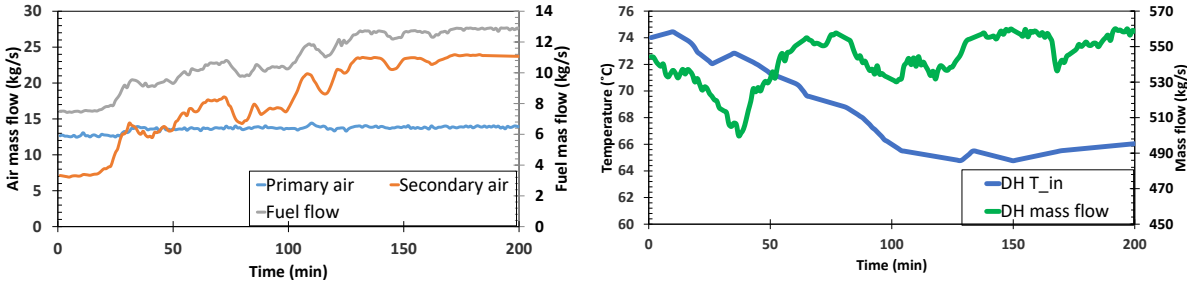

a) CFB gas side b) CFB water-steam side

Figure 18. Inputs to the model for the transient validation of the CFB mode. Source: **Paper III**.

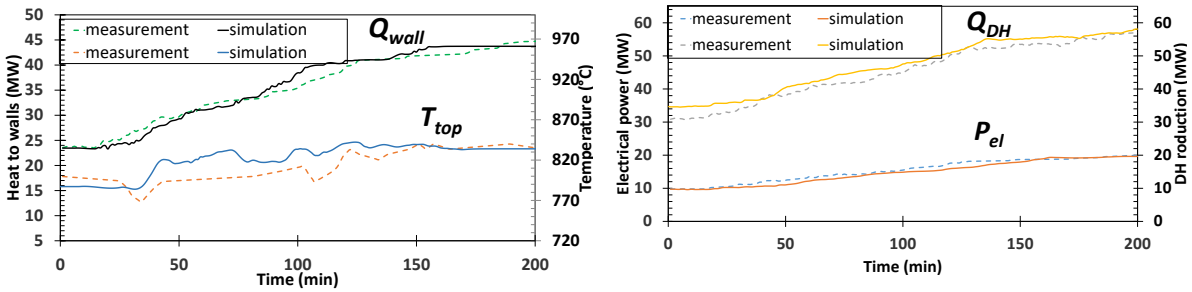

a) CFB gas side b) CFB water-steam side

Figure 19. Comparison of the model outputs (simulation) and the plant measurements of the CFB plant. Source: **Paper III**.

As for the CFB configuration, the model validation for the BFB plant mode is displayed in Figures 20 (input values) and 21 (comparison of simulated and measured variables). In general, the model is found to predict satisfactorily the behaviors of the reference plant across the 120 minutes simulated. Greater discrepancies are noticed only within the first 20 minutes of transient operation, which is the period during which the fuel flow and STC production are

temporarily decreased (see inputs in Figure 20). This reduced model performance is likely due to discrepancies in the parameters of the supervisory and regulatory control layers (for more details, see **Paper IV**).

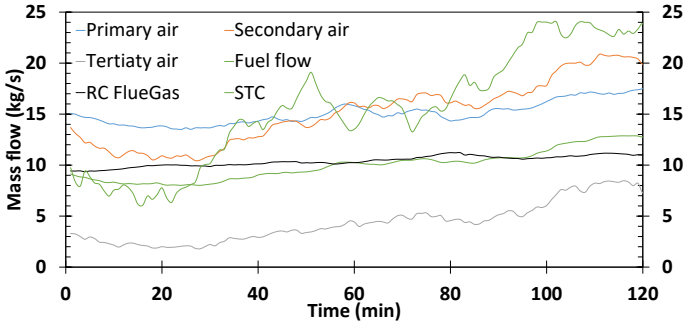

Figure 20. Inputs to the model for the transient validation of the BFB mode. Source: **Paper IV**.

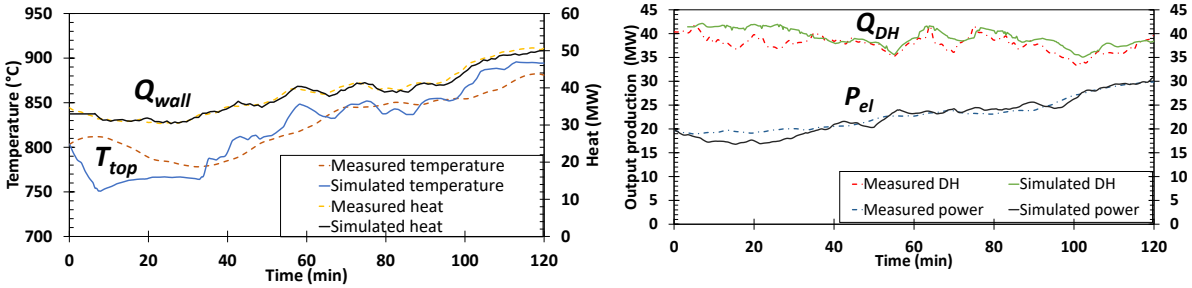

a) BFB gas side b) BFB water-steam side

Figure 21. Comparison of the model outputs (simulation) and the plant measurements of the BFB plant. Source: **Paper IV.**

When evaluating the whole time series shown in Figures 19 and 21, it is concluded that despite the deviations discussed above, the ability of the model to predict transient industrial operation of CFB and BFB plants is valid for the purpose of this work. This is, the model can satisfactorily predict i) the steady-state values of key process variables at reactor and plant levels across the 50-100% load span and ii) the system inertia and control loops involved when the load is changed at ramping rates typical of industrial operation. Nevertheless, it is important to point out that changes at faster rates than those employed for the transient validation (0.2 MW/min for the CFB and 0.4 MW/min for the BFB) are not validated with the current datasets.

4.1.2. Load-changing dynamics

The results at the reactor level show that the dynamic responses of BFB furnaces after load changes are largely governed by the changes in effective gas emissivity that are driven by the gas residence time within the furnace. In contrast, CFB furnaces exhibit longer stabilization times because they depend upon the characteristic times of the heat transfer and fuel conversion mechanisms along the furnace. At the plant level, it is found that the stabilization times of the water-steam side (found to be in the order of 5-20 minutes) as compared to those of the gas side are: i) within the same order of magnitude in CFB plants and ii) one order of magnitude larger in BFB plants.

In addition, several patterns have been identified regarding the transient operation of fuel-fed FB plants. These include: i) shorter stabilization times when the changes imply a heat removal from the system (e.g., decreasing the fuel or DH load or increasing the fuel moisture) rather than the inverse; and ii) faster dynamics when the plants are running at higher loads.

Operational and control strategies can temporarily overcome the limitations imposed by the inherent process dynamics of FBC plants. More specifically, strategies that make use of the live steam control valve offer fast ramp capabilities during short periods of time, although they could eventually damage certain items of equipment such as the steam turbine. In contrast, strategies that manipulate the combustion load offer slower (albeit smooth and stable) load-changing capabilities.

Inherent dynamics

The stabilization times (t_s) after load reductions in the two reference fuel-fed FB units at the reactor level, i.e., within the gas side, are plotted in Figure 22 (and explained in detail in **Papers I** and **II**). For all the cases investigated, and due to the larger heat capacity of the bottom region (consequence of the larger solids inventory), the temperature response in the bottom region is slower than that at the furnace top. In the BFB furnace (Figure 22b), the differences in heat capacity between the bottom and top regions are more pronounced, which explains the larger differences observed in these regions for the stabilization times of the temperatures (around 20 minutes and a few seconds, respectively). As a direct function of the furnace temperature, the dynamics of Q_{wall} reach stabilization just before/after (with ~20 seconds of difference) the temperature at the furnace top stabilizes.

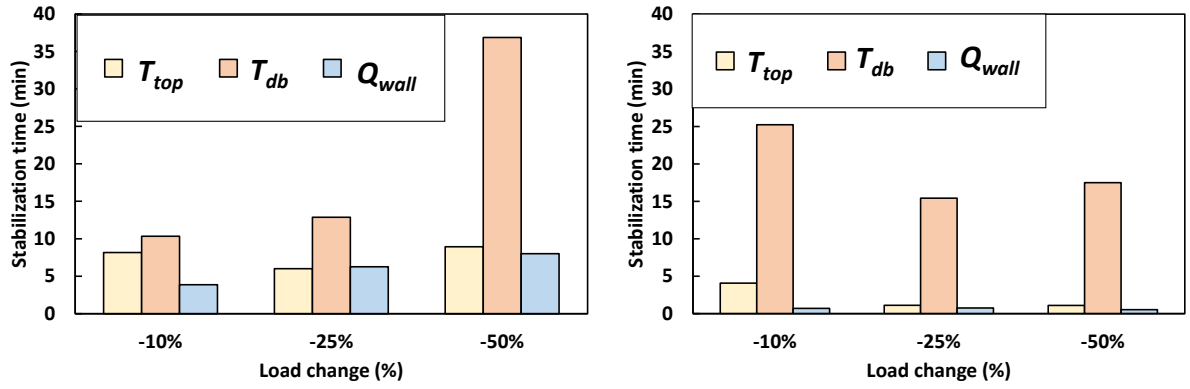

a) CFB gas side b) BFB gas side

Figure 22. Stabilization times of the CFB and BFB reference furnaces after load changes of different magnitudes. Source: **Paper I.**

To analyze the dependencies of the stabilization times of the gas side on the three main mechanisms taking place in the furnace (fluid dynamics, fuel conversion and heat transfer), additional open-loop tests are performed for the -25% load reduction, whereby the characteristic times of each of the mechanisms (defined as shown in Table 12) are varied independently according to the variables listed in Table 12 (for details, see **Paper II**). Based on the simulation results, Table 13 formulates simplified mathematical expressions that relate the stabilization times of the three gas-side variables monitored (heat extracted from the furnace and temperatures at the furnace bottom and top of the furnace) to the characteristic times of the above-mentioned furnace mechanisms.

Table 12. Characteristic times of the main in-furnace mechanisms of CFB and BFB furnaces. The table shows how these have been varied in the model to evaluate their impacts on the gas-side dynamics. Note that the characteristic time of the fluid dynamics in the BFB furnace has not been varied. Source: **Paper II**.

Mechanism	**Characteristic time**		**Variable varied**	
	CFB	BFB	CFB	BFB
Fluid dynamics	$\tau_{FD,CFB} = \tau_{riser} + \tau_{cyclone} + \tau_{loop-seal}$	$\tau_{FD,BFB} = \tau_{gas}$	Size of loop seal (for CFB)	-
Fuel conversion	$\tau_{FC} = t_{char}$		Char conversion time	
Heat transfer	$\tau_{HT} = \frac{\sum M_i C_{p,i}}{\sum F_i C_{p,i}}$		Solids heat capacity	

The relationships listed in Table 13 reveal that in BFB furnaces, the stabilization times at the furnace bottom (11-21 minutes) correspond approximately to the sum of the characteristic times of the two mechanisms present in the dense bed, i.e., the fuel conversion and the heat transfer (see Equation 13). In contrast, the temperature at the furnace top and the heat transfer to the walls stabilize in 60–80 seconds and 40–70 seconds, respectively, for all the cases assessed. This is a consequence of Q_{wall} being driven by the change in effective gas emissivity forced by the varied presence of solids fines entrained by the gas. Given the very low thermal inertia of the upper regions of the BFB furnace, its temperature dynamic behavior can be expressed as a function of the residence time of the gas triggering the change in gas emissivity, and to a minor extent (see Equation 14), the stabilization time of the temperature at the surface of the bottom region. Since Q_{wall} depends mainly on the gas temperature and effective emissivity, its stabilization time can be approximated as that of the temperature at the furnace top (Equation 15).

On the contrary, a relatively uniform effect of the three mechanisms considered for the CFB conditions is observed on the gas-side temperatures of CFB combustors. Furthermore, in the bottom region, the stabilization time can be directly approximated as the sum of the three characteristic times (Equation 16). Thus, even though the changes in fluid dynamics, fuel conversion and heat transfer are occurring in parallel, the tails of each of these mechanisms follow each other and add up sequentially to give the total stabilization time. As for the temperature in the furnace top, its stabilization generally occurs some 30% faster than that at the furnace bottom (Equation 17). Lastly, the dynamics of the heat transfer to the waterwalls are found to be sensitive to all the investigated variations, although they are predominantly influenced by the fuel conversion time (Equation 18).

Table 13. Simplified expressions for the dependency of the stabilization times (t_s) of the gas side on the characteristic times (τ) of the three in-furnace mechanisms considered (fuel conversion, FC, heat transfer, HT, and fluid dynamics, FD). Source: **Paper II**.

FB type	Variable	Expression	
BFB	T_{db}	$t_{s,db} \approx \tau_{FC} + \tau_{HT}$	(13)
	T_{top}	$t_{s,top} \approx \tau_{FD} + 0.05\, t_{s,db}$	(14)
	Q_{wall}	$t_{s,Q} \approx t_{s,top}$	(15)
CFB	T_{db}	$t_{s,db} \approx \tau_{FC} + \tau_{HT} + \tau_{FD}$	(16)
	T_{top}	$t_{s,top} \approx 0.7\, t_{s,db}$	(17)
	Q_{wall}	$t_{s,Q} \approx 0.9\tau_{FC} + 0.2\, \tau_{FD} + 0.4\, \tau_{HT}$	(18)

When expanding the analysis to the plant level, i.e., including the water-steam side, the computed stabilization times of the main process variables for load changes of ±20% are plotted in Figure 23. Note that the dynamics of the water-steam side are the same for CFB and BFB plants (as the process equipment used is the same, the dynamics mainly depend on equipment size and flows [37], which for the reference cases used are on the same order of magnitude). Therefore, only the results from the CFB plant are included here (see **Paper IV** for the BFB case).

First, Figure 23 reveals that the process stabilizes faster (on average, 15% shorter stabilization time) when heat is added to the system, i.e., when the fuel load is increased. When comparing the stabilization times of the different variables, the electricity production as well as pressure and mass flow of live steam are found to be the fastest to reach stabilization within the water-steam side, averaging 5 minutes for the investigated cases, which is comparable to the gas-side variables added in Figure 23, i.e., T_{db} and Q_{wall}. The outlet DH temperature and the condenser heat load are the slowest variables to reach stabilization, with average times of 10 and 13 minutes, respectively. When the same analysis is carried out for the process running at 70% load (Figure 23), all variables are found to stabilize more slowly than they do when starting from the 80% load case. This difference ranges from 9% slower in the case of the DH outlet temperature up to 25% slower for the electricity production. This effect has been reported earlier for thermal power plants [62], and is attributed to the intrinsic decrease in flows during partial-load operation, which increases the residence time of the fluid in both the gas and water-steam sides.

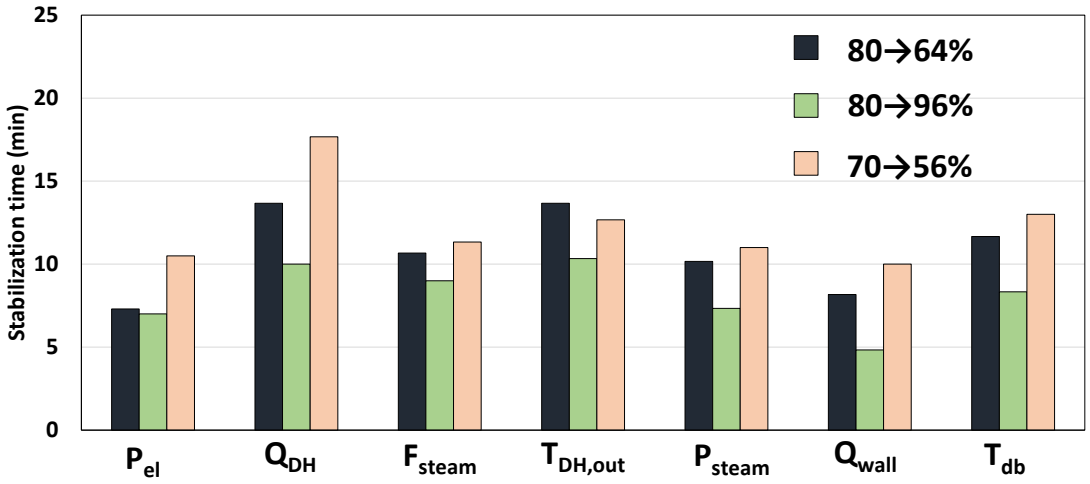

Figure 23. Stabilization times of the CFB reference plant (gas and water-steam sides) after load changes of different magnitudes. Source: **Paper III**.

Controlled dynamics

Figure 24 shows the responses of the generated power (in percent of the design load, i.e., 100%) for each of the control strategies when implemented in the reference CFB plant (for further details, see **Paper III**). For the slow cases, both BF and TF strategies are capable of providing load changes at the same rate as the set-point (SP) is changed. However, in the faster cases is observed that while BF provides very fast power output changes that always follow the SP, TF is considerably slower. These results show the dynamic effect of the control valve using the energy accumulated in the drum and steam lines to generate fast temporary changes in the steam pressure and mass flow, which quickly propagate to the turbine.

Since the fast changes in power output reported in Figures 24c and 24d occur due to the rapid dynamics of steam throttling, the live steam pressure under the fast load change is plotted in Figure 25 for a closer examination. The rapid changes in power output provided by the BF strategy occur at the expense of steam throttling when the control valve is rapidly closed. The overshoot in the pressure trajectory is +30% for the BF case as compared with ±0.01% for the TF strategy. In the case of BF operation, the temporary increase in the live steam pressure is directly linked to exergy losses and, therefore, the loss of available work, with a negative impact on process efficiency during the transient Thus, even though TF operation provides a slower response due to the longer characteristic times of the combustor, it maximizes process efficiency during both transient and partial-load operation. These results highlight the tradeoff that exists between flexibility and efficiency and component lifetime, as well as the operational constraints associated with power plant flexibilization.

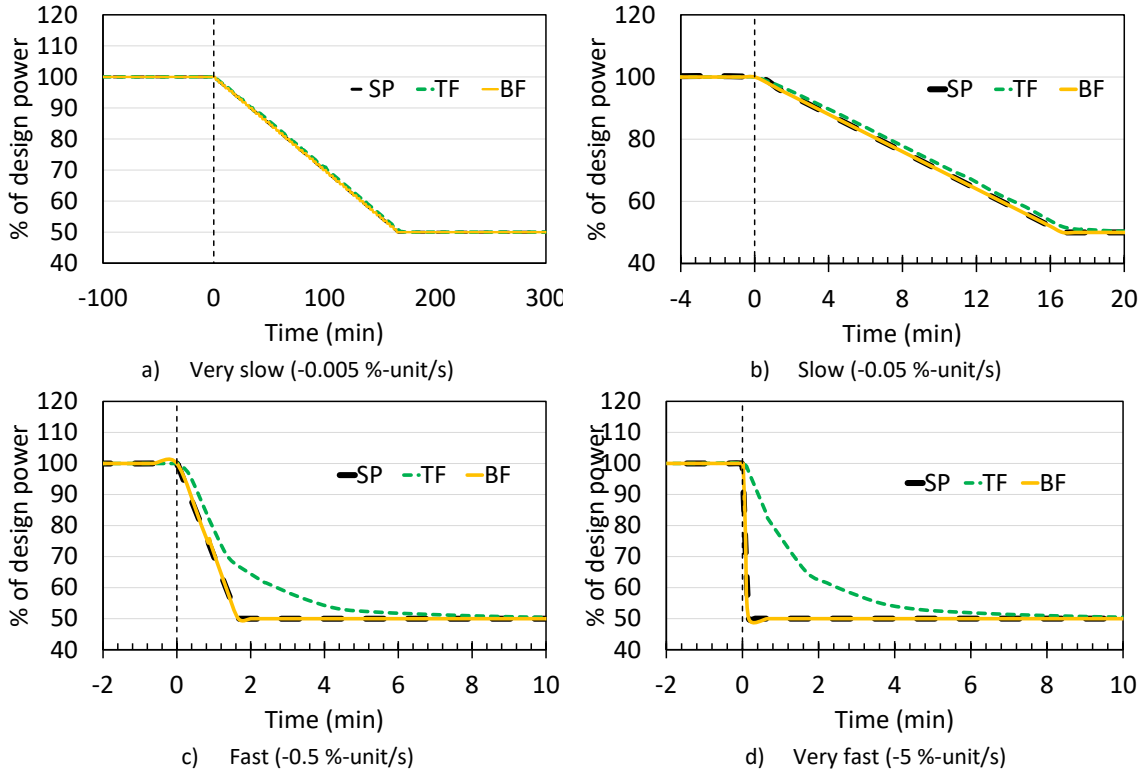

Figure 24. Power output of the CFB reference plant with after ramping rates of different magnitudes with turbine-following (TF) and boiler-following (BF) control structures in place. Source: **Paper III**.

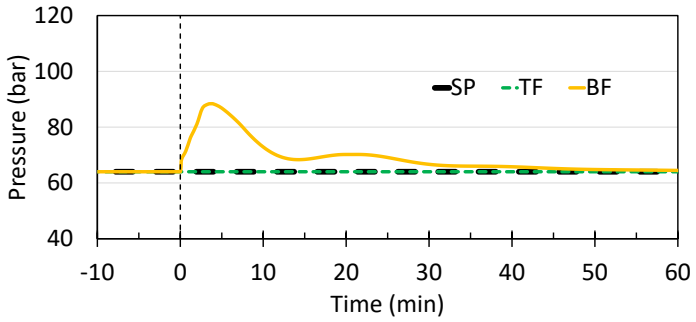

Figure 25. Pressure of the live steam prior to the steam control valve for the ramping rates and control structures tested. Source: **Paper III**.

Figure 26 shows the responses of the CFB plant after the bypass valve is opened. It is clear that the rise time of the electrical power output (Figure 26a) lies in the range of 25-60 seconds, and that it increases in line with the bypass flow. The response of the DH output (Figure 26b) is slower than that of the electrical output, with stabilization times in the range of 6–8 minutes. When the valve is closed (Figure 26, c and d) the power is increased with rise times of 1 minute, regardless of the magnitude of the bypass flow. These results are in line with those published previously [133]. The fuel flow in the combustor during the bypass opening has been added in Figure 26, a and c, and as expected, it remains constant, which is important for emissions control, combustion efficiency and intraday trading.

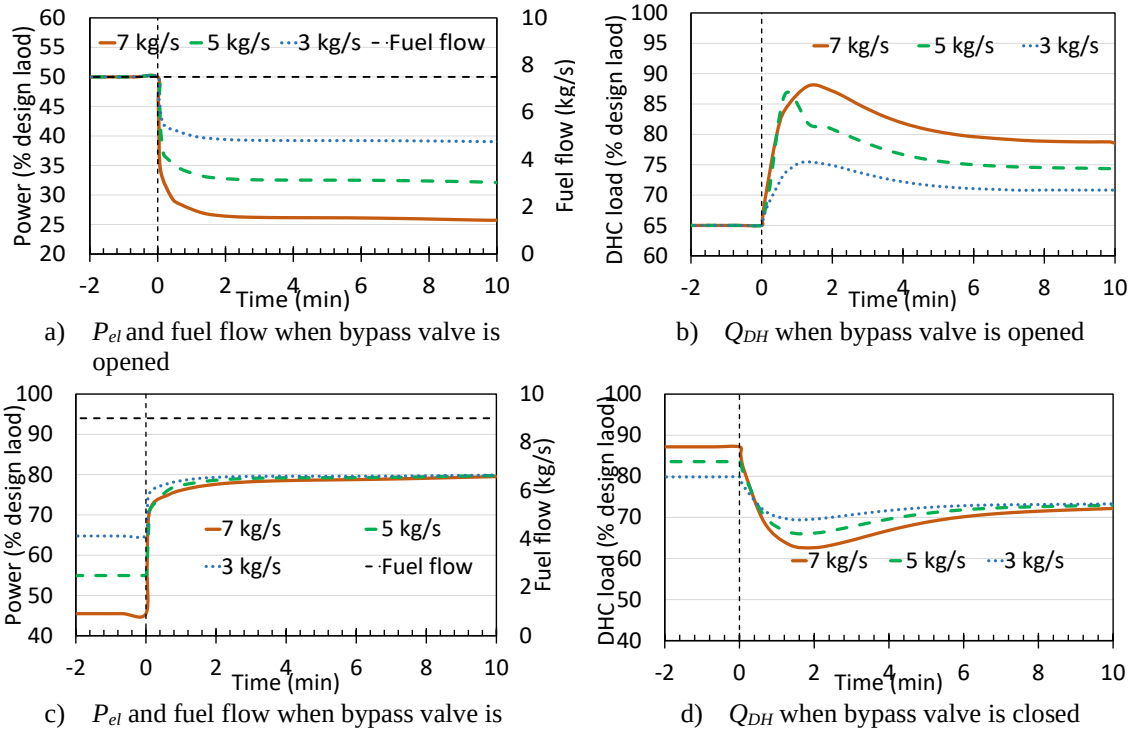

a) P_{el} and fuel flow when bypass valve is opened

b) Q_{DH} when bypass valve is opened

c) P_{el} and fuel flow when bypass valve is closed

d) Q_{DH} when bypass valve is closed

Figure 26. Simulated responses of the electrical power output and DH production for different bypass flows when the valve is open (a) and b)) and closed (c) and d)). Source: **Paper III**.

4.2. Techno-economics of VRE-fed FB plants

4.2.1. Solar-charged layouts

From a technical point of view, VRE-fed FB plants based on Co offer the highest energetic efficiencies for dispatchable power production. These can be as high as those of conventional thermal power plants, especially when deployed with Brayton cycles. The results show that the generation of valuable byproducts (carbon capture and pure O2, respectively) is done at the expense of electrical efficiency and dispatchability

Different cost structures are found for each of the process layouts: while Ca-based investment costs are dominated by the reactors cost, Co-based plants are driven by the cost of the solid material required. The economic performance of VRE-fed FB plants can be benefitted as from the production of additional by-products. In this regard, Ca-based FB plants offering CO_2-capture services to nearby emitters simultaneous to the heat and power production represent a key two-fold solution with high potential for future energy systems.

This section presents the results regarding the technical and economic performance of the solar-charged process layouts presented in Section 3.2 and analyzed in detail in **Papers V** and **VI:** *CaL-TCES*, *CaL-TCES-CCS*, *CoL-TCES-OEA* and *CoL-TCES-O_2*.

Figure 27 shows the yearly electricity generated or consumed by the charging and discharging sections respectively for the reference scale of 100 MW thermal input (i.e., 430 GWh/year). It can be seen that the electricity production in the *CoL-TCES-OEA* is higher than that of the *CaL-TCES*, which is attributed to the larger extent of reaction, larger reaction enthalpy (i.e., energy density) as well as the use of the Brayton cycle. Consequently. the energy efficiency of the

CoL-TCES-OEA ($\eta_{t,el}$ = 45%) is the highest of the processes assessed. It can also be seen in Figure 27 that in both *TCES-focused* layouts (i.e., *CaL-TCES* and *CaL-TCES-OEA*) the charging side is a net electricity consumer (most of the parasitic electricity consumption comes from the solids conveying). Hence, as also seen in Figure 27, the dispatchability ratios r_{disp} of these two processes are slightly larger than 1, i.e., all the electricity is generated in the discharging section, and therefore all the delivered energy is dispatchable.

When the generation of a more valuable by-product is considered (i.e., *CaL-TCES-CCS* and *CoL-TCES-O₂*), Figure 27 reveals that the total electricity production is reduced as compared to the corresponding *TCES-focused* layouts. This effect is due to i) the condensation of the steam used as a compound that can be separated from the more valuable streams and/or ii) the decrease in extent of reaction linked to the modified process conditions. Hence, the generation of a more valuable by-product comes on the expense of a drop in energy efficiency of 7 and 6 %-points respectively for the Ca- and Co-based processes. Note that due to the increased use of steam in the charging side the share of non-dispatchable electricity generation increases for the layouts with valuable by-product. Thus, the dispatchability ratio of these processes is also reduced (0.69 and 0.76 for the *CaL-TCES-CCS* and *CoL-TCES-O₂* respectively).

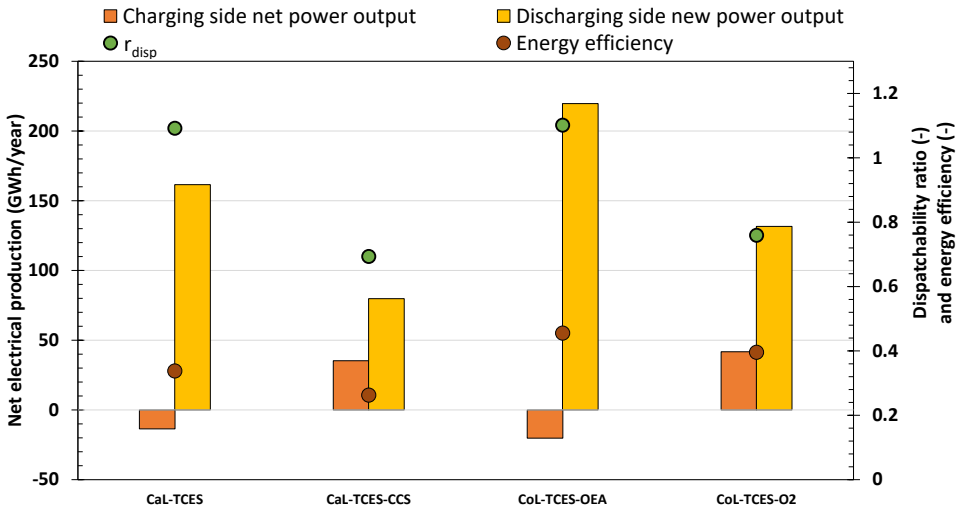

Figure 27. Net electrical production *(per year)* of the charging and discharging sides, energy efficiency ($\eta_{t,el}$) and dispatchability ratio (r_{disp}) for each of the processes assessed. Source: **Paper V**.

Regarding the economic assessment Figure 28 provides an overview of the total cost, its breakdown and the BESP of each process layout for three different process sizes (Q_{in}, see Section 3.2.2). The total investment costs range between 230-379 M$ for the 100 MW of the reference thermal input (and within 140-780 M$ for the whole range). For any of the three sizes studied, *CaL-TCES* provides the lowest plant cost and *CoL-TCES-OEA* the highest, i.e., the variation of scale does not modify the comparative performance.

For the CaL processes, the reactors account for the largest share of the investments (around 80%) regardless of the process size. It should be noted that the reactor cost includes the heat transfer surfaces (for the charging reactor) as well as the steam-related systems in the case of atmospheric discharging reactor, i.e., in the *CaL-TCES-CCS* layout. In contrast, the cost structure of the Co-based processes is driven both by the cost of the inventory material (as predicted by Bayon et al. [134]), together with the cost of the reactors. This observation indicates that while the Ca-based processes are suitable for covering energy storage periods

much longer than the 12h-period used as reference in this work without strong alteration of the costs reported here, the cost of the Co-based processes is largely dependent on the storage time. In fact, the results displayed in Figure 28 make evident that despite the favorable technical performance of the *CoL-TCES-OEA* process the *CaL-TCES* shows a better economic performance due to the significantly lower material cost. The weight of the heat input cost (largest fraction within the O&M variable costs in Figure 28) is on average 45% for the CaL processes and 33% for the CoL processes for the cost considered here (20 $/MWh$_{heat}$). In **Papers V** and **VI** the addition of a high temperature solar collector within the process frame is also considered (rather than purchasing a heat inflow), resulting in a BESP increase of 10-30%.

In addition, Figure 28 reveals that the BESP is generally reduced for the layouts offering a valuable by-product despite the drop in thermodynamic performance (i.e., lower energy efficiency and dispatchability ratio) discussed above. The increased economic performance is in average 3% for the CaL processes and 19% for the CoL. Note that the benefit of implementing the *CaL-TCES-CCS* as compared to the *CaL-TCES* is more noticeable at larger process sizes (up to 18% reduction in BESP for the 250 MW case), whereas for the 50 MW size the implementation of the advance layout is not profitable as compared to the *TCES-focus* layout. The main reason for this is that the *CaL-TCES-CCS* layout is formulated with an atmospheric discharging reactor that includes a steam-generation system (see **Papers V** and **VI**), which is much more expensive than the adiabatic carbonator in the *CaL-TCES* scheme. Thus, the cost of the reactor is favored by economy of scale and the side-profit obtained from the carbon capture service scales linearly with size. Consequently, the *CaL-TCES-CCS* becomes the most competitive process at the 250 MW scale (while the *CoL-TCES-*O_2 layout offers the lowest BESP for the 50 and 100 MW scales).

It is important to note that the method employed values equally the dispatchable and non-dispatchable electricity production. In reality, these will be priced differently (as the dispatchable electricity can be intentionally sold in periods of high electricity prices) which would enhance the economic performance of the layouts with larger r_{disp}, i.e., the *CaL-TCES* and *CoL-TCES-OEA*.

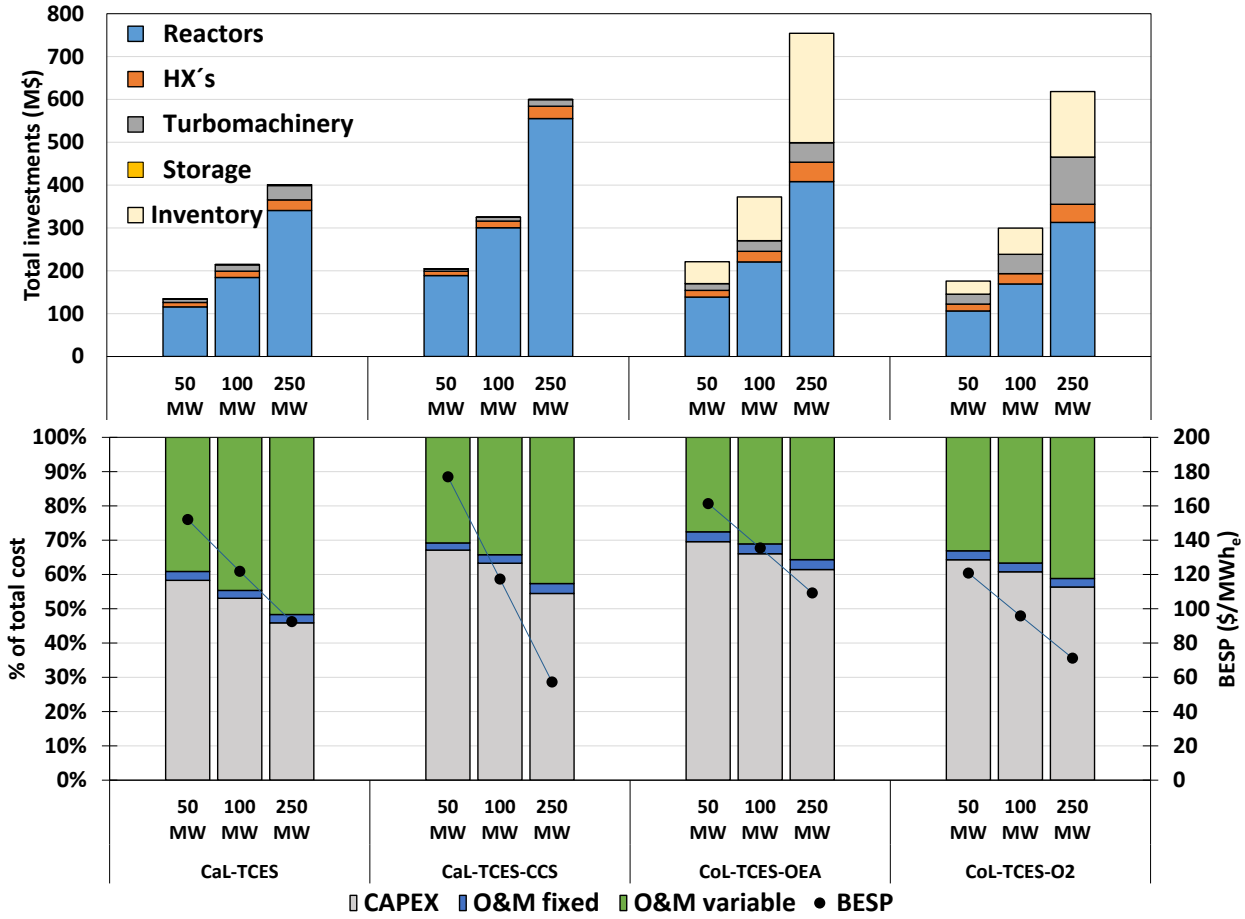

Figure 28. Disclosure of the total investments (in M$), total costs (distribution between OPEX and CAPEX) and BESP of the four solar-charged FB plants assessed. $ refers to USD.

Due to the low TRL of the process layouts assessed the reported costs entail large uncertainties. A parametric study is carried out in **Paper V** to examine how the BESP reacts to the variations of key assumed parameters. Results from such study indicate that the *CaL-TCES* cost is the most robust to the variations considered in the study. Secondly, that although the economic performances of the two Co-based processes are affected by the material cost and the by-product selling price, the BESP remains within the same order of magnitude (80-155 $/MWh for all cases studied).

4.2.2. Electricity-charged layouts

The retrofit of existing fuel-fed FB plants into electricity-charged Fe-based FB plants is evaluated through a Swedish case study. The technical performance is superior for layouts utilizing high-temperature electrolyzers, which largely increase the dispatchability of the process to the expense of 4%-points of energy efficiency. The results reveal that the retrofit of the entire Swedish FB fleet is feasible when compared to the estimated national reserves and yearly extraction flows of iron ore.

The cost structure of the proposed Fe-based plants is largely dependent on the equipment for generating the chemical agent, i.e., the cost for the electrolyzers (if H_2). In addition, results show that i) the cost-optimal layout is that with low-temperature electrolyzers; and ii) the economic performance of electricity-charged FB plants is improved in scenarios with high variability of the electricity price.

This section presents the technical and economic performance of the retrofit of FB plants into the electricity-charged process layouts formulated in Section 3.2.1 and analyzed in detail in **Paper VII**. First, the overall energy balances for the two types of electrolyzers are presented, followed by the required installed capacities and electricity and material consumption from a plant and national level. Lastly, the cost-optimal layout is shown, and its cost structure is analyzed for different scenarios.

The total energy efficiency and dispatchability ratios (r_{disp}) of the low and high temperature electrolyzer layouts are plotted in Figure 29. It can be seen that while the low-temperature electrolyzer presents a higher energy efficiency (of around 90% against 86% for the high-temperature case), the share of dispatchable heat produced is lower (r_{disp} = 44%) than that of the high-temperature electrolyzer (r_{disp} = 79%). This is due to the much higher level of non-dispatchable heat delivered in the reduction section for the case with low-temperature electrolyzers, as a consequence of their having heat recovery via heat pump (and therefore higher electricity consumption).

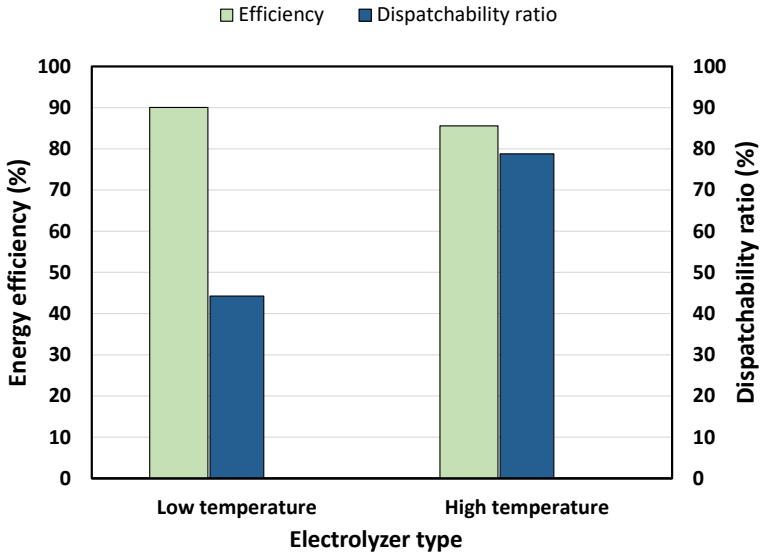

Figure 29. Dispatchability ratios and energy efficiencies (electricity-to-heat, η_t) of the electricity-charged FB plant layouts with low and high temperature electrolyzers. Source: **Paper VII.**

The inventories of reduced solid material (in tonnes) and the sizes of the storage silos (in m^3) are displayed in Figure 30 for the different scenarios. Note that a second storage tank of similar size is required for the oxidized material. It can be noted in Figure 30 that since the required storage correlates linearly with the *ADV* (see Chapter 3), the *Only_VRE* threshold requires the largest storage for all electricity mixes (5,534-87200 tonnes) while the *No_peak* requires the smallest material inventories (2500-4200 tonnes), as only electricity demand peaks with durations of 7-12 hours are to be covered by the storage. When translating the storage sizes into volumes the computed values (1000-30000 m^3) are in the same order of magnitude of those of conventional process industries (refineries often hold tanks from 10000 to 100000 m^3).

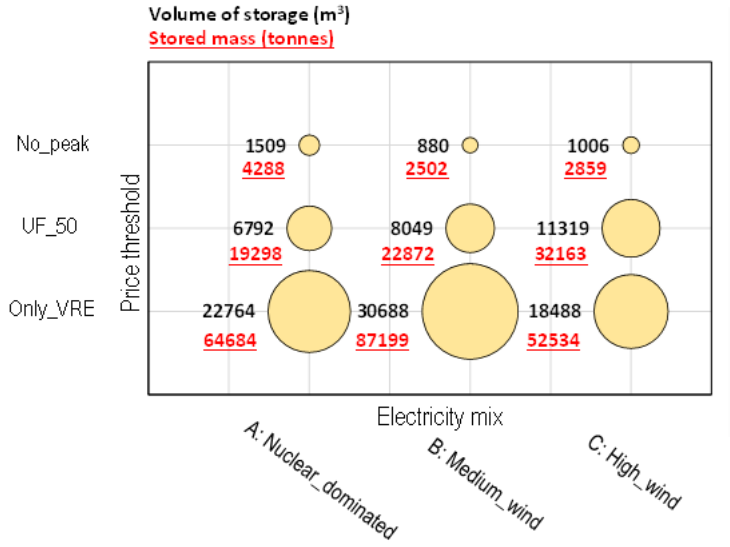

Figure 30. Resulting sizes of the reduced material stored (in tonnes) and equivalent volumes in order to store electricity for the objective time periods under the nine cases investigated (see Table 9). Source: **Paper VII.**

The Fe inventory requirement of the reference 100 MW plant can be understood when put in context with the national Fe production rates. If the results obtained for the intermediate scenario (i.e., *UF_50* applied to the *Medium_wind* electricity mix) are extrapolated, a retrofit of the total Swedish FB-DH fleet would require an initial inventory of 2.8 Mt of Fe powder. This represents about 0.23% of the Swedish national Fe reserves and approximately 11% of the national annual production of Fe ore [135], so it falls into the feasible national mining capabilities. Similarly, the make-up flows (depicted in detail in **Paper VII**) required to cover material losses and deactivation would amount to about 40 kt/yr for the entire Swedish FB-DH installed capacity, which represents around 0.15% of the national production of Fe ore.

The required installed capacities of the charging section units are plotted in Figure 31 in terms of the power capacities of the electrolyzers (MW) and the mass inflows of solids for the reduction reactor (kg/s). Note that since both variables correlate directly with the running hours of the reduction step the scenarios computed for the *Only_VRE* threshold show the largest capacities and the *No_peak* scenarios result in the smallest capacities. When utilizing low-temperature electrolyzers, the computed capacity to be installed is in the range of 196–1150 MW, while the capacities of the more efficient high-temperature electrolyzers are on average 30% smaller (see discussion on Figure 29). The reduction reactor's inlet mass flow is between 82 kg/s for an UF value close to 1 and 475 kg/s for the scenario with the lowest UF value (0.17).

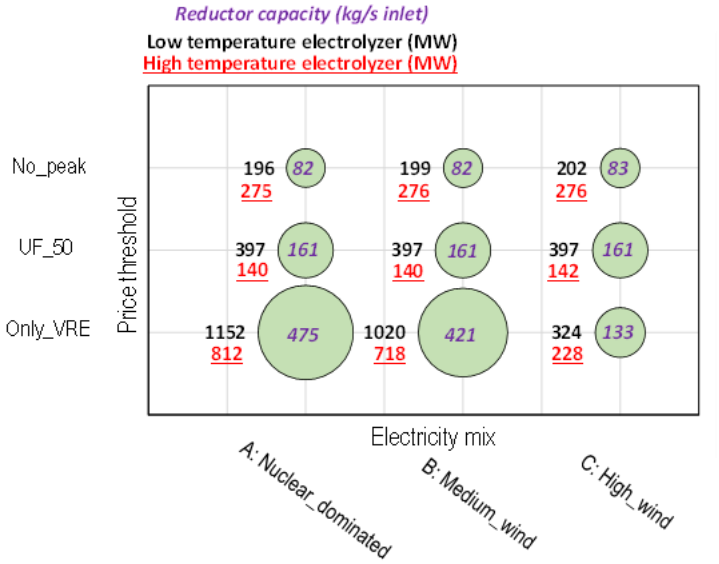

Figure 31. Capacities of the charging reactor, i.e., F_{ch} (in kg/s of solid material) and electrolyzers (in MW) for the nine cases investigated. Source: **Paper VII.**

When assessing the cost-optimal structure of the retrofit, the layout with low-temperature electrolyzer over-competes the one with high-temperature electrolyzer for all electricity mixes (see [132]). Figure 32 shows the cost-optimal disclosure for the three electricity mixes considered as well as the computed BHSP. It can be seen that the cost of the electrolyzers represent the largest investment followed by the purchase of the inventory material, as the processes are sized to store energy for up to weeks. This is also why the share of the inventory material cost increases as the electricity price variations raise (from *Nuclear_dominated* to *High_wind*). This increase in electricity price variations (and consequent larger investment in charging section and storage sizes) leads also to a decreased cost of electricity use (O&M variable cost in Figure 32), from 49.5% of the total cost to 15.6%. Nonetheless, such a shift in the cost structure leads to an overall reduction of the BHSP of around 10%, which indicates that the economic performance of the process benefits from electricity price variations.

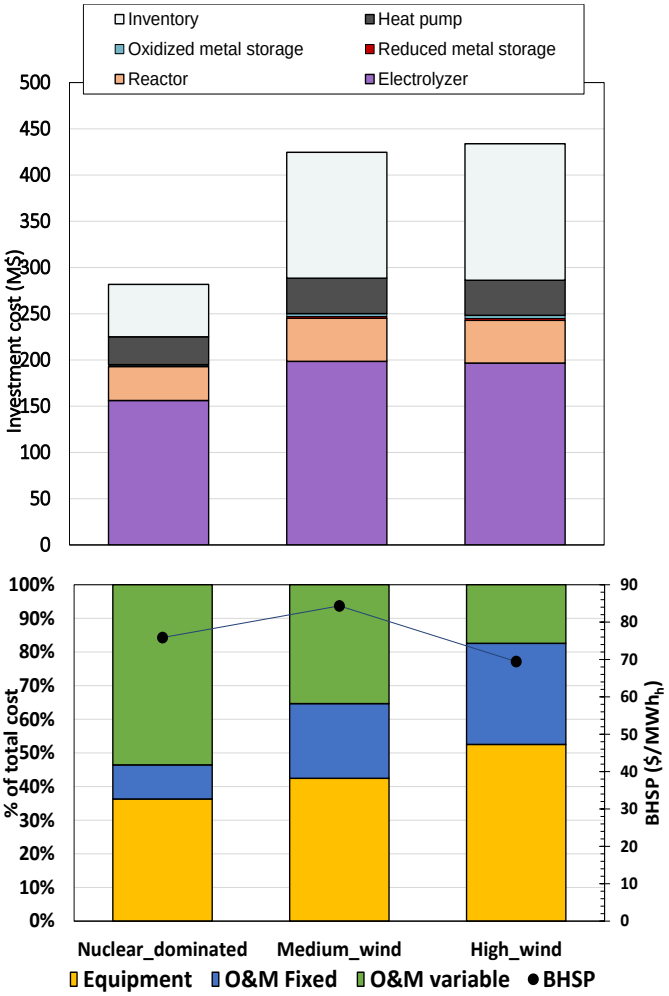

Figure 32. Disclosure of the total investments (in M$), total costs (distribution between OPEX and CAPEX) and BHSP of the electricity-charged FB plants for the three different electricity mixes considered. $ refers to USD.

5. Discussion

The capabilities of FB plants in future energy systems can be assessed based on the results presented in Chapter 4, together with additional results from the appended papers. More specifically, this section discusses the capabilities of FB plants for: i) transient operation; ii) providing different VMS to the power system; and iii) the additional provision of high-value streams and services besides heat and power (combustible biogenic gas, carbon capture, and hydrogen on-demand).

5.1. Transient operation of FB plants

As reviewed in Section 2.2, a quasi-static behavior for the gas side is a commonly used assumption when modeling the dynamics of combustion plants because i) it yields substantial savings related to the complexity and computational cost of the model; and ii) the dynamic gas-solids interactions are complex and there is a lack of measurements under industrial conditions. The validity of this assumption can be explored based on the results on the dynamic interplay between the gas and water-steam sides in FB plants obtained in **Papers I–III**.

The simulated inherent stabilization times (t_s) of the reference fuel-fed FB plants for the open-loop load changes (-20% in fuel load) are summarized in Table 14. The inherent stabilization time of a parameter is of importance since it indicates the minimum ramping rate for which a quasi-static behavior can be assumed. A sensitivity analysis of the load ramping rate on gas side parameters illustrates this, which is shown in **Paper I**.

It is evident from Table 14 that the stabilization times are of the same order of magnitude in both the gas sides and the water-steam sides in CFB furnaces (very roughly around 10 minutes). Alternatively, in BFBs, the relevant in-furnace parameters interfacing with the water-steam side – Q_{walls} and T_{top} – exhibit dynamics that are one order of magnitude faster (around 1 minute) than the water-steam side (10-20 minutes). Note that although the times reported in Table 14 refer to the specific sizes investigated (100-140 MW_{th}), they are a function of the fluid residence time and chemical processes involved, both rather independent of unit size.

Table 14. Summary of the inherent stabilization times of the gas and water-steam sides of the investigated fuel-fed FB plants.

Variable	**Inherent stabilization times (min)**	
Gas side	CFB furnace	BFB furnace
Temperatures	6–15	T_{db}: 10–26 T_{top}: 1–1.5
Heat transfer to waterwalls	2–10	0.5–1.0
Water-steam side		
Live steam pressure and mass flow	10–15	
Power generation	8–15	
DH temperatures and heat flows	13–25	

Based on the above, it can be concluded that i) for fuel-fed CFB plants, the description of the dynamics of the gas side is crucial for an accurate prediction of the transient performance when the changes of interest are shorter than 10-20 minutes; while ii) for fuel-fed BFB plants, assuming a quasi-static behavior of the gas side might suffice as the dynamics are governed by the water-steam side; and iii) for changes that are larger than 25 minutes, quasi-static behavior can be assumed for the whole plant in both CFB and BFB cases.

These results are relevant when assessing the transient capabilities of FBC plants to provide load changes in short timeframes, as needed for instance for primary control reserve (characterized by response times in the order of 30 seconds in most European markets). For such dynamic plant simulations, the above results indicate that the assumption of quasi-static behavior of the gas side is not valid and thus the dynamics of the gas side need to be modeled. Furthermore, fast load ramping would temporarily yield undesired emissions (as indicated by the results in **Paper I**), highlighting the importance of a holistic dynamic model of the gas side for a complete assessment of the flexibility capabilities of FB units.

Further, the knowledge on FB dynamics gained through this thesis can serve to preliminarily assess to what extent VRE-fed plants can cope with the timescales required to operate transiently and to provide the VMS discussed in Section 5.2. While the dynamics of the water-steam side computed for the fuel-fed plants apply to the VRE-fed layouts (since water-steam side equipment does not vary significantly), the characteristic times within the gas side of VRE-fed reactors need futher study. For this, the expressions derived in Section 4.1.2 (Table 13) can be used to estimate the behavior of VRE-fed units as long as the fluidization regime is kept similar to that of FB boilers, i.e. a low aspect ratio of the reactor geometry and of the solids bed, and Geldart B solids [136]. An estimation of the timescale of each of the in-furnace mechanisms for each of the reactors in the VRE-fed layouts considered in this thesis (Section 3.2.1) is provided in Table 15.

Table 15. Estimation of the characteristic times of the in-furnace mechanisms within the different VRE-fed FB reactors evaluated in this thesis.

Mechanism	**Charging reactors**			**Discharging reactors**	
	Thermal reductor	Chemical reductor	Calciner	Carbonator	Oxidator
Fluid dynamics	$\leq 10^0$ minutes	$<10^0$ minutes	$<10^0$ minutes	$<10^0$ minutes	$<10^0$ minutes
Chemical conversion	10^1 minutes	$<10^2$ minutes	$<10^1$ minutes	$<10^1$ minutes	10^1 minutes
Heat transfer	depends on design of heat supply	depends on thermal mass (solids inventory and heat capacity)	depends on design of heat supply	depends on thermal mass (solids inventory and heat capacity)	depends on thermal mass (solids inventory and heat capacity)

The characteristic times for the fluid dynamics depend on several parameters, but will remain within the second-minute timescale for gas velocities in the order of 1-7 m/s. Regarding the chemical conversion, most of the process conditions were chosen (see Section 3.2 and **Papers V** and **VII**) to allow for a reaction time <10 minutes, except for the chemical reduction of Fe with H_2, which is on the <100 minutes timescale. Lastly, regarding the heat transfer, for discharging reactors it can be estimated through the expressions derived for fuel-fed units once a solids inventory and heat capacity are given. Similarly, for chemically charged units (which are refractory-lined) the heat transfer is governed by the thermal mass of the unit. For thermally charged reactors (calciner and thermal reductor), the characteristic time of the heat transfer becomes largely dependent on the design of the heat supply, e.g., directly/indirectly irradiated, electrically heated, etc. (see [14]).

In conclusion, it can be expected that the dynamics of VRE-fed plants will remain within the same order of magnitude as fuel-fed plants, i.e., in the 10^1 minutes timescale. According to the estimations presented in Table 15, the bottleneck for transient operation will most likely lay on the chemical conversion of the solid material, especially for the chemical reduction. Nonetheless, improvements can be made in this regard by decreasing the solids particulate size within the accepted limits or manipulating the reactor pressure and temperature.

5.2. Provision of variation management strategies

This subsection discusses the implications of the results presented in Chapter 4 in relation to the variation management strategies (VMS) introduced in Section 2.1. Table 16 lists the different VMS explored within the present thesis with their links to the appended papers, their identified key features and the characteristics of the energy systems that would benefit most from each VMS, respectively.

Table 16. VMS explored in this thesis (and related appended papers) together with their pros, cons, and energy system types that would benefit the most from each.

VMS	Solution	Applicable to	Pros	Cons	Paper
Shifting	Storage of solar thermal energy	Systems with high share of CSP	Unlimited storage time potential. Stored energy can be freighted. Efficiency up to 45%. Low storage cost.	High investment cost. Challenging reactor design.	**Papers V-VI**
	Storage of electricity	Systems with high share of renewable electricity.	Unlimited storage time potential. Stored energy can be freighted. Low storage cost.	Higher costs than batteries.	**Paper VII**
Absorbing	Electricity to DH	Systems with high demand for DH.	Efficiency up to 90%. Unlimited storage time potential.	High electrolyzer cost. Challenging reactor design.	**Paper VII**
	Electricity to H_2	Systems with a high demand for H_2, (e.g., H_2-based transportation)	Avoids costly H_2 storage	Complex 3-reactor system	**Paper VII**
	Electricity to partially-reduced Fe oxide	Systems with a developed metal industry	Distributes the reduction of Fe, creates backups	Needs transport to the steel production plants	**Paper VII**
Complementing	Load-following operation	Systems with high shares of solar and wind power	Capabilities in the 10^1 minutes timescale. Faster ramp-up than ramp-down	Decreased lifetime of components. Increased emissions.	**Papers I-IV**

Shifting

Shifting strategies shape the net load curve by shifting electricity in time [23]. In this work, the storage of non-dispatchable VRE has been explored, which can be in the form of i) high-temperature non-dispatchable heat (e.g., CSP solar) or ii) non-dispatchable electricity. The investigated VRE-fed FB process layouts show a relatively high levels of efficiency (20%-45%) when storing energy for dispatchable electricity production, offering theoretically unlimited storage times. In addition, the cost analyses show that despite the relatively high plant costs, the storage costs for most of the layouts (Ca- and Fe-based processes) are low. The latter makes the VRE-fed plants assessed here a beneficial solution for systems that are dominated by variations characterized by low amplitude and low frequency, i.e., systems with high shares of wind power [25] wherein the variations are characterized by longer time scales (typically weeks). On the other end, for systems that are dominated by solar photovoltaics (with

variations times in the order of hours), FB plants are hardly competitive against other shifting technologies such as batteries, with investment costs in the order of 0.1-0.2 M$/MWh$_{stored}$ [4] (as compared to the 0.16-1.00 M$/MWh$_{stored}$ of the processes computed here). Regarding the storage of solar thermal energy, the economic performance of the TCES plants assessed here is slightly worse than the well-established thermal energy storage (TES) solutions, with BESP in the range of 30-320 $/MWh for the 100MW$_{th}$ size [137]. Nonetheless, further development of TCES may be pursued since TES is limited by i) a storage temperature (500-600 ºC) which restricts the discharge in form of electricity production, and ii) a limited storage time.

An important aspect of the VRE-fed layouts is their potential for freighting the solid material acting as energy carrier, which enables energy trading between regions and shifting of the net load curve both temporally and spatially. Note that if shipping is accounted for, the efficiencies reported would need to incorporate the energy used for transportation.

Absorbing

Absorbing strategies use the excess electricity in the grid to create another energy carrier. In this work, the main absorbing strategy investigated is the electricity-charged FeL process layout, which produces dispatchable heat. This layout is especially useful in systems with a DH demand (e.g., in the Nordic countries). The reported energy efficiency for this process is around 90% (considering the use of a heat pump that recovers the energy losses from the electrolyzers), which can be compared to other power-to-heat technologies such as electric boilers. Nonetheless, the main difference lays on that the process presented here provides dispatchable heat, i.e., offering both absorbing and shifting strategies. Thus, a fair comparison could be established with electric boiler (or heat pump) with thermal energy storage, with investment costs in the order of 0.2-5 M$/MWh$_{stored}$ [138] noting that the storage time of the TCES process presented here is theoretically unlimited. This is especially important as curtailment can often occur during the summer months, which would rule out the use of power-to-heat technologies that lack storage. Additionally, a recent cost assessment [132] revealed that the economic feasibility of power-to-heat technologies is worsen with increased electricity price variations, which differs from the processes investigated in this thesis (see Section 4.2.2)

The possibility to produce H_2 on-demand is also explored in Paper VII (and later discussed in Section 5.3.3). This technology could potentially outcompete conventional electrolysis schemes that include H_2 storage technologies, as the results from [132] suggested. Nonetheless, the installation and operation of a 3-reactor system are costly and can be complex, and such layout requires a demand for H_2 (such as for heavy transport, or to be burnt in a gas turbine for absorbing and shifting VMS). Lastly, partially-reduced Fe as an energy carrier and/or raw material for the steel industry is a possibility, especially in regions that have the existing infrastructure and where zero-emissions steel production is being promoted such as in Sweden. Decentralizing the reduction of Fe can also offer advantages in terms of production backup and more useful utilization of the waste heat.

Previous work [25], [23] has shown that absorbing strategies are more efficient at promoting wind power than shifting strategies, except in systems that have large shares of hydropower. In other words, the value of absorbing strategies surges in systems with high shares of wind power. When added to the fact that the BHSP is reduced as the variations in electricity price increase (see Section 4.2.2), this indicates that the FeL process explored here has a high

potential as a strategy for flexible, VRE-fed, FB plants in future energy systems with large shares of wind power.

Complementing

Complementing strategies target to produce additional electricity when required. This relates to the results on load ramping capabilities of fuel-fed FB plants presented in Section 4.1.2 and discussed in Section 5.1. Note that while those results focus on load reduction, it has been shown [**Paper I-IV**] that increasing the load (a feature needed for complementing strategies) stabilizes in average 10-15% faster than decreasing the load (downregulation). Thus, the results presented in Section 4.1.2 are considered valid for assessing the capabilities of fuel-fed FB plants as complementing providers.

As described in Section 5.1, ∼0.08 %/s is the fastest simulated ramping rate at which FB plants can provide load changes using boiler-following control strategies and up to ∼25 %/s using turbine-following control strategies. While aspects such as component lifetime and emissions of unburnt gases will most likely limit the capabilities of the latter strategy, these results indicate that FB plants could potentially be operated to cover variations in the minute timeframe at the expense of increased O&M cost. Slower load ramps in the order of 0.05-0.005 %/s not impacting the O&M costs can be achieved which, deployed together with wind power, would have the ability to replace base-load and mid-load technologies in systems with a low share of wind power [25].

The part-load efficiency and operational boundaries (see Section 2.1.2) are also relevant when it comes to complementing strategies. In this regard, operation with turbine bypass has been shown to increase temporarily the electrical power boundaries of the plants, thereby reducing the minimum power load without altering the combustor. In addition, operation with turbine bypass allows for the decoupling of heat and power production levels, effectively increasing the plant product flexibility.

As biomass prices are expected to surge owing that it is a limited resource with envisioned applications in the industrial and transport sectors, complementing services could also be provided by VRE-fed layouts (as long as the dynamics of the discharging reactor are kept within the same order of magnitude as those of fuel-fed reactors, see Section 5.1). For existing fuel-fed FB plants, the remaining lifetime can be decisive when it comes to deciding the role to take: i) to continue running on biomass and obtain the revenue from offering complementing strategies; or ii) to invest in in a new reactor and storage units and make use of competitively-priced electricity while benefiting from providing shifting, absorbing and complementing strategies.

5.3. Additional products and services

This section discusses the potential of FB plants to expand their portfolio by providing additional services and products besides heat and power, based on the results presented in Chapter 4 and with supporting results from the appended papers.

5.3.1. Combustible biogenic gas

FB combustors can be retrofitted to add biogenic products to their current output mix. This retrofit consists of adding an integrated gasification/pyrolysis chamber (hereinafter called *gasifier* for simplicity). This type of retrofit increases the yearly utilization of the plant as it partially decouples the plant operation from the heat and power demands. To assess the dynamic performance of this retrofit concept, the addition of a BFB gasifier providing 31.5 MW of biogenic gas to the reference plants described in Section 3.1.1 (see details in Appendix B and [52]) was considered in the dynamic process models presented in **Paper I** and **III**.

For a combustion load change at constant gasifier load, simulations indicate that the stabilization times for a load change are increased (20% on average) as compared with the original plant configuration (Section 4.1.2, Figure 23). This increase is expected because the retrofit involves the addition of bed material and new equipment both in the gas side (gasifier and loop seals, which increase the fluid-dynamics time of the solids) and the water-steam side (new heat exchangers for DH production and fuel drying), which introduces further thermal inertia into the process. A further contribution to the slower dynamics for the retrofit case lays in that the fuel burnt in the combustor consists of char to a larger extent than in the original configuration, yielding larger fuel conversion times. This effect is exacerbated at lower combustor loads, yielding even slower dynamics of the retrofit in periods with low DH demand (which adds up to the findings on slower dynamics at low loads for the original configuration, presented in Section 4.1).

Nonetheless, the retrofit concept offers an additional operational strategy for speeding the load-changing in fuel-fed FB plants: the injection into the combustor of some of the raw gas produced in the gasifier. Figure 33 shows the inherent stabilization times of the retrofitted CFB plant when applying this strategy. As seen, the inherent dynamics are reduced by an average of 18% compared to the original configuration. Thus, fuel-fed FB plants retrofitted with a gasification reactor not only have the potential to overcome the slower dynamics caused by the retrofit, but can yield higher operational flexibility when allowing the combustion of a fraction of the generated gas.

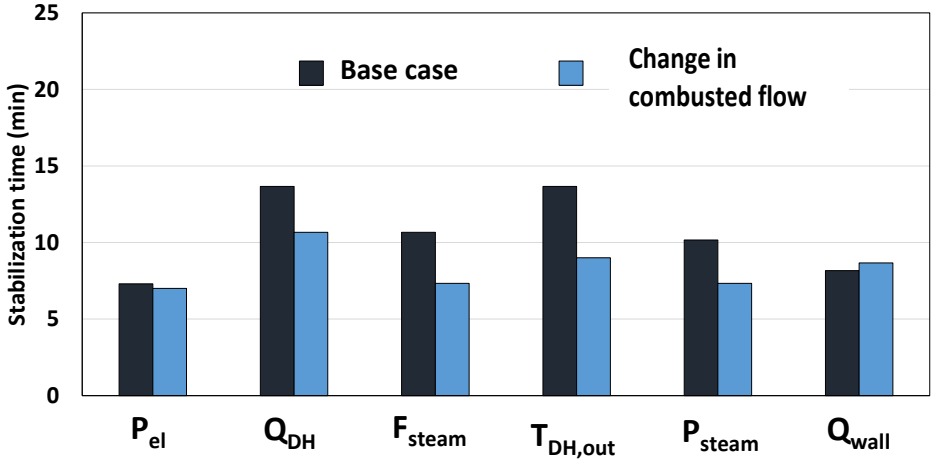

Figure 33. Stabilization times of the reference CFB plant after the addition of a FB gasifier (see Appendix B) when a fraction of the produced combustible gas is combusted in the furnace and used as a load-changing strategy. For comparison, the results from the base case (see Section 4.1.2), i.e., prior to the retrofit have been included.

5.3.2. CO_2 capture from nearby facilities

The *CaL-TCES-CCS* process layout (formulated in Section 3.2.1 and explored in detail in **Paper VI**) has been assessed in Section 4.2 as a heat and power plant with a side revenue associated with the capture of CO_2 from nearby emitters. However, to facilitate the comparison with other CO_2-capture technologies, the process can also be assessed as a CO_2-capture plant with co-production of electricity.

To study the process economic performance in terms of capture cost ($/$t_{CO2\ captured}$), the two revenues of the plant must be considered: the incoming cash flow from the CO_2 capture services (defined as *IncomeCC*) is here varied between 10, 50 and 100 $/$t_{CO2}$ [139], while the electricity selling price (*ESP*) is varied between 20, 40 and 80 $/MWh [140]. Figure 34 displays the economic performance of the process for four different process capacities (Q_{in}, see Section 3.2), for varying *IncomeCC* (vertical black bars) and *ESP* (for *IncomeCC* fixed at the base case value, 50 $/ $t_{CO2\ captured}$). Note that negative cost values indicate that the plant would be making a profit before the process lifetime set for the analysis (20 years, see Section 3.2). As seen, the obtained capture costs range from -27 to 45 $/$t_{CO2\ captured}$ for the base case (i.e., *IncomeCC* = 50 $/ $t_{CO2\ captured}$ and *ESP* = 40 $/MWh). It should be noted that this analysis i) disregards the price of the heat input (which accounts roughly for an additional 40% of the investments, see Section 4.2); and ii) assumes a solids degree of conversion of 0.15, which is an uncertain value that depends on factors outside the scope of this study. On the latter regard, if a solids conversion of 0.25 is assumed instead, cost reductions of around 20% are observed, and a residual capture cost of around 16 $/$t_{CO2\ captured}$ is reached for solids conversion values >0.5. The latter cost value falls within the predictions by Fenell and Anthony [90], who reported captured costs of the calcium looping process within the range of 20-40 $/$t_{CO2\ captured}$ albeit accounting for the heat flow within the OPEX.

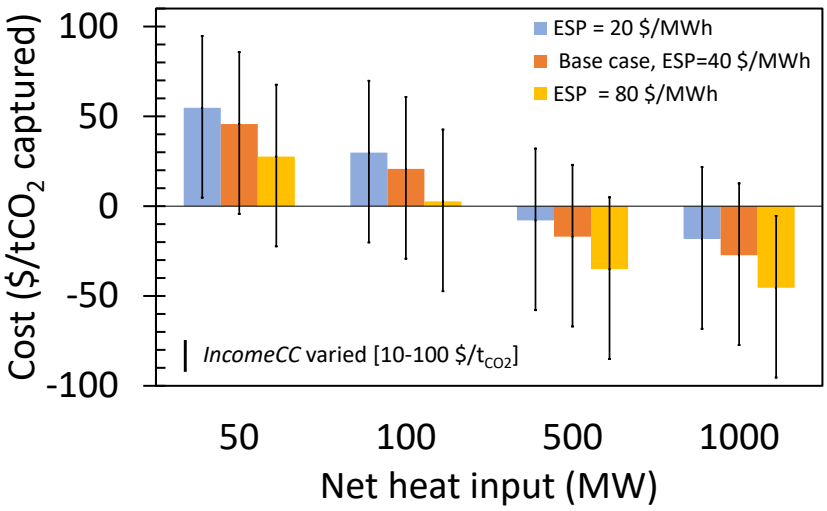

Figure 34. Economic performance the *CaL-TCES-CCS* process layout expressed as a capture cost when the revenues associated with the CO_2 capture (*IncomeCC*, vertical black lines) and the sale of electricity (*ESP*, colored bars) are varied. Note that the cost of the heat input or heat generation components are excluded from this calculations Source: **Paper VI**.

5.3.3. H_2 on-demand

On-demand H_2 production is of great interest for several sectors, e.g., heavy transport, for which transporting H_2 to remote locations and storing it becomes a major challenge. FB plants can facilitate the on-demand production of H_2 through the so-called wet metal cycle (see Figure 35 and **Paper VII**). This process modifies the electricity-charged process layout depicted in Section 3.2.1 by splitting the oxidation step into two stages using steam (for H_2 production) and air (for heat production), respectively. Since the metal is reduced during low-electricity-price periods and can be stored indefinitely, the production of H_2 in the steam oxidation reactor can adapt to the demand and be decoupled from the electricity prices without the need for costly H_2 storage.

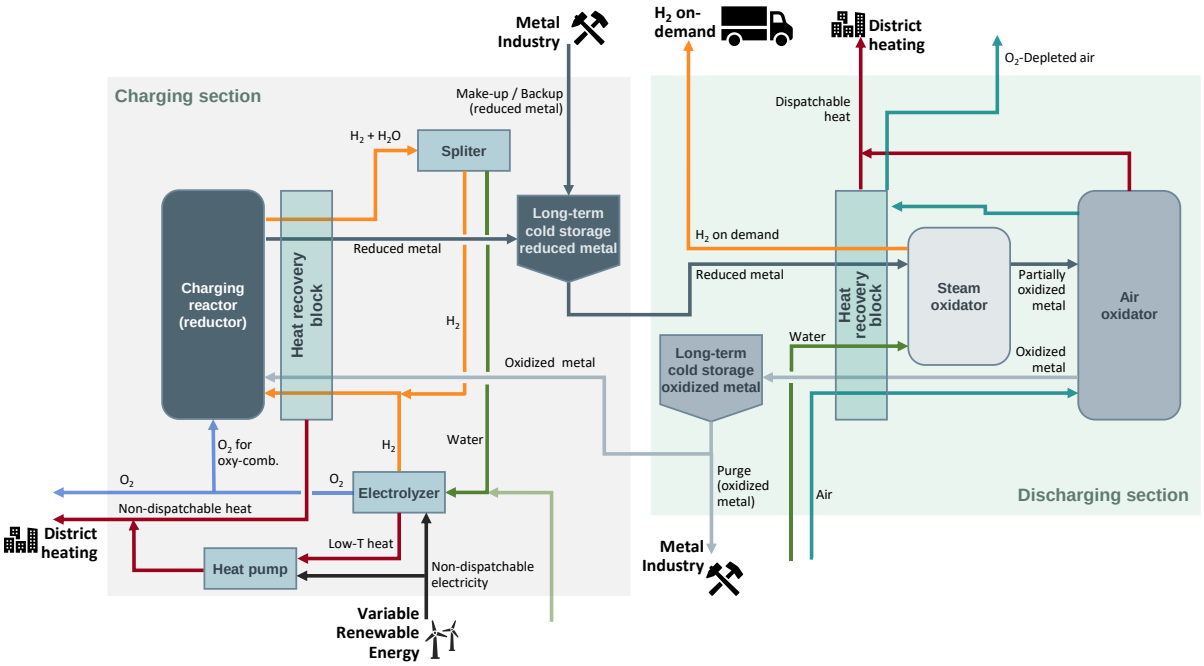

Figure 35. Schematic of an electricity-fed FB plant layout with on-demand production of H_2. The discharging section is split between two oxidations: first partially with steam, second fully with air. Source: **Paper VII.**

The different operational modes of this layout are a function of the availability of competitive-priced electricity and the demands for heat and H_2 (for a detailed operational map see **Paper VII**). It is important to note that H_2 can also be outputted from the charging section by running the electrolyzers at higher loads than those required by the reduction reactor, which is attractive for H_2 demand periods with competitive electricity prices. Instead, periods of high electricity price represent an opportunity for the plant to sell the electricity generated in the air oxidation reactor.

6. Conclusion

FB plants are found to be a versatile technology capable to adapt to the flexibility needs of different future energy systems. Regarding the two pathways explored:

- Transient operation of fuel-fed FB plants is governed by the dynamics of the water-steam side. Hence, their capabilities for load-changing operation are similar to other Rankine-based thermal technologies.
- FB plants can benefit from turning into VRE-fed facilities if the generation of additional byproducts and services (such as H_2 on-demand or CO_2 capture) is considered.

As the main outcome, this thesis elucidates new operational and design opportunities for FB plants to contribute towards net-zero energy systems, both from the energy supply and demand sides. This is needed since FB plants have traditionally been designed for converting carbon-based fuels and operated under slow load-changing conditions. For this, dynamic process modeling and techno-economic modeling have been applied to different FB layouts.

Related to the four research questions of the thesis (listed in Section 1.2.1), the following conclusions are drawn:

- Regarding **fuel-fed** FB plants:

1. *Research question 1:* What are the mechanisms governing the dynamics of the gas side of fuel-fed FB plants and what are their characteristic times in comparison to those of the water-steam side?

    - The governing in-furnace mechanisms for FB reactors (heat transfer, fuel conversion and fluid dynamics) are included in the dynamic modeling of FB plants. Their magnitudes and dependencies of their stabilization times for each furnace type (BFB/CFB) have been characterized. As main difference between the furnace types, BFB units (the dynamics of which are largely driven by the fluid dynamics within the furnace) display stabilization times that range from a few seconds to 1 minute, which are one order of magnitude faster than those of CFB furnaces (driven instead by the fuel conversion and heat transfer).

    - Characteristic response times of the gas side are not longer than those of the water-steam side (similar times in the case of CFB furnaces, and one order of magnitude shorter in the case of BFB designs). Thus, the bottleneck for fast load-changing operation involves the water-steam equipment. This challenges the traditional understanding that FB plants would be less-suited for fast load changes, and suggests instead that they hold capabilities similar to those of other thermal technologies equipped with Rankine cycles.

2. *Research question 2:* Can control and operational strategies enable faster load-changing capabilities than those required today in fuel-fed FB plants?

    - Operational and control structures that aim to reduce the plant ramping rate can overcome the inherent dynamics of the gas side. In addition, they enhance the product flexibility of FB plants by temporarily decoupling the production of heat and power. However, they may lead to temporary efficiency losses, undesired emissions and a greater need for component maintenance and replacement.

- Regarding **VRE-fed** FB plants:

3. *Research question 3:* Which FB-based process layouts can offer large-scale energy storage to the system?

    - Large-scale VRE-fed layouts for solar- and electricity-charging applications are formulated based on three different metallic chemical systems: i) carbonation/calcination (calcium); ii) thermally reduced redox (cobalt oxides); and iii) chemically reduced redox (iron oxides). Two different process layouts are proposed for each material in order to evaluate the production of additional services.

4. *Research question 4:* What are the technical and economic performances of the layouts formulated in 3) and how do they depend on the characteristics of the energy systems in which they are deployed?

    - Within the solar-charged layouts, the Co-based layouts provide the best technical performance mainly due to their larger extent of reaction and energy density. Nonetheless, the Ca-based processes show better economic performance as the cost structures of cobalt-based processes are largely affected by the material cost. Energy systems with a carbon tax around 80-100 $/t$CO_2$ would provide the conditions for VRE-fed calcium-based FB plants to provide variation management strategies to the grid at both demand and supply sides while capturing CO_2 from hard-to-abate facilities

    - The electricity-charged layouts based on FeO/Fe_2O_3 represent a cost-efficient solution for retrofitting existing FB boilers into units providing absorbing and shifting VMS to the grid. The initial inventories and makeup flows of solid material required by this layout are feasible when compared to the reserves and mining rates of Fe ore in e.g., Sweden.

7. Recommendations for further work

The following is a brief list of recommendations for future research to be carried out based on the outcomes of this thesis.

- The dynamics of VRE-fed plants remain to be explored. Even though the water-steam side of VRE-fed schemes remains basically the same as that of fuel-fed plants, the gas side may differ. Understanding and controlling the transient performances of VRE-fed plants is mandatory to fulfil their dual role as VMS-providers in the supply and demand sides as proposed in the present work.

- The dynamic process model of fuel-fed FB plants presented in this thesis results in a large set of non-linear equations, yielding long computational times (around 3 hours for the initialization and simulation of a given scenario). Thus, reducing the complexity of the model through reduced-order modeling or surrogate modeling techniques is needed to use the model for optimization and model predictive control applications.

- The transient operation included in this work focuses exclusively on changes that occur during operation, with the start-up sequence lying outside the scope of the work. Therefore, the start-up procedure should be modeled and optimized, to allow a broader assessment of the full capabilities of FB plants to provide rapid load changes to the grid.

- The analyses provided in this work could be developed by including i) the income related to the VMS provided; and ii) the costs related to the lifetime reductions of critical equipment due to thermal stresses and fatigue caused by flexible operation. These two items would enable the definition of an optimal operational map for a given FB plant.

- The impact of FB plants as flexibility providers on regional and national energy systems must be explored in order to refine the system boundaries used for the assessments. This is especially critical when evaluating VRE-fed FB plants, as their impacts on the energy system are on both the supply and demand sides.

- Experimental investigations are required to bring forward the development and upscaling of the gas-solids TCES technology. Given the fact that FB is the preferred reactor technology for large-scale deployment, the fluidization behavior of metal powders gains additional relevance. Further, the effect of the cyclic cooling/heating of the solids on the mechanical and reactive properties should be studied, as this is an important aspect of TCES layouts that differs from other well-tested processes such as CLC.

Appendix A. Linear cost optimization model

The cost-optimal size and operation of the electricity-charged FB plants are assessed in this thesis using an existing linear optimization model presented in [132] and based on that from Toktarova et al. [141]. The overall objective of the model is to minimize the total cost (i.e., the sum of the investments and the operating costs) while ensuring that the heat demand is met. The model has an hourly resolution and a temporal scope of 1 year.

Table A1 lists all the sets, parameters and variables of the model. The set *P* represents both of the heat production capacities (namely the waste heat recovered from the electrolyzer and from the charging reactor (non-dispatchable) and the heat output from the discharging reactor (dispatchable)), as well as the storage units. The total plant cost to be minimized is defined as in Equation 19, while the constraint defined in Equation 20 ensures that the heat demand D_t^{heat} is satisfied in every time-step *t*.

Table A1: Sets, parameters and variables of the cost optimization model.

Sets	
T	Set of time-steps
P	Set of all units
P^{hpr}	Subset of *P* that includes all heat production equipment
p^{str}	Subset of *P* that includes all storages
Variables	
C_p^{inv}	Investment costs of equipment *p*
$C_p^{O\&M,fix}$	Fixed operating and maintenance cost of process *p*
C_p^{run}	Running cost of process p in time-step *t*
C_{tot}	Total heat production cost
i_p	Capacity of process *p*
$g_{p,t}$	Generation of heat and production of commodities of process *p* at time-step *t*
$soc_{p,t}$	State of charge of storage *p* at time-step *t*
z_p^{ch}	Charging of storage *p* at time-step *t*
z_p^{dis}	Discharging of storage *p* at time-step *t*
Parameters	
D_t^{heat}	Heat demand at time-step *t*
e_p	Efficiency of storage *p*

$$\min C^{tot} = \sum_{p\in P}\left(C_p^{inv} + C_p^{O\&M,fix}\right) + \sum_{p\in P}\sum_{t\in T} C_{p.t}^{run} g_{p,t} \quad (19)$$

$$\sum_{p\in P^{hpr}} g_{p,t} \geq D_t^{heat} \quad (20)$$

Lastly, Equation 21 describes the utilization of the storage units, i.e., the filling levels in each tank (of charged and discharged material) in every time-step ($soc_{p,t}$). In addition, the levels of stored materials have to be lower or equal to the total storage capacity (i_p) at all times, as expressed by Equation 22:

$$soc_{p,t} = soc_{p,t-1} + e_p z_{p,t}^{ch} - z_{p,t}^{dis}, \qquad \forall p \in P^{str}, \quad \forall t \in T \quad (21)$$

$$soc_{p,t} \leq i_p, \qquad \forall p \in P^{str} \quad (22)$$

Appendix B. Retrofit of a fuel-fed FB plant for CHP into a poly-generation plant

The poly-generation concept explored in this thesis (Section 5.2.1) comprises the addition of an indirect BFB pyrolysis reactor (*gasifier*) to the reference plants presented in Section 3.1.1. A schematic drawing of the retrofit is shown in Figure B1. In this system, dried fuel is fed to the gasifier, where it is partially converted to gas. The heat required by the process is supplied by a stream of bed material transported from the combustor, which is also returned to the combustor along with the unreacted char (for more details of the DFB gasification system, see [51]). The retrofit, in the case of an external gasifier, includes two loop seals (LS) for transporting the solids to and from the combustor, one rotating drum dryer that works with preheated air, a gas cooler and a scrubber (the latter two for the adequation of the product gas). Medium-pressure steam is extracted from the turbine train to fluidize the gasifier and loop seals, as well as to preheat the air required for drying the fuel. The cooler and scrubber generate heat that can be utilized to produce DH. Lastly, the retrofit includes the possibility for burning part of the raw gas in the combustor, if so desired. Table B1 lists the design conditions of the evaluated retrofit, and the details are available in [52].

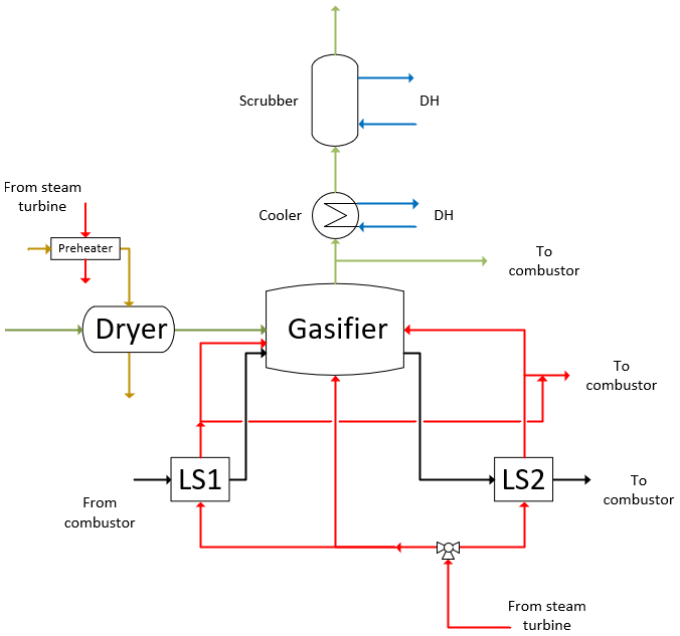

Figure B1: Schematic diagram of the retrofit assessed within the project. The same layout applies to the CFB and BFB reference plants. LS: loop seal. Source: [52]

Table B1: Design parameters of the retrofit.

	Units	CFB plant	BFB plant
Gasifier capacity (gas power)	MW	31.5	31.5
Fuel type (standard case)	-	GROT*	GROT*
Gasifier area	m^2	7	5
Steam mass flow	kg/s	0.2625	0.8476
Loop seals steam flow	kg/s	0.010	0.042
Gasifier operation temperature	°C	800	800
Fuel feeding moisture content	%	20	20
Cooling temperature	°C	300	300
Tar condensing power (design load)	MW	1.40	3.21

*GROT: branches and tops from forestry

Figure B2 shows a schematic of the overall input/output structure of the gasifier model when connected to the models of the gas and water-steam sides of fuel-fed FB plants (described in Section 3.1.2).

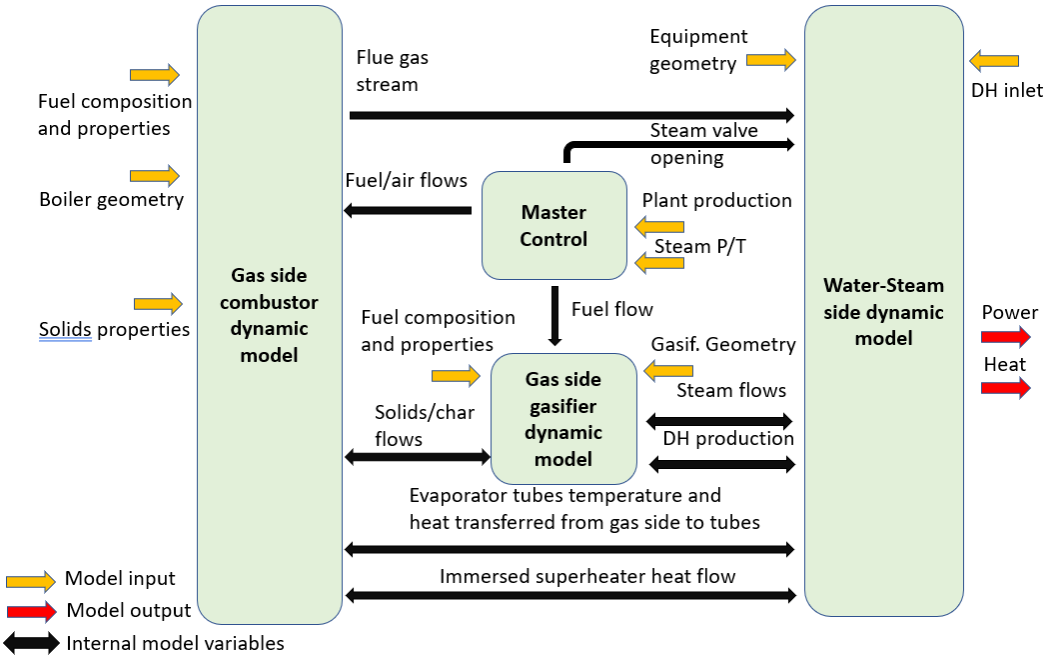

Figure B2: Input/output scheme of the integrated dynamic models including the master control.

References

[1] IPCC, “Summary for Policymakers: Climate Change 2022: Impacts, Adaptation and Vulnerability.,” 2022. doi: 10.1017/9781009325844.Front.

[2] IEA, “The role of CCUS in low-carbon power systems,” 2020. doi: 10.1787/7be68d30-en.

[3] European Commission, “Roadmap 2050,” *Policy*, no. April, pp. 1–9, 2012, doi: 10.2833/10759.

[4] International Energy Agency, “World Energy Outlook 2021 : Part of the World Energy Outlook,” Paris, 2021. [Online]. Available: https://www.iea.org/reports/world-energy-outlook-2021

[5] IEA, “Electrification,” Paris, 2022. [Online]. Available: https://www.iea.org/reports/electrification

[6] IEA, “Harnessing variable renewables: a guide to the balancing challenge,” 2011.

[7] M. A. Gonzalez-Salazar, T. Kirsten, and L. Prchlik, “Review of the operational flexibility and emissions of gas- and coal-fired power plants in a future with growing renewables,” *Renew. Sustain. Energy Rev.*, vol. 82, no. July 2017, pp. 1497–1513, 2018, doi: 10.1016/j.rser.2017.05.278.

[8] F. Johnsson, D. Johansson, U. Persson, and E. Pihl, *Pathways to Sustainable European Energy Systems*. Molndal: PR-offset, 2011.

[9] International Energy Agency, “Net Zero by 2050: A Roadmap for the Global Energy Sector,” 2021.

[10] M. Gao, F. Hong, and J. Liu, “Investigation on energy storage and quick load change control of subcritical circulating fluidized bed boiler units,” *Appl. Energy*, vol. 185, pp. 463–471, 2017, doi: 10.1016/j.apenergy.2016.10.140.

[11] H. Zhang, M. Gao, F. Hong, J. Liu, and X. Wang, “Control-oriented modelling and investigation on quick load change control of subcritical circulating fluidized bed unit,” *Appl. Therm. Eng.*, vol. 163, no. September, p. 114420, 2019, doi: 10.1016/j.applthermaleng.2019.114420.

[12] J. Kjärstad and F. Johnsson, “The European power plant infrastructure-Presentation of the Chalmers energy infrastructure database with applications,” *Energy Policy*, vol. 35, no. 7, pp. 3643–3664, 2007, doi: 10.1016/j.enpol.2006.12.032.

[13] S. Padula, C. Tregambi, R. Solimene, R. Chirone, M. Troiano, and P. Salatino, “A novel fluidized bed ‘thermochemical battery’ for energy storage in concentrated solar thermal technologies,” *Energy Convers. Manag.*, vol. 236, p. 113994, 2021, doi: 10.1016/j.enconman.2021.113994.

[14] G. Zsembinszki, A. Sole, C. Barreneche, C. Prieto, A. I. Fernández, and L. F. Cabeza, “Review of reactors with potential use in thermochemical energy storage in concentrated solar power plants,” *Energies*, vol. 11, no. 9, 2018, doi: 10.3390/en11092358.

[15] L. André and S. Abanades, “Recent advances in thermochemical energy storage via solid–gas reversible reactions at high temperature,” *Energies*, vol. 13, no. 22, 2020, doi: 10.3390/en13225859.

[16] S. Seddighi, P. T. Clough, E. J. Anthony, R. W. Hughes, and P. Lu, “Scale-up challenges and opportunities for carbon capture by oxy-fuel circulating fluidized beds,” *Appl.*

Energy, vol. 232, no. October, pp. 527–542, 2018, doi: 10.1016/j.apenergy.2018.09.167.

[17] R. Veneman, Z. S. Li, J. A. Hogendoorn, S. R. A. Kersten, and D. W. F. Brilman, "Continuous CO_2 capture in a circulating fluidized bed using supported amine sorbents," *Chem. Eng. J.*, vol. 207–208, pp. 18–26, 2012, doi: 10.1016/j.cej.2012.06.100.

[18] S. Sengupta *et al.*, "Circulating Fluid-Bed Studies for CO_2 Capture from Flue Gas using K_2CO_3/Al_2O_3 Adsorbent," *Energy and Fuels*, vol. 32, no. 8, pp. 8594–8604, 2018, doi: 10.1021/acs.energyfuels.8b01383.

[19] H. Thunman, C. Gustavsson, A. Larsson, I. Gunnarsson, and F. Tengberg, "Economic assessment of advanced biofuel production via gasification using cost data from the GoBiGas plant," *Energy Sci. Eng.*, vol. 7, no. 1, pp. 217–229, 2019, doi: 10.1002/ese3.271.

[20] A. Gómez-Barea and B. Leckner, "Modeling of biomass gasification in fluidized bed," *Prog. Energy Combust. Sci.*, vol. 36, no. 4, pp. 444–509, 2010, doi: 10.1016/j.pecs.2009.12.002.

[21] S. J. Davis *et al.*, "Net-zero emissions energy systems," *Science (80-.).*, vol. 360, no. 6396, 2018, doi: 10.1126/science.aas9793.

[22] Office of Energy Efficiency and Renewable Energy, "Confronting the duck curve: how to address over-generation of solar energy," *US Gov*, 2023. https://www.energy.gov/eere/articles/confronting-duck-curve-how-address-over-generation-solar-energy

[23] L. Göransson and F. Johnsson, "A comparison of variation management strategies for wind power integration in different electricity system contexts," *Wind Energy*, vol. 21, no. 10, pp. 837–854, 2018, doi: 10.1002/we.2198.

[24] L. Göransson, "Balancing Electricity Supply and Demand in a Carbon-Neutral Northern Europe," *Energies*, vol. 16, no. 8, 2023, doi: 10.3390/en16083548.

[25] V. Johansson and L. Göransson, "Impacts of variation management on cost-optimal investments in wind power and solar photovoltaics," *Renew. Energy Focus*, vol. 32, no. March, pp. 10–22, 2020, doi: 10.1016/j.ref.2019.10.003.

[26] J. Beiron, F. Normann, F. Johnsson, and G. Lisa, "Flexibility provision by combined heat and power plants – An evaluation of benefits from a plant and system perspective," *Energy Convers. Manag. X*, vol. 16, p. 100318, 2022, doi: 10.1016/j.ecmx.2022.100318.

[27] S. Garðarsdóttir, L. Göransson, F. Normann, and F. Johnsson, "Improving the flexibility of coal-fired power generators: Impact on the composition of a cost-optimal electricity system," *Appl. Energy*, vol. 209, no. June 2017, pp. 277–289, 2018, doi: 10.1016/j.apenergy.2017.10.085.

[28] J. Beiron, "Combined heat and power plants in decarbonized energy systems," Chalmers University of Technology, 2022. [Online]. Available: https://research.chalmers.se/en/publication/531778

[29] R. M. Montañés, "Transient performance of combined cycle power plant with absorption based post-combustion CO_2 capture: dynamic simulations and pilot plant testing," NTNU, 2018.

[30] W. Wang, Y. Sun, S. Jing, W. Zhang, and C. Cui, "Improved boiler-turbine coordinated control of CHP units with heat accumulators by introducing heat source regulation," *Energies*, vol. 11, no. 10, 2018, doi: 10.3390/en11102815.

[31] D. Zhang, Y. Hu, and Y. Gao, “Flexibility Improvement of CHP Unit for Wind Power Accommodation,” *J. Mod. Power Syst. Clean Energy*, vol. 10, no. 3, pp. 731–742, 2022, doi: 10.35833/MPCE.2020.000630.

[32] S. Kahlert and H. Spliethoff, “Investigation of different operation strategies to provide balance energy with an industrial combined heat and power plant using dynamic simulation,” *J. Eng. Gas Turbines Power*, vol. 139, no. 1, pp. 1–8, 2017, doi: 10.1115/1.4034184.

[33] C. Gustavsson and C. Hulteberg, “Co-production of gasification based biofuels in existing combined heat and power plants - Analysis of production capacity and integration potential,” *Energy*, vol. 111, pp. 830–840, 2016, doi: 10.1016/j.energy.2016.06.027.

[34] G. Martinez Castilla, M. Biermann, R. M. Montañés, F. Normann, and F. Johnsson, “Integrating carbon capture into an industrial combined-heat-and-power plant: performance with hourly and seasonal load changes,” *Int. J. Greenh. Gas Control*, vol. 82, no. January, pp. 192–203, 2019, doi: 10.1016/j.ijggc.2019.01.015.

[35] M. Richter, G. Oeljeklaus, and K. Görner, “Improving the load flexibility of coal-fired power plants by the integration of a thermal energy storage,” *Appl. Energy*, vol. 236, no. October 2018, pp. 607–621, 2019, doi: 10.1016/j.apenergy.2018.11.099.

[36] E. Mollenhauer, A. Christidis, and G. Tsatsaronis, “Increasing the Flexibility of Combined Heat and Power Plants With Heat Pumps and Thermal Energy Storage,” vol. 140, no. February, pp. 1–8, 2018, doi: 10.1115/1.4038461.

[37] F. Alobaid, N. Mertens, R. Starkloff, T. Lanz, C. Heinze, and B. Epple, “Progress in dynamic simulation of thermal power plants,” *Prog. Energy Combust. Sci.*, vol. 59, pp. 79–162, 2017, doi: 10.1016/j.pecs.2016.11.001.

[38] I. Avagianos, D. Rakopoulos, S. Karellas, and E. Kakaras, “Review of Process Modeling of Solid-Fuel Thermal Power Plants for Flexible and Off-Design Operation,” *Energies*, vol. 13, no. 6587, 2020, doi: doi:10.3390/en13246587.

[39] W. L. Luyben, *Process modeling, simulation, and control for chemical engineers*, Second Edi. McGraw-Hill, 1996.

[40] S. Stultz and J. Kitto, “Controls for Fossil Fuel-Fired Steam Generating Plants,” in *Steam: its generation and use*, The Babcok and Wilcox Company, 2005, pp. 41–1, 41–21. doi: 10.1515/9783110214130.489.

[41] S. Skogestad and I. Postlethwaite, *Multivariable Feedback Control. Analysis and design*. Wiley, 2006.

[42] IPCC, *Climate Change 2014: Mitigation of Climate Change*. Cambridge University Press, 2014. doi: 10.1017/CBO9781107415416.

[43] M. Steyn *et al.*, “Global Status of CCS 2022,” *Glob. Status CCS*, 2022, [Online]. Available: https://status22.globalccsinstitute.com/wp-content/uploads/2022/12/Global-Status-of-CCS-2022_Download_1222.pdf

[44] T. Kuramochi, A. Ramírez, W. Turkenburg, and A. Faaij, “Comparative assessment of CO_2 capture technologies for carbon-intensive industrial processes,” *Prog. Energy Combust. Sci.*, vol. 38, no. 1, pp. 87–112, 2012, doi: 10.1016/j.pecs.2011.05.001.

[45] M. Biermann, “Partial CO_2 capture to facilitate cost-efficient deployment of carbon capture and storage in process industries,” Chalmers University of Technology, 2022.

[Online]. Available: https://research.chalmers.se/en/publication/531680

[46] P. Basu, “Combustion of coal in circulating fluidized-bed boilers: A review,” *Chem. Eng. Sci.*, vol. 54, no. 22, pp. 5547–5557, 1999, doi: 10.1016/S0009-2509(99)00285-7.

[47] F. Winkler, “Verfahren zum Herstellen von Wassergas,” DE437970c, 1922

[48] J. R. Grace, X. Bi, and N. Ellis, *Essentials of fluidization technology*. Wiley-VCH, 2020. doi: 10.1002/9783527699483.

[49] J. Koornneef, M. Junginger, and A. Faaij, “Development of fluidized bed combustion — An overview of trends , performance and cost,” *Prog. Energy Combust. Sci.*, vol. 33, no. October, pp. 19–55, 2007, doi: 10.1016/j.pecs.2006.07.001.

[50] K. Laursen and J. R. Grace, “Some implications of co-combustion of biomass and coal in a fluidized bed boiler,” *Fuel Process. Technol.*, vol. 76, no. 2, pp. 77–89, 2002, doi: 10.1016/S0378-3820(02)00021-8.

[51] A. Larsson, M. Seemann, D. Neves, and H. Thunman, “Evaluation of Performance of Industrial-Scale Dual Fluidized Bed Gasifiers Using the Chalmers 2 − 4-MW,” 2013.

[52] D. Pallarès, G. Martinez, F. Johnsson, A. Larsson, C. Gustavsson, and G. Gustafsson, “Kostnadseffektiva och flexibla samproduktionsanläggningar för maximalt,” 2021. [Online]. Available: https://www.energimyndigheten.se/forskning-och-innovation/projektdatabas/sokresultat/?registrationnumber=2018-004058

[53] D. Pallarès and F. Johnsson, *Modeling of fluidized bed combustion processes*. 2013. doi: 10.1533/9780857098801.2.524.

[54] K. Atsonios, A. Nesiadis, N. Detsios, K. Koutita, N. Nikolopoulos, and P. Grammelis, “Review on dynamic process modeling of gasification based biorefineries and bio-based heat & power plants,” *Fuel Process. Technol.*, vol. 197, no. March 2019, p. 106188, 2020, doi: 10.1016/j.fuproc.2019.106188.

[55] F. Johnsson, H. Thunman, and D. Pallarès, “Future applications of circulating fluidized-bed technology,” in *Proceedings of CFB-13 conference*, 2021, pp. 26–35.

[56] W. L. Luyben, *Plantwide dynamic simulators in chemical processing and control*. New York: Marcel Dekker, 2002.

[57] D. Pallarès and F. Johnsson, “Macroscopic modelling of fluid dynamics in large-scale circulating fluidized beds,” *Prog. Energy Combust. Sci.*, vol. 32, no. 5–6, pp. 539–569, 2006, doi: 10.1016/j.pecs.2006.02.002.

[58] E. Oko and M. Wang, “Dynamic modelling , validation and analysis of coal-fired subcritical power plant,” *FUEL*, vol. 135, pp. 292–300, 2014, doi: 10.1016/j.fuel.2014.06.055.

[59] A. Benato, A. Stoppato, and A. Mirandola, “Dynamic behaviour analysis of a three pressure level heat recovery steam generator during transient operation,” *Energy*, vol. 90, pp. 1595–1605, 2015, doi: 10.1016/j.energy.2015.06.117.

[60] R. M. Montañés, S. GarÐarsdóttir, F. Normann, F. Johnsson, and L. O. Nord, “Demonstrating load-change transient performance of a commercial-scale natural gas combined cycle power plant with post-combustion CO_2 capture,” *Int. J. Greenh. Gas Control*, vol. 63, no. May, pp. 158–174, 2017, doi: 10.1016/j.ijggc.2017.05.011.

[61] F. Alobaid *et al.*, “Dynamic simulation of a municipal solid waste incinerator,” *Energy*, vol. 149, pp. 230–249, 2018, doi: 10.1016/j.energy.2018.01.170.

[62] J. Beiron, R. M. Montañés, F. Normann, and F. Johnsson, “Dynamic modeling for assessment of steam cycle operation in waste-fired combined heat and power plants Absolute Percentage Deviation,” *Energy Convers. Manag.*, vol. 198, no. August, p. 111926, 2019, doi: 10.1016/j.enconman.2019.111926.

[63] A. Cammi, F. Casella, M. E. Ricotti, and F. Schiavo, “An object-oriented approach to simulation of IRIS dynamic response,” *Prog. Nucl. Energy*, vol. 53, no. 1, pp. 48–58, 2011, doi: 10.1016/j.pnucene.2010.09.004.

[64] R. M. Montañés, J. Windahl, J. Pålsson, and M. Thern, “Dynamic Modeling of a Parabolic Trough Solar Thermal Power Plant with Thermal Storage Using Modelica,” *Heat Transf. Eng.*, vol. 39, no. 3, pp. 277–292, 2018, doi: 10.1080/01457632.2017.1295742.

[65] P. J. Dechamps, “Modelling the transient behavior of combined cycle plants,” *Proc. ASME Turbo Expo*, vol. 4, 1994, doi: 10.1115/94GT238.

[66] P. J. Dechamps, “Modelling the transient behaviour of heat recovery steam generators,” *Proc. Inst. Mech. Eng. Part A J. Power Energy*, pp. 265–273, 1995, doi: https://doi.org/10.1243/PIME_PROC_1995_209_005_01.

[67] J. Sandberg, R. B. Fdhila, E. Dahlquist, and A. Avelin, “Dynamic simulation of fouling in a circulating fluidized biomass-fired boiler,” *Appl. Energy*, vol. 88, no. 5, pp. 1813–1824, 2011, doi: 10.1016/j.apenergy.2010.12.006.

[68] M. Zlatkovikj, V. Zaccaria, I. Aslanidou, and K. Kyprianidis, “Simulation study for comparison of control structures for BFB biomass boiler,” in *61st SIMS Conference on Simulation and Modelling*, 2020, no. September.

[69] S. Suojanen, E. Hakkarainen, M. Tähtinen, and T. Sihvonen, “Modeling and analysis of process configurations for hybrid concentrated solar power and conventional steam power plants,” *Energy Convers. Manag.*, vol. 134, no. December, pp. 327–339, 2017, doi: 10.1016/j.enconman.2016.12.029.

[70] C. K. Park and P. Basu, “A model for prediction of transient response to the change of fuel feed rate to a circulating fluidized bed boiler furnace,” *Chem. Eng. Sci.*, vol. 52, no. 20, pp. 3499–3509, 1997, doi: 10.1016/S0009-2509(97)00128-0.

[71] Y. Majanne and P. Köykkä, “Dynamic model of a circulating fluidized bed boiler,” *IFAC Proc. Vol.*, vol. 42, no. 9, pp. 255–260, 2009, doi: 10.3182/20090705-4-SF-2005.00046.

[72] B. Deng, M. Zhang, L. Shan, G. Wei, J. Lyu, and H. Yang, “Modeling study on the dynamic characteristics in the full-loop of a 350 MW supercritical CFB boiler under load regulation,” *J. Energy Inst.*, vol. 97, pp. 117–130, 2021, doi: 10.1016/j.joei.2021.04.014.

[73] Y. Chen and G. Xiaolong, “Dynamic modeling and simulation of a 410 t/h Pyroflow CFB boiler,” *Comput. Chem. Eng.*, vol. 31, no. 1, pp. 21–31, 2006, doi: 10.1016/j.compchemeng.2006.04.006.

[74] S. Kim, S. Choi, J. Lappalainen, and T. H. Song, “Dynamic simulation of the circulating fluidized bed loop performance under the various operating conditions,” *Proc. Inst. Mech. Eng. Part A J. Power Energy*, vol. 233, no. 7, pp. 901–913, 2019, doi: 10.1177/0957650919838111.

[75] J. Ritvanen, J. Kovacs, S. Mikko, M. Hultgren, A. Tourunen, and T. Hyppänen, “1-d

dynamic simulation study of oxygen fired coal combustion in pilot and large scale CFB boilers," in *21st International Conference on Fluidized Bed Combustion*, 2012.

[76] A. Tourunen, J. Hämäläinen, T. Hyppänen, J. Saastamoinen, K. Paakkinen, and A. Kettunen, "Study of operation of a pilot CFB-reactor in dynamic conditions," in *17th International Fluidized Bed Combustion Conference*, 2003.

[77] J. Peters, F. Alobaid, and B. Epple, "Operational flexibility of a CFB furnace during fast load change-experimental measurements and dynamic model," *Appl. Sci.*, vol. 10, no. 17, 2020, doi: 10.3390/app10175972.

[78] D. Stefanitsis, A. Nesiadis, and K. Koutita, "Simulation of a CFB Boiler Integrated With a Thermal Energy Storage System During Transient Operation," vol. 8, no. September, pp. 1–14, 2020, doi: 10.3389/fenrg.2020.00169.

[79] J. Lappalainen, A. Tourunen, H. Mikkonen, M. Hänninen, and J. Kovács, "Modelling and dynamic simulation of a supercritical, oxy combustion circulating fluidized bed power plant concept-Firing mode switching case," *Int. J. Greenh. Gas Control*, vol. 28, pp. 11–24, 2014, doi: 10.1016/j.ijggc.2014.06.015.

[80] J. Haus, E. U. Hartge, S. Heinrich, and J. Werther, "Dynamic flowsheet simulation of gas and solids flows in a system of coupled fluidized bed reactors for chemical looping combustion," *Powder Technol.*, vol. 316, pp. 628–640, 2017, doi: 10.1016/j.powtec.2016.12.022.

[81] J. Findejs, V. Havlena, J. Jech, and D. Pachner, "Model based control of the circulating fluidized bed boiler," *IFAC Proc. Vol.*, vol. 42, no. 9, pp. 44–49, 2009, doi: 10.3182/20090705-4-SF-2005.00010.

[82] T. Kataja and Y. Majanne, "Dynamic Model of a Bubbling Fluidized Bed Boiler," in *14th Nordic Process Control Workshop*, pp. 140–149.

[83] N. Selçuk and E. Degirmenci, "Dynamic Simulation of Fluidized Bed Combustors and its Validation Against Measurements Dynamic Simulation of Fluidized Bed Combustors and its Validation Against Measurements," *Combust. Sci. Technol.*, vol. 167, no. December, pp. 1–27, 2001, doi: 10.1080/00102200108952175.

[84] M. S. Yasar, N. Selçuk, and G. Kulah, "Performance and validation of a radiation model coupled with a transient bubbling fluidized bed combustion model," *Int. J. Therm. Sci.*, vol. 176, no. 1, p. 107496, 2022, doi: 10.1016/j.ijthermalsci.2022.107496.

[85] A. Galgano, P. Salatino, S. Crescitelli, F. Scala, and P. L. Maffettone, "A model of the dynamics of a fluidized bed combustor burning biomass," *Combust. Flame*, vol. 140, no. 4, pp. 371–384, 2005, doi: 10.1016/j.combustflame.2004.12.006.

[86] M. Hultgren, E. Ikonen, and J. Kova, "Once-through Circulating Fluidized Bed Boiler Control Design with the Dynamic Relative Gain Array and Partial Relative Gain," 2017, doi: 10.1021/acs.iecr.7b03259.

[87] M. Hultgren and E. Ikonen, "Integrated control and process design for improved load changes in fluidized bed boiler steam path," vol. 199, pp. 164–178, 2019, doi: 10.1016/j.ces.2019.01.025.

[88] S. Kim, S. Choi, and T. Song, "Dynamic simulation study of the steam temperature in a ultra-supercritical circulating fluidized bed boiler system," in *Proc. iMechE Part A: Journal of Power and Energy*, 2020, pp. 1–15. doi: 10.1177/0957650920915304.

[89] N. Zimmerman, K. Kyprianidis, and C.-F. Lindberg, "Waste Fuel Combustion:

Dynamic Modeling and Control," *Processes*, vol. 6, no. 11, p. 222, 2018, doi: 10.3390/pr6110222.

[90] P. Fenell and B. Anthony, *Calcium and Chemical Looping Technology for Power Generation and Carbon Dioxide (CO_2) Capture*, vol. 1, no. 82. Cambridge: Woodhead Publoshing Series, 2015.

[91] E. Alonso and M. Romero, "Review of experimental investigation on directly irradiated particles solar reactors," *Renew. Sustain. Energy Rev.*, vol. 41, pp. 53–67, 2015, doi: 10.1016/j.rser.2014.08.027.

[92] J. Baron, E. M. Bulewicz, S. Kandefer, M. Pilawska, W. Zukowski, and A. N. Hayhurst, "Combustion of hydrogen in a bubbling fluidized bed," *Combust. Flame*, vol. 156, no. 5, pp. 975–984, 2009, doi: 10.1016/j.combustflame.2008.11.014.

[93] Y. Yan, K. Wang, P. T. Clough, and E. J. Anthony, "Developments in calcium/chemical looping and metal oxide redox cycles for high-temperature thermochemical energy storage: A review," *Fuel Process. Technol.*, vol. 199, no. November 2019, p. 106280, 2020, doi: 10.1016/j.fuproc.2019.106280.

[94] L. André, S. Abanades, and G. Flamant, "Screening of thermochemical systems based on solid-gas reversible reactions for high temperature solar thermal energy storage," *Renew. Sustain. Energy Rev.*, vol. 64, pp. 703–715, 2016, doi: 10.1016/j.rser.2016.06.043.

[95] C. Ortiz, J. M. Valverde, R. Chacartegui, L. A. Perez-Maqueda, and P. Giménez, "The Calcium-Looping ($CaCO_3$/CaO) process for thermochemical energy storage in Concentrating Solar Power plants," *Renew. Sustain. Energy Rev.*, vol. 113, no. July, p. 109252, 2019, doi: 10.1016/j.rser.2019.109252.

[96] J. C. Abanades, "Calcium looping for CO_2 capture in combustion systems," *Fluid. Bed Technol. Near-Zero Emiss. Combust. Gasif.*, no. Edited by Fabrizio Scala, pp. 931–970, 2013, doi: 10.1533/9780857098801.4.931.

[97] C. Ortiz, J. Manuel Valverde, R. Chacartegui, L. A. Pérez-Maqueda, and P. Gimenez-Gavarrell, "Scaling-up the Calcium-Looping Process for CO_2 Capture and Energy Storage," *KONA Powder Part. J.*, no. March, pp. 1–20, 2021, doi: 10.14356/kona.2021005.

[98] A. N. Antzara, A. Arregi, E. Heracleous, and A. A. Lemonidou, "In-depth evaluation of a ZrO_2 promoted CaO-based CO_2 sorbent in fluidized bed reactor tests," *Chem. Eng. J.*, vol. 333, no. October 2017, pp. 697–711, 2018, doi: 10.1016/j.cej.2017.09.192.

[99] W. E. Wentworth and E. Chen, "Simple thermal decomposition reactions for storage of solar thermal energy," *Sol. Energy*, vol. 18, no. 3, pp. 205–214, 1976, doi: 10.1016/0038-092X(76)90019-0.

[100] A. Lyngfelt, "Chemical Looping Combustion : Status and Development Challenges," *Energy and Fuels*, vol. 34, pp. 9077–9093, 2020, doi: 10.1021/acs.energyfuels.0c01454.

[101] S. Abanades, P. Charvin, G. Flamant, and P. Neveu, "Screening of water-splitting thermochemical cycles potentially attractive for hydrogen production by concentrated solar energy," *Energy*, vol. 31, no. 14, pp. 2805–2822, 2006, doi: 10.1016/j.energy.2005.11.002.

[102] C. Agrafiotis, M. Roeb, and C. Sattler, "A review on solar thermal syngas production via redox pair-based water/carbon dioxide splitting thermochemical cycles," *Renew.*

Sustain. Energy Rev., vol. 42, pp. 254–285, 2015, doi: 10.1016/j.rser.2014.09.039.

[103] S. Chuayboon and S. Abanades, "An overview of solar decarbonization processes, reacting oxide materials, and thermochemical reactors for hydrogen and syngas production," *Int. J. Hydrogen Energy*, vol. 45, no. 48, pp. 25783–25810, 2020, doi: 10.1016/j.ijhydene.2020.04.098.

[104] P. Pardo, A. Deydier, Z. Anxionnaz-Minvielle, S. Rougé, M. Cabassud, and P. Cognet, "A review on high temperature thermochemical heat energy storage," *Renew. Sustain. Energy Rev.*, vol. 32, pp. 591–610, 2014, doi: 10.1016/j.rser.2013.12.014.

[105] B. Wong, L. . Brown, F. . Schaube, R. . Tamme, and S. C.;, "Oxide based thermochemical heat storage," in *SolarPACES*, 2010.

[106] B. Ehrhart, E. Coker, N. Siegel, and A. Weimer, "Thermochemical cycle of a mixed metal oxide for augmentation of thermal energy storage in solid particles," *Energy Procedia*, vol. 49, no. April 2015, pp. 762–771, 2014, doi: 10.1016/j.egypro.2014.03.082.

[107] Modelon AB, "Modelon Home," 2018. https://www.modelon.com/

[108] U. Lackermeier and J. Werther, "Flow phenomena in the exit zone of a circulating fluidized bed," *Chem. Eng. Process.*, vol. 41, pp. 771–783, 2002.

[109] F. Johnsson, A. Vrager, T. Tiikma, and B. Leckner, "Solids flow pattern in the exit region of a CFB-furnace. Influence of geometry," in *Proceedings of the 15th international con- ference on fluidized bed combustion*, 1999.

[110] F. Johnsson and B. Leckner, "Vertical distribution of solids in a CFB-furnace," in *13th International conference on fluidized-bed combustion*, 1995, p. 719.

[111] F. Johnsson, W. Zhang, and B. Leckner, "Characteristics of the formation of particle wall layers in CFB boilers," in *2nd Int. Conf. on Multiphase Flow, Kyoto, Japan, Vol 3*, 1995.

[112] T. Djerf, D. Pallarès, and F. Johnsson, "Solids flow patterns in large-scale Circulating Fluidised Bed boilers: Experimental evaluation under fluid-dynamically down-scaled conditions," *Chem. Eng. Sci.*, vol. 231, no. December, p. 116309, 2020, doi: 10.1016/j.ces.2020.116309.

[113] H. Ström and H. Thunman, "A computationally efficient particle submodel for CFD-simulations of fixed-bed conversion," *Appl. Energy*, vol. 112, pp. 808–817, 2013, doi: 10.1016/j.apenergy.2012.12.057.

[114] S. Oka, *Fluidized bed combustion*. New York, 2004.

[115] F. L. Dryer and C. K. Westbrook, "Simplified Reaction Mechanisms for the Oxidation of Hydrocarbon Fuels in Flames," *Combust. Sci. Technol.*, vol. 27, no. 1–2, pp. 31–43, 1981, doi: 10.1080/00102208108946970.

[116] C. Breitholtz, B. Leckner, and A. P. Baskakov, "Wall average heat transfer in CFB boilers," *Powder Technol.*, vol. 120, no. 1–2, pp. 41–48, 2001, doi: 10.1016/S0032-5910(01)00345-X.

[117] J. R. Howell, *A catalog of radiation configuration factors*. McGraw-Hill, 1982.

[118] J. Eborn, "On model libraries for thermo-hydraulic applications," *Dep. Autom. Control. Lund Inst. Technol.*, p. 135, 2001, [Online]. Available: http://www.control.lth.se/documents/2001/ebo01phd.pdf

[119] Springer, Ed., *VDI Wärmeatlas*, 9th Editio. Springer, 1997. [Online]. Available: https://www.springer.com/gp/book/9783540778769

[120] F. Casella and A. Leva, "Modelica open library for power plant simulation: design and experimental validation," *Proc. 3rd Int. Model. Conf.*, no. December, pp. 41–50, 2003, [Online]. Available: http://scholar.google.com/scholar?hl=en&btnG=Search&q=intitle:Modelica+open+library+for+power+plant+simulation+:+design+and+experimental+validation#0

[121] R. Paranjape, "Modeling and control of a supercritical coal fired boiler," Texas Tech University, 1996. doi: 10.1080/00431672.1996.9925425.

[122] R. Beebe, "Condition monitoring of steam turbines by performance analysis," *J. Qual. Maint. Eng.*, vol. 9, no. 2, pp. 102–112, 2003, doi: 10.1108/13552510310482361.

[123] S. Skogestad, "Probably the best simple PID tuning rules in the world," in *AIChE Annual Meeting*, 2001, no. November 2001.

[124] E. Hairer and G. Wanner, "Stiff differential equations solved by Radau methods," *J. Comput. Appl. Math.*, vol. 111, no. 1–2, pp. 93–111, 1999, doi: 10.1016/S0377-0427(99)00134-X.

[125] D. Seborg, T. Edgar, D. Mellichamp, and F. Doyle, *Process dynamics and control*. John Wiley & Sons, 2011.

[126] D. Spreitzer and J. Schenk, "Iron Ore Reduction by Hydrogen Using a Laboratory Scale Fluidized Bed Reactor : Kinetic Investigation — Experimental Setup and Method for Determination," *Metall. Mater. Trans. B*, vol. 50, no. 5, pp. 2471–2484, 2019, doi: 10.1007/s11663-019-01650-9.

[127] J. Beiron, R. M. Montañés, F. Normann, and F. Johnsson, "Combined heat and power operational modes for increased product flexibility in a waste incineration plant," vol. 202, 2020, doi: 10.1016/j.energy.2020.117696.

[128] L. Göransson, M. Lehtveer, E. Nyholm, M. Taljegard, and V. Walter, "The benefit of collaboration in the North European electricity system transition—System and sector perspectives," *Energies*, vol. 12, no. 24, 2019, doi: 10.3390/en12244648.

[129] Y. Liu, Q. Zhu, T. Zhang, X. Yan, and R. Duan, "Analysis of chemical-looping hydrogen production and power generation system driven by solar energy," *Renew. Energy*, vol. 154, pp. 863–874, 2020, doi: 10.1016/j.renene.2020.02.109.

[130] G. Manzolini, E. MacChi, and M. Gazzani, "CO_2 capture in Integrated Gasification Combined Cycle with SEWGS - Part B: Economic assessment," *Fuel*, vol. 105, pp. 220–227, 2013, doi: 10.1016/j.fuel.2012.07.043.

[131] IRENA, "Renewable Energy Technologies: Cost analysis series. Concentrating Solar Power," 2012. doi: 10.1016/B978-0-12-812959-3.00012-5.

[132] J. Cortes Romea, "Electrified District Heating Plants using Thermochemical Energy Storage," Chalmers University of Technology, 2023. [Online]. Available: https://upcommons.upc.edu/handle/2117/385637

[133] J. Beiron, R. M. Montañés, and F. Normann, "Operational Flexibility of Combined Heat and Power Plant With Steam Extraction Regulation," in *Proceedings of 11th International Conference on Applied Energy*, 2019, pp. 1–4.

[134] A. Bayon *et al.*, "Techno-economic assessment of solid–gas thermochemical energy storage systems for solar thermal power applications," *Energy*, vol. 149, pp. 473–484,

2018, doi: 10.1016/j.energy.2017.11.084.

[135] LKAB, “Annual and Sustainability Report,” Luleå, 2021.

[136] D. Geldart, “Types of Gas Fluidization,” *Powder Technol.*, vol. 7, pp. 285–292, 1973.

[137] S. Thaker, A. Olufemi Oni, and A. Kumar, “Techno-economic evaluation of solar-based thermal energy storage systems,” *Energy Convers. Manag.*, vol. 153, no. October, pp. 423–434, 2017, doi: 10.1016/j.enconman.2017.10.004.

[138] P. Holmér, J. Ullmark, L. Göransson, V. Walter, and F. Johnsson, “Impacts of thermal energy storage on the management of variable demand and production in electricity and district heating systems: a Swedish case study,” *Int. J. Sustain. Energy*, vol. 39, no. 5, pp. 446–464, 2020, doi: 10.1080/14786451.2020.1716757.

[139] P. Psarras, S. Comello, P. Bains, P. Charoensawadpong, S. Reichelsten, and J. Wilcox, “Carbon Capture and Utilization in the Industrial Sector,” *Environ. Sci. Technol.*, vol. 51, pp. 11440–11449, 2017.

[140] EU, “Eurostat electricity price statistics.” https://ec.europa.eu/eurostat/statistics-explained/index.php?title=Electricity_price_statistics#Electricity_prices_for_non-household_consumers

[141] A. Toktarova, L. Göransson, and F. Johnsson, “Design of Clean Steel Production with Hydrogen : Impact of Electricity System Composition,” *Energies*, vol. 14, no. 8349, 2021.